We thank the Referee for the insightful comments. We have revised our manuscript according to the suggestions of the Referee's comments and our responses to the comments are as follows. The Referee's comments are in black, authors' responses are in blue, and changes to the manuscript are in red color text.

This study investigates the formation of secondary organic aerosols from the photooxidation of furan at different NOx and RH levels. SOA yields were measured using NaCl seeds to provide surface area for the partitioning of SOA-forming vapors. The chemical composition, in particular organic functional groups and a selection of molecular products, was characterized by FTIR and ESI-MS. The authors found a strong dependence of the measured SOA concentration, mass yield, and the intensity of individual functionalities on the initial VOC/NOx ratios and RH levels in a series of experiments conducted, and suggested that NOx and RH play an important role in the SOA formation from furan oxidation by altering the chemical pathways, e.g., aqueous phase chemistry, that essentially lead to SOA. This conclusion, however, is heavily drawn from the inadequate data analysis and interpretation, and lacks fundamental understanding of the predominant chemistry that occurs in the chamber experiments performed.

NOx dependence of SOA yields

In this study, photolysis of NO2 was used to generate O3, which further undergoes photolysis and reaction with H2O to generate OH radicals. The initial VOC/NOx ratio in the performed experiments ranges from ~7 to ~48. With the presence of hundreds of ppb levels of furan at the beginning of the experiment, furan is not completely oxidized at the end and the measured SOA mass is mostly composed of the very first few generations of oxidation products. As the initial VOC/NOx ratio decreases, more NO2 will be available for the formation of O3 and consequently OH radicals. **The observed 'NOx-effect' here is essentially the OH effect: higher OH levels result in more furan consumed, thus producing more SOA mass and higher SOA yield.**

This OH effect on SOA production has been well studied and understood in the community.

Author reply:

In our experiments, the OH radical was indeed produced during the photooxidation of furan instead of being added before the experiments started. But the original intension of our study was not to determine the OH effect on furan SOA formation. As indicated previously, SOA yields increase with increasing NOx concentration at low NOx levels and then decrease at higher NOx concentration (Sarrafzadeh et al., 2016a; Loza et al., 2014; Hoyle et al., 2011; Chan et al., 2010). All these studies demonstrated that the increase of SOA yield at low NOx levels was attributed to an increase of OH concentration. After eliminating the effect of OH concentration on the SOA mass growth, the SOA yield only decreased with increasing NOx concentration.

To control the effect of OH concentration on furan SOA formation in the present work, four more experiments have been added with additional injection of H_2O_2 as OH precursor before the experiments started. The results suggested that there remains a positive correlation between SOA formation and NOx concentration as shown in Table S1 and Fig. 3. To further understand the effect of NOx level on SOA formation, four more experiments were carried out for HESI-Q Exactive-Orbitrap MS detection. The MS results revealed the formation of a number of cyclical hydroxyl nitrates and dihydroxyl dinitrates with low-volatility, which can significantly contribute to the SOA formation (Schwantes et al., 2019). To provide a better illustration of the NOx effect on SOA formation, the following changes have been made to the revised manuscript.

Page 7, line 2:

"To further assess the effect of OH produced during the furan-NOx photooxidation, four experiments (Table S1, Exp.13-16) were conducted by injecting H_2O_2 in the chamber before the experiments started. For Exp.6-12, different RH levels coupled with similar furan/NOx ratios were monitored to assess the RH impact on SOA formation. To analyze the SOA composition, five additional experiments (Table S2, Exp. 17-21) were carried out to analyze the HESI-Q Exactive-Orbitrap MS, which intended to compare the role of NOx and RH on the SOA formation."

Page 9, line 5:

"It is generally accepted that experiments with low NOx levels lead to higher SOA yields than those with higher NOx levels at the same VOC concentration (Song et al., 2005). However, as shown in Fig. 3, an increasing SOA mass concentration and SOA yield with increasing NOx was observed. There are two possible explanations to this phenomenon: (i) The concentration of OH radicals produced *in situ* in the present study before additional source of OH was insufficient to produce a considerable amount of SOA under low-NOx conditions. As shown in Fig. S3, the OH concentration exhibits a gradual increase with NOx concentration and there appears to be a correlation between NOx concentration, OH concentration and SOA yield. Therefore, at low-NOx conditions, the increase of SOA yield was attributed to an increase of OH concentration, which was affected by OH recycling following reaction (R6) (see Fig. 1) and contributed to the enhancement of SOA formation. This result is consistent with a previous study concerning the impact of NOx and OH on SOA formation from β-pinene photooxidation, which has proved that the positive correlation between SOA yield and NOx levels ($[VOC]_0/[NOx]_0 > 10$ ppbC/ppb) was caused by the NOx–induced increase of OH concentration (Sarrafzadeh et al., 2016b). (ii) Differently, Sarrafzadeh et al. found that after eliminating the effect of OH concentration on SOA mass growth, SOA yield only decreased with increasing NOx levels (Sarrafzadeh et al., 2016b). To further investigate the NOx effect on furan generated SOA formation under adequate OH conditions, four more experiments (see Table S1) were carried out with additional injection of H_2O_2 as the OH radical source before the start of each experiment. The SOA yield trend at different C_4H_4O/NOx ratios is also shown in Fig. 3. The continuous growth trend of SOA yield with increasing NOx concentration at a relative high NOx level may result from the partitioning of generated semi/low-volatility compounds (multifunctional nitrates and dinitrates) into the particle phase, leading to significant furan SOA formation under high NOx conditions. Similarly, SOA from OH-initiated isoprene oxidation under high-NOx conditions was comprehensively investigated by Schwantes et al., who suggested that low volatility hydroxyl nitrates and dihydroxyl dinitrates generated conspicuously more aerosol than previously thought (Schwantes et al., 2019). Our results showing the increase of SOA mass formation at high-NOx conditions also agree with a previous study, which indicated that a high level of NO_2 can participate in the OH-induced reaction of guaiacol, consequently leading to the formation of organic nitrates and the enhancement of guaiacol SOA formation (Liu et al., 2019a). "

Page 11, line 21:

"The MS spectra of generated species from different NOx level and RH conditions, which show evidence for the OH-furan reaction, are presented in Fig. 7 and Fig. 8, respectively. The major peaks are m/z^+ 85.0018, 101.0894, and 185.0504 in the positive ion mode, and m/z^- 146.0161, 225.0125 and 263.0132 in the negative ion mode. The prominent peaks in the HR-MS spectra detected on negative ion mode are comprised of various functionalized hydroxyl nitrates and dihydroxyl dinitrates. However, in the positive ion mode analysis, most carbonyl components were detected. The assignments of these ion peaks, the molecular weights of the products observed, and proposed structures are summarized in Table 3. These detected compounds provide additional evidence for the proposed radical reaction mechanism."

Page 12, line 4:

"(i) decompose and then react with O_2 to yield a 1,4-aldoester (A), (ii) react with $NO_2/NO/O_2$ to form hydroxyl nitrate compound isomers with m/z^- 146., or (iii) react with O_2 to form unsaturated products and hydroxyfuranone (B) and 1,4-aldoacid (C). The ring-opened alkylperoxy radical generated from (d) can decompose to generate an unsaturated 1,4-dialdehyde (D). The formation of 1,4-dialdehyde with m/z^+ 85 detected in the positive ion mode suggests that these unsaturated 1,4-dicarbonyls are formed after initial OH addition at 2- or 5-positions. We note that OH radical addition at 2, 3-positions would lead to carbonyl product isomers with same m/z^+ 101. In addition, some dihydroxyl dinitrates with m/z^- 225 were also detected in negative ion mode. However, the pathways favouring the generation of these dihydroxyl dinitrates could only take place under high NOx levels. Scheme 1 shows the formation of second-generation products hemiacetals (E) via the reactions of the hydroxyfuranone (B) with 1,4-dialdehyde (D). After uptake from the gas-phase, the combination of hydroxyfuranone with 4-dialdehyde appeared to occur by H-abstraction, followed by dehydration, thus forming m/z^+ 185 compounds. This reaction pathway has also been identified in previous studies of OH-initiated reactions of furans (Strollo and Ziemann, 2013; Aschmann et al., 2014). According to the results of HR-MS, this aqueous phase reaction is more favoured in aqueous particles."

Page 13, line 4:

"However, in the present study, an increasing trend of SOA formation was observed with the increase of NOx concentration. As shown in the HESI-Q Exactive Orbitrap-MS results, all the detected primary products are carbonyl-rich, and even the organonitrates have at least two carbonyl functional groups. These carbonyl-containing products have lower volatility and contribute to the SOA formation. The peak intensities in the MS of the products (m/z^+ 85, 101) generated by the pathways involving HO_2 (as indicated by the scheme 1) decreased with the increase of NOx concentration. Additionally, more products of dihydroxyl dinitrates (m/z^- 225) with multifunctional groups were detected under high NOx conditions. As shown in Scheme 1, the multifunctional organonitrates detected in negative ion mode are produced mostly from later-generation chemistry. Hydroxyl nitrates with m/z^- 149 can be formed through pathways 1-a, 2-a, and 3-a by the reaction of RO_2 with NOx. We note that the m/z^- 149 compound was detected both at low NOx levels and high NOx levels. However, the peak intensity of this product was decreased with increasing NOx concentration. This phenomenon might be caused by the later-reaction of the unsaturated hydroxyl nitrates going through a second

OH-initiated reaction and leading to the formation of the dihydroxyl dinitrate with m/z^- 225. In addition, the peak intensities changes of SOA products detected in the positive mode, such as, the peaks at m/z^+ 85 and 101 were reduced under high NOx conditions, which resulted from the fact that the RO_2 radical fate was dominated by the pathway of RO_2+NO or RO_2+NO_2. This result supports that the fate of RO_2 is not a single channel reaction. There exists a competition between RO_2 reacting with NOx and with HO_2 under high NOx conditions but the former pathway is more favourable. There are two pathways for hydroxyl nitrates formation from RO_2 radicals in the presence of NOx according to which RO_2 radicals may react with NO and NO_2 to form $RONO_2$ and $ROONO_2$, respectively (Kroll and Seinfeld, 2008). However, the formed peroxynitrates could easily thermally dissociate and convert to $RONO_2$.

Furthermore, by analyzing the OH concentration and products components, we conclude that there are two possible explanations for the increasing trend of SOA yield as the NOx level increases: (i) the SOA production is closely related to the oxidation capacity in the photooxidation experiments. Experiments conducted under different NOx levels indicate that the OH concentration is controlled by the NOx level if there is no additional OH precursor added before the start of the experiment. As shown in Fig. S3, an increase in NOx level results in more OH generation and a faster furan decay rate. This justifies the observed higher SOA mass concentration and higher SOA yield. (ii) HRMS fragments associated with multifunctional organonitrates are enhanced under high NOx conditions (Fig. 7). As presented in Scheme 1, the furan dihydroxyl dinitrates are generated from the first-generation hydroxyl nitrate reacting with OH to form a peroxy radical, which reacts thereafter with NO. Together with multifunctional hydroxyl nitrates, these low-volatility species can easily partition into the particle phase and increase the SOA mass concentration. More importantly, the seed particle added initially plays an important role in the processes of gas-particle partitioning as indicated by a recent study, which showed that sufficient seed surface area at the start of the reaction largely suppressed the effects of vapour wall losses of low-volatility compounds (Schwantes et al., 2019).

Therefore, the NaCl seed particle added in the present work promoted the partitioning of the formed low-volatility functional organonitrates."

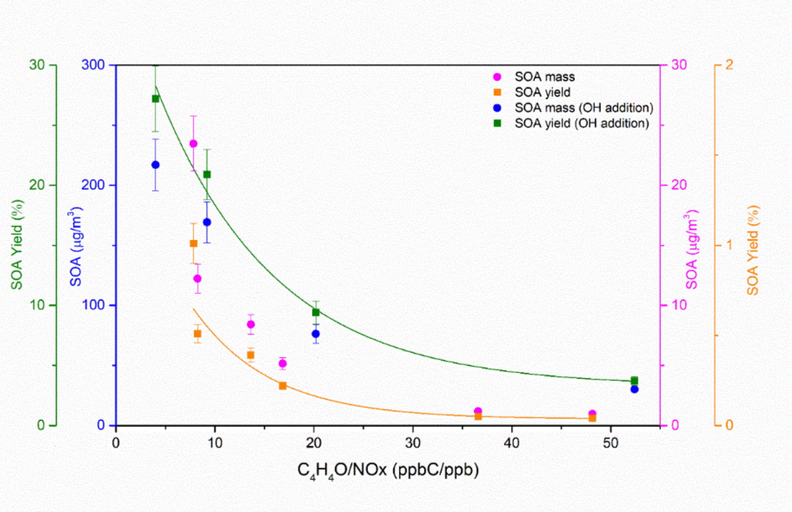

Figure 3: Dependence of the SOA mass concentration and SOA yield on the C_4H_4O/NOx ratio. Since the particle wall loss has a weak RH dependence in our chamber, a mean value of 3.6×10^{-5} s^{-1} was used for wall loss correction. A density of 1.4 g cm^{-3} was used in SMPS (Jia and Xu, 2018; Kostenidou et al., 2007).

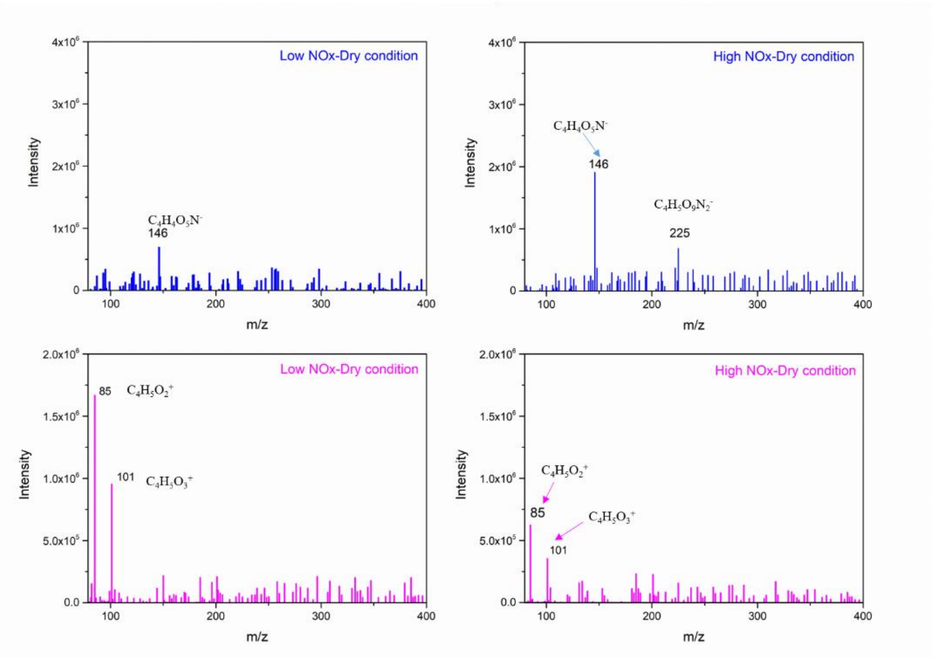

Figure 7: Selected background-subtraction HESI-Q Exactive-Orbitrap MS results of SOA in both negative (blue) and positive (pink) ion modes from the photooxidation of furan under different RH conditions.

Table S1. Summary of experimental conditions with the additional injection of H_2O_2 in the study of the NOx effect on SOA formaiton.

No.	$[furan]_0$ (ppb)	$[H_2O_2]_0$ (ppm)	$[NOx]_0$ (ppb)	RH (%)	C_4H_4O/NOx (ppbC/ppb)	SOA^e (μg m^{-3})	SOA yield (%)
13	802	1.7	15.3	< 10	52.4	30.1	3.7
14	811	1.6	40.2	< 10	20.2	76.3	9.4
15	807	1.7	87.5	< 10	9.2	169.2	20.9
16	797	1.7	200.1	< 10	4.0	216.9	27.2

Table S2. Summary of experimental conditions for HESI-Q Exactive-Orbitrap MS detection.

No.	$[furan]_0$ (ppb)	$[H_2O_2]_0$ (ppm)	$[NOx]_0$ (ppb)	RH (%)	C_4H_4O/NOx (ppbC/ppb)	Aim
17	723.5	3.5	26.4	<5	36.3	for HESI-Q Exactive-Orbitrap MS
18	748.3	6.5	152.6	<5	5.8	
19	764.8	7.2	163.5	30	5.9	
20	755.1	7.3	149.8	62	5.9	

RH dependence of SOA yields

Again, as H2O is used to generate OH radicals, higher RH levels result in more OH radicals, which lead to more SOA mass produced from furan photooxidation. **The**

observed 'RH effect' is essentially another 'OH effect' by promoting the generation of OH radicals and accelerating the oxidation processes of furan. The authors suggest that relative humidity affects the SOA yield through aqueous phase chemistry. However, the deliquescence point of sodium chloride is around 70% RH, below which the water content in the NaCl particles is close to zero, meaning that there would be minimal aqueous phase chemistry occurring in the particle phase.

Author reply:

The DRH and ERH of NaCl are about 75.5% and 47.6-46.3% (Gupta et al., 2015), respectively. NaCl seed aerosols were generated via atomization of NaCl aqueous solution with a constant-rate atomizer. The seed particles would be in the form of droplets after produced from the atomizer (Ge et al., 2016). Being dried through a self-made diffusion dryer, the NaCl seeds experienced efflorescence behavior during the dehydration process. It has been previously shown that SOA formation decreases both the ERH and DRH of the seed particles and results in the uptake of water by the particles (Liu et al., 2018; Takahama et al., 2007; Smith et al., 2012). There is a high possibility that the NaCl seeds will effloresce and deliquesce early after being coated by the new formed SOA. This assumption has been mentioned in the manuscript on Page 14, line 17. Additionally, we have monitored the aerosol liquid water content after the experiments. The details for the detection of ALW have been presented on Page 5, line 23 in our manuscript. Furthermore, as displayed in the manuscript, the ALW content has been indeed detected at 54% RH. Therefore, there is a high possibility that aqueous phase chemistry may play an important role in the SOA formation. This assumption was further confirmed by the results of HESI-Q Exactive-Orbitrap MS. The appearance of m/z^+ 185 and m/z^- 262 demonstrated that aqueous phase reactions indeed took place under high RH conditions by aqueous phase reaction of the hydroxyfuranone (B) and 1,4-dialdehyde (D) (Strollo and Ziemann, 2013). Alternatively, the moist surface under high RH conditions is more favorable for the condensation of the products with carbonyl functional groups, leading to the increasing production of SOA formation. As shown in Fig. 8, the intensities of multifunctional hydroxyl nitrates and dihydroxyl dinitrate (m/z^- 146, 225) exhibited positive correlations with RH conditions. Slight peak intensity increases of m/z+ 85 and 101 products were also observed under high RH conditions, indicating that the gas-particle phase partitioning of low-volatility compounds was enhanced at these conditions. The discussion concerning the effect of RH on furan SOA formation has been rewritten to provide more information.

Page 9, line 28:

"It is worth note that under high RH conditions, as shown in Fig. 1, the NO_2 hydrolysis (reaction (R11)) can generate nitrous acid (HONO), which has been considered as a major source of OH. As indicated in Fig. 4, the SOA yields obtained in the present work clearly show a gradual increase with RH. Also shown in Fig. S3 is the dependence of OH and furan concentrations on RH during the experiments determined from the decay of furan using a reaction rate coefficient of k(OH+furran) = 4.01×10^{-11} cm^3 $molecules^{-1}$ s^{-1} (Atkinson et al., 1983). It is therefore probable that the increase of RH results in high levels of HONO formation in the chamber, which leads to an increase in OH concentration, a faster furan decay rate, and higher aerosol mass yields. This result is in reasonable good agreement with previous studies, which proposed that the amount of products that can partition into the particle phase increases with the increasing rate of hydrocarbon oxidation (Healy et al., 2009; Chan et al., 2007). Moreover, the increasing RH might also enhance the SOA formation due to the fact that the functionalized gas phase components were more favoured to condense on the surface of wet particles (Liu et al., 2019b)."

Page 13, line 3:

"3.4 Effect of RH on SOA formation

Experiments 6-12 were conducted under seven different RH conditions ranging from 5% to 85%. In this RH range, the SOA yield increases from 1.01% to 5.03%.

With almost identical initial conditions except RH, the yield of furan-derived SOA formed at high RH can be a factor of two higher than that formed at low RH. A similar trend was also observed by Yu et al., who found that the SOA mass concentrations increased by a factor of six when RH increased from 18% to 82% (Yu et al., 2011). As shown in Fig. S3, an increase in RH leads to higher OH concentrations resulting from higher HONO levels generated by the reaction of NO_2 with H_2O. Previously, Anglada et al. confirmed, using quantum mechanical calculations, that the water component could increase the OH production (Anglada et al., 2011). The positive correlation between initial water vapour concentration and OH concentration has also been previously observed experimentally (Healy et al., 2009; Tillmann et al., 2010). Additionally, Healy et al. have also reported that increasing OH concentration promoted the decay of VOC and enhanced SOA formation (Healy et al., 2009). Similarly, in the present work, a faster decay rate of furan was also observed as RH increased, as shown in Fig. S3. It is possible that the faster rate of gas phase oxidation under higher OH concentrations will lead to the generation of less volatile compounds as presented previously (Chan et al., 2007). A higher OH concentration promotes oxidation reactions, influences the distribution of organic products, and facilitates the SOA formation (Sarrafzadeh et al., 2016b).

An obvious increase of SOA yield was observed when the RH increased from 37% to 54%. This phenomenon was mainly caused by the efflorescence transition when the seed particles were coated with SOA. It has been previously shown that SOA formation decreases both the efflorescence RH and deliquescence RH of the seed particles and results in the uptake of water by the particles (Liu et al., 2018; Takahama et al., 2007; Smith et al., 2012). It is highly possible that the NaCl seeds effloresce and deliquesce early after being coated by the new formed SOA. The effect of efflorescence contributes to the water uptake by the particles, leading to the obvious trend-changing of SOA yield. It is noted that with the NaCl seed aerosols serving as nuclei, the ALW was high at high RH. Products with water solubility produced from the photooxidation of furan can dissolve into the ALW of aerosol particles. As a result, ALW in the formed aerosols plays an important role in gas/particle partitioning. As shown in Fig. 4, the ALW was detected when the RH was higher than 54%, which was based on the deliquescence of NaCl under high RH conditions. The increase of ALW could partially explain the increase of SOA mass concentration and SOA yield. It is highly probable that the particle surface area increases with increasing amount of ALW as shown in Fig. S7, which likely promotes the dissolution of semi-volatile matters produced during the experiments. According to the HESI-Q Exactive-Orbitrap MS results shown in Fig. 8, the intensities of multifunctional hydroxyl nitrates and dihydroxyl dinitrate (m/z^- 146 and 225, respectively) exhibited positive correlations with RH. Slight peak intensities increases of m/z^+ 85 and 101 products were also observed under high RH conditions. This phenomenon indicates that the gas-particle phase partitioning of low-volatility compounds was enhanced under high RH conditions. Furthermore, the increased surface area under high RH conditions may also be attributed to the condensation of the produced multifunctional compounds.

Another possibility for the increasing trend of SOA yield with the increase of RH might result from the SOA formation through aqueous chemistry in wet aerosols (Grgic et al., 2010; Lim et al., 2010). In these atmospheric processes, alcohols, aldehydes, and ketones formed from the photooxidation of furan in the gas phase can be absorbed into the humid surface of the hygroscopic SOA at high RH. This process further contributes to the formation of low-volatility products on the SOA surface. In addition, the aqueous photochemistry of highly soluble small compounds that portioned in ALW could produce additional organic compounds and result in larger SOA yield under high RH conditions (Faust et al., 2017; Jia and Xu, 2014). The appearance of m/z^+ 185 and m/z^- 262 detected by the HESI-Q Exactive-Orbitrap MS further demonstrated that aqueous phase reactions indeed took place under high RH conditions. As shown in Scheme 1, the peak of m/z^+ 185 could form by aqueous phase reaction of the hydroxyfuranone (B) and 1,4-dialdehyde (D). The formation of hemiacetal (E) has also been detected by a previous study of the OH-initiated reaction of 3-methylfuran in the presence of NOx (Strollo and Ziemann, 2013). The proposed hemiacetal compound (E) plays a substantial role in the obvious increase of m/z^+ 185 product formation under high RH conditions. A pathway of organonitrate (m/z^- 262) formation in the aqueous particles with the presence of NO_3^- was suggested in the present study based on a previous work, which indicated a radical-radical reaction pathway for organosulfate formation from aqueous OH oxidation of glycolaldehyde in the presence of sulfuric acid (Perri et al., 2010). Increasing the RH also resulted in an overall addition of peak intensities in the negative ion mode, due to the fact that the sample obtained at high RH during the SOA generation had a larger particle surface. Specifically, a relatively stronger intense band of $C_8H_8O_9N^-$ (m/z^-=262) was found under a high RH. Consequently, the heterogeneous products in wet seed particles will further contribute to the formation of SOA, because higher aerosol liquid water content enables more aqueous phase reactions.

In conclusion, the reasons for the increasing trend of SOA formation under high RH conditions may be summarized as following: firstly, higher concentration of OH radical will certainly promote the SOA formation as RH increases. A faster decay rate of furan will also contribute to the formation of products that can partition into the particle phase. In addition, it is possible that the aqueous surface of seed particles provides a new substrate for the photooxidation of furan. Previously, N_2O_5 and HNO_3 have been proven to be the key products in the VOC-NOx irradiation experiments (Wang et al., 2016). The moist surface under high RH conditions is more favorable for the condensation of products with low vapor pressure, leading to the increasing production of SOA formation. The high RH environment favors the formation of the hemiacetal compound. Moreover, the effect of RH on SOA formation in furan photooxidation can also be determined by the aqueous photochemistry under high RH conditions as discussed above. The aqueous phase reactions at the surface of particles promotes the formation of hemiacetal-like products, which likely plays an important role in the process of SOA formation. Previously, unsaturated first-generation reaction product of 3-methyl furan has also been suggested to undergo acid-catalyzed condensed-phase reactions, with SOA yields up to 15% (Strollo and Ziemann, 2013).

In addition, the reinforced effect of RH on SOA yield was also ascribed from the photooxidation of other aromatic compounds, such as, benzene (Ng et al., 2007), toluene (Hildebrandt et al., 2009; Kamens et al., 2011), and xylene (Zhou et al., 2011)."

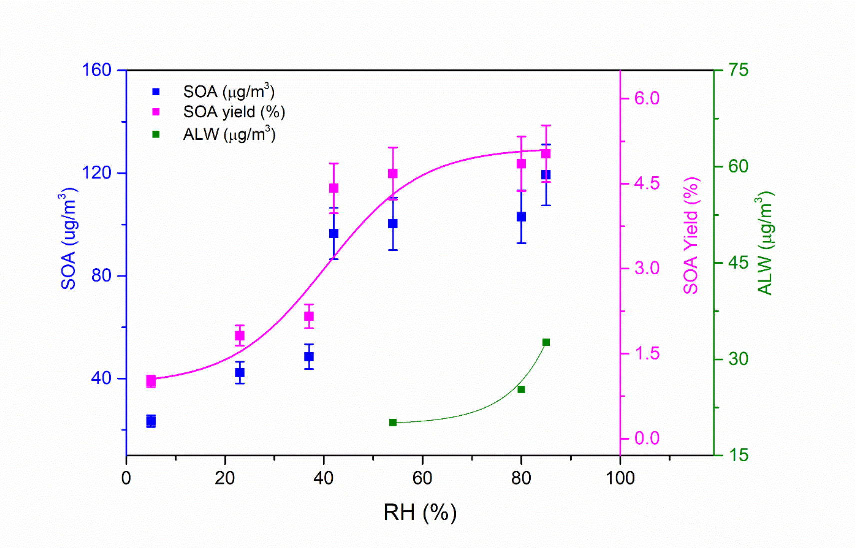

Figure 4: Dependences of the SOA mass concentration, SOA yield and ALW on relative humidity (RH).

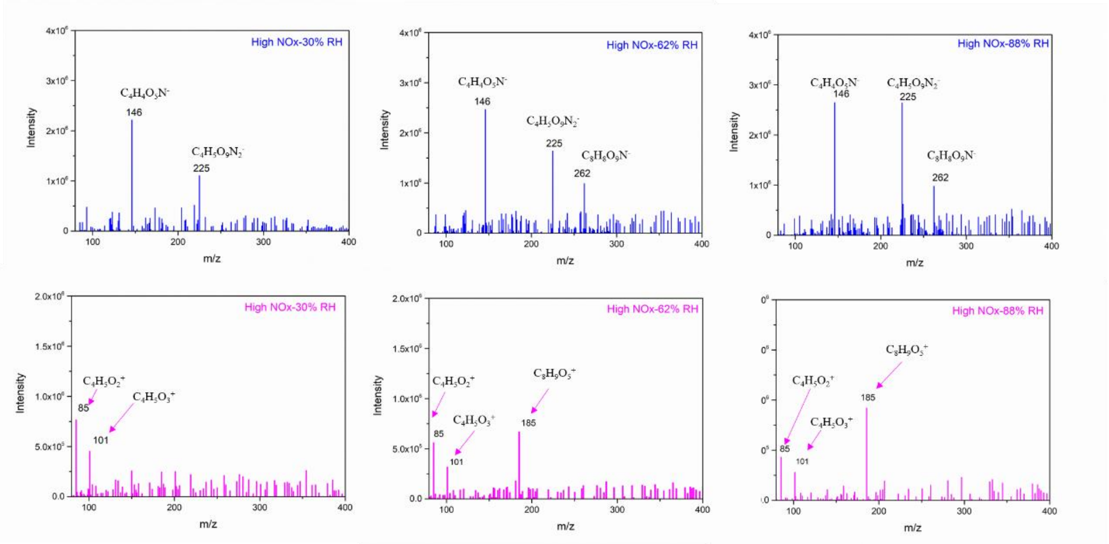

Figure 8: Selected background-subtraction HESI-Q Exactive-Orbitrap MS results of SOA in both negative (blue) and positive (pink) ion modes from the photooxidation of furan under different RH conditions.

SOA measurements at high RH levels

It is well known that using DMA to measure aerosol size distribution and mass leadings under high RH is subject to many certainties, e.g., arcing at high voltage caused by high water content in the aerosols. While the authors used a diffusion drier in front of the DMA inlet, which could certainly minimize the arcing effect that interferes the measurement of big particles, the drying efficiency was not characterized. Have the authors measured the RH of the aerosol flow upon the exit of the diffusion drier? Did aerosols generated under high RH (e.g., 80%) still carry a certain amount of water after drying? Additionally, the authors need to consider how the drying processes affect the repartitioning of water-soluble components between gas and particle phases in order to obtain an accurate SOA yield.

Author reply:

Indeed, the Nafion dryer was added to determine the liquid water content in the aerosols under high RH after the reaction ended. After modifying to the dry mode, the humid air in SMPS was quickly replaced by dry air through venting the sheath air at 5 L min^{-1}, and then the dry aerosol was measured by SMPS. The ALW was determined by the difference of the particle mass concentrations before and after the modification of the dry mode. After the dry mode treatment, the RH in the sampling air and sheath air reduced to 10 % and 7 %, respectively. The drying process for ALW determination is based on a widely used method developed by Engelhart (Engelhart et al., 2011), which has been proven to remove 90% of the water vapor. Consequently, the aerosols treated after the drying process were thought to carry seldom water content. We agree with the Referee that there is a possibility of the water-soluble components repartitioning betweent gas and particle phases. The fact that the SOA concentration for high RH conditions were slightly underestimated due to the ALW measurement. Thus, we added some sentences to reply comment on how the ALW meaurement affects our results on Page 5 in the revised manuscript.

“It should be noted that the dissloved water-soluble species would evaporate back into the gas phase during the ALW measurement when the aerosol water is removed. In fact, the repartitioning of water-soluble components between gas and particle phases was not taken into consideration. The SOA concentrations for high RH conditions were slightly underestimated, but the underestimation is extremely low and can be negligible."

Treatment of wall losses

The particle and vapor wall loss rates are chamber specific quantities that depend on a number of different parameters, i.e., the chamber size (volume to surface area ratio), the wall materials, the humidity in the enclosure air that affects the static charges on the chamber wall surface, and the mixing conditions (static or active mixing), among many others. The interaction patterns of particles with the chamber walls have been well studied for decades, and the particle wall loss rate has been found to vary substantially, by orders of magnitude, among different chamber environments. That the authors simply took the particle wall loss parameterizations obtained in other chambers to correct their own experiment would no doubt introduce significant uncertainties in their SOA mass measurements, resulting in unreliable SOA yield calculations.

Author reply:

We agree with the Referee that the wall loss rates of different chambers are different and the difference is dependent on many parameters, such as, the chamber size, the wall materials, and the chamber environments. The particle and vapor wall loss parameterizations used in this study are based on a previous study carried out in the same chamber reactor in our lab. Besides the chamber size and wall material, the experimental environments of these two studies are also similar: i) both studies were conducted in the ~5%-80% humidity range; ii) in both studies, NaCl seeds were added at the beginning of each experiment to provide sufficient seed surface area to limit the effects of vapor wall losses; iii) during all experiments in these two studies, two ironing air blowers were around the reactor to get rid of the electric charge on the surface of the reactor. Consequently, the citation of wall loss parameterizations detected from the same chamber reactor and similar experimental experiments will not introduce much uncertainties in the present study. After careful analysis of our experiments, we believe that our results are reliable and credible. To clarify the statement, we modified the sentences in the revised manuscript. The new one reads as follows:

"The wall loss rate constants for O_3, NOx and aerosol particles were 3.3×10^{-7} s^{-1}, 4.1×10^{-7} s^{-1}, and 3.6×10^{-5} s^{-1}, respectively, which were detected from our previous study conducted in the same set-up and similar experimental conditions (Ge et al., 2017a)."

References

Anglada, J. M., Gonzalez, J., and Torrent-Sucarrat, M.: Effects of the substituents on the reactivity of carbonyl oxides. A theoretical study on the reaction of substituted carbonyl oxides with water, Phys. Chem. Chem. Phys., 13, 13034-13045, 10.1039/c1cp20872a, 2011.

Aschmann, S. M., Nishino, N., Arey, J., and Atkinson, R.: Products of the OH radical initiated reactions of furan, 2-and 3-methylfuran, and 2,3-and 2,5-dimethylfuran in the presence of NO, J. Phys. Chem. A, 118, 457-466, 10.1021/jp410345k, 2014.

Atkinson, R., Aschmann, S. M., and Carter, W. P.: Kinetics of the reactions of O_3 and OH radicals with furan and thiophene at 298±2 K, Int. J. Chem. Kinet., 15, 51-61, 0.1002/kin.550150106, 1983.

Chan, A. W. H., Kroll, J. H., Ng, N. L., and Seinfeld, J. H.: Kinetic modeling of secondary organic aerosol formation: Effects of particle- and gas-phase reactions of semivolatile products, Atmos. Chem. Phys., 7, 4135-4147, 10.5194/acp-7-4135-2007, 2007.

Chan, A. W. H., Chan, M. N., Surratt, J. D., Chhabra, P. S., Loza, C. L., Crounse, J. D., Yee, L. D., Flagan, R. C., Wennberg, P. O., and Seinfeld, J. H.: Role of aldehyde chemistry and NOx concentrations in secondary organic aerosol formation, Atmos. Chem. Phys., 10, 7169-7188, 10.5194/acp-10-7169-2010, 2010.

Engelhart, G. J., Hildebrandt, L., Kostenidou, E., Mihalopoulos, N., Donahue, N. M., and Pandis, S. N.: Water content of aged aerosol, Atmos. Chem. Phys., 11, 911-920, 10.5194/acp-11-911-2011, 2011.

Faust, J. A., Wong, J. P. S., Lee, A. K. Y., and Abbatt, J. P. D.: Role of aerosol liquid water in secondary organic aerosol formation from volatile organic compounds, Environ. Sci. Technol., 51, 1405-1413, 10.1021/acs.est.6b04700, 2017.

Ge, S., Xu, Y., and Jia, L.: Secondary organic aerosol formation from propylene irradiations in a chamber study, Atmos. Environ., 157, 146-155, 10.1016/j.atmosenv.2017.03.019, 2017.

Grgic, I., Nieto-Gligorovski, L. I., Net, S., Temime-Roussel, B., Gligorovski, S., and Wortham, H.: Light induced multiphase chemistry of gas-phase ozone on aqueous pyruvic and oxalic acids, Phys. Chem. Chem. Phys., 12, 698-707, 10.1039/b914377g, 2010.

Gupta, D., Kim, H., Park, G., Li, X., Eom, H. J., and Ro, C. U.: Hygroscopic properties of NaCl and NaNO3 mixture particles as reacted inorganic sea-salt aerosol surrogates, Atmos. Chem. Phys., 15, 3379-3393, 10.5194/acp-15-3379-2015, 2015.

Healy, R. M., Temime, B., Kuprovskyte, K., and Wenger, J. C.: Effect of relative humidity on gas/particle partitioning and aerosol mass yield in the photooxidation of p-Xylene, Environ. Sci. Technol., 43, 1884-1889, 10.1021/es802404z, 2009.

Hildebrandt, L., Donahue, N. M., and Pandis, S. N.: High formation of secondary organic aerosol from the photo-oxidation of toluene, Atmos. Chem. Phys., 9, 2973-2986, 10.5194/acp-9-2973-2009, 2009.

Hoyle, C. R., Boy, M., Donahue, N. M., Fry, J. L., Glasius, M., Guenther, A., Hallar, A. G., Hartz, K. H., Petters, M. D., Petaja, T., Rosenoern, T., and Sullivan, A. P.: A review of the anthropogenic influence on biogenic secondary organic aerosol, Atmos. Chem. Phys., 11, 321-343, 10.5194/acp-11-321-2011, 2011.

Jia, L., and Xu, Y.: Effects of relative humidity on ozone and secondary organic aerosol formation from the photooxidation of benzene and ethylbenzene, Aerosol Sci. Tech., 48, 1-12, 10.1080/02786826.2013.847269, 2014.

Jia, L., and Xu, Y.: Different roles of water in secondary organic aerosol formation from toluene and isoprene, Atmos. Chem. Phys., 18, 8137-8154, 10.5194/acp-18-8137-2018, 2018.

Kamens, R. M., Zhang, H., Chen, E. H., Zhou, Y., Parikh, H. M., Wilson, R. L., Galloway, K. E., and Rosen, E. P.: Secondary organic aerosol formation from toluene in an atmospheric hydrocarbon mixture: Water and particle seed effects, Atmos. Environ., 45, 2324-2334, 10.1016/j.atmosenv.2010.11.007, 2011.

Kostenidou, E., Pathak, R. K., and Pandis, S. N.: An algorithm for the calculation of secondary organic aerosol density combining AMS and SMPS data, Aerosol Sci. Tech., 41, 1002-1010, 10.1080/02786820701666270, 2007.

Kroll, J. H., and Seinfeld, J. H.: Chemistry of secondary organic aerosol: Formation and evolution of low-volatility organics in the atmosphere, Atmos. Environ., 42, 3593-3624, 10.1016/j.atmosenv.2008.01.003, 2008.

Lim, Y. B., Tan, Y., Perri, M. J., Seitzinger, S. P., and Turpin, B. J.: Aqueous chemistry and its role in secondary organic aerosol (SOA) formation, Atmos. Chem. Phys., 10, 10521-10539, 10.5194/acp-10-10521-2010, 2010.

Liu, C., Liu, J., Liu, Y., Chen, T., and He, H.: Secondary organic aerosol formation from the OH-initiated oxidation of guaiacol under different experimental conditions, Atmos. Environ., 207, 30-37, 10.1016/j.atmosenv.2019.03.021, 2019a.

Liu, S., Tsona, N. T., Zhang, Q., Jia, L., Xu, Y., and Du, L.: Influence of relative humidity on cyclohexene SOA formation from OH photooxidation, Chemosphere, 231, 478-486, 10.1016/j.chemosphere.2019.05.131, 2019b.

Liu, T., Huang, D. D., Li, Z., Liu, Q., Chan, M., and Chan, C. K.: Comparison of secondary organic aerosol formation from toluene on initially wet and dry ammonium sulfate particles at moderate relative humidity, Atmos. Chem. Phys., 18, 5677-5689, 10.5194/acp-18-5677-2018, 2018.

Loza, C. L., Craven, J. S., Yee, L. D., Coggon, M. M., Schwantes, R. H., Shiraiwa, M., Zhang, X., Schilling, K. A., Ng, N. L., Canagaratna, M. R., Ziemann, P. J., Flagan, R. C., and Seinfeld, J. H.: Secondary organic aerosol yields of 12-carbon alkanes, Atmos. Chem. Phys., 14, 1423-1439, 10.5194/acp-14-1423-2014, 2014.

Ng, N. L., Kroll, J. H., Chan, A. W. H., Chhabra, P. S., Flagan, R. C., and Seinfeld, J. H.: Secondary organic aerosol formation from m-xylene, toluene, and benzene, Atmos. Chem. Phys., 7, 3909-3922, 10.5194/acp-7-3909-2007, 2007.

Perri, M. J., Lim, Y. B., Seitzinger, S. P., and Turpin, B. J.: Organosulfates from glycolaldehyde in aqueous aerosols and clouds: Laboratory studies, Atmos. Environ., 44, 2658-2664, 10.1016/j.atmosenv.2010.03.031, 2010.

Sarrafzadeh, M., Wildt, J., Pullinen, I., Springer, M., Kleist, E., Tillmann, R., Schmitt, S. H., Wu, C., Mentel, T. F., and Zhao, D.: Impact of NOx and OH on secondary organic aerosol formation from β-pinene photooxidation, Atmos. Chem. Phys., 16, 11237-11248, 10.5194/acp-16-11237-2016, 2016a.

Sarrafzadeh, M., Wildt, J., Pullinen, I., Springer, M., Kleist, E., Tillmann, R., Schmitt, S. H., Wu, C., Mentel, T. F., Zhao, D., Hastie, D. R., and Kiendler-Scharr, A.: Impact of NOx and OH on secondary organic aerosol formation from beta-pinene photooxidation, Atmos. Chem. Phys., 16, 11237-11248, 10.5194/acp-16-11237-2016, 2016b.

Schwantes, R. H., Charan, S. M., Bates, K. H., Huang, Y., Nguyen, T. B., Mai, H., Kong, W., Flagan, R. C., and Seinfeld, J. H.: Low-volatility compounds contribute significantly to isoprene secondary organic aerosol (SOA) under high-NOx conditions, Atmos. Chem. Phys., 19, 7255-7278, 10.5194/acp-19-7255-2019, 2019.

Smith, M. L., Bertram, A. K., and Martin, S. T.: Deliquescence, efflorescence, and phase miscibility of mixed particles of ammonium sulfate and isoprene-derived secondary organic material, Atmos. Chem. Phys., 12, 9613-9628, 10.5194/acp-12-9613-2012, 2012.

Song, C., Na, K. S., and Cocker, D. R.: Impact of the hydrocarbon to NOx ratio on secondary organic aerosol formation, Environ. Sci. Technol., 39, 3143-3149, 10.1021/es0493244, 2005.

Strollo, C. M., and Ziemann, P. J.: Products and mechanism of secondary organic aerosol formation from the reaction of 3-methylfuran with OH radicals in the presence of NOx, Atmos. Environ., 77, 534-543, 10.1016/j.atmosenv.2013.05.033, 2013.

Takahama, S., Pathak, R. K., and Pandis, S. N.: Efflorescence transitions of ammonium sulfate particles coated with secondary organic aerosol, Environ. Sci. Technol., 41, 2289-2295, 10.1021/es0619915, 2007.

Tillmann, R., Hallquist, M., Jonsson, A. M., Kiendler-Scharr, A., Saathoff, H., Iinuma, Y., and Mentel, T. F.: Influence of relative humidity and temperature on the production of pinonaldehyde and OH radicals from the ozonolysis of alpha-pinene, Atmos. Chem. Phys., 10, 7057-7072, 10.5194/acp-10-7057-2010, 2010.

Wang, Y., Luo, H., Jia, L., and Ge, S.: Effect of particle water on ozone and secondary organic aerosol formation from benzene-NO_2-NaCl irradiations, Atmos. Environ., 140, 386-394, 10.1016/j.atmosenv.2016.06.022, 2016.

Yu, K.-P., Lin, C.-C., Yang, S.-C., and Zhao, P.: Enhancement effect of relative humidity on the formation and regional respiratory deposition of secondary organic aerosol, J. Hazard. Mater., 191, 94-102, 10.1016/j.jhazmat.2011.04.042, 2011.

Zhou, Y., Zhang, H., Parikh, H. M., Chen, E. H., Rattanavaraha, W., Rosen, E. P., Wang, W., and Kamens, R. M.: Secondary organic aerosol formation from xylenes and mixtures of toluene and xylenes in an atmospheric urban hydrocarbon mixture: Water and particle seed effects (II), Atmos. Environ., 45, 3882-3890, 10.1016/j.atmosenv.2010.12.048, 2011.

We greatly value the careful reading and the detailed comments provided by the Referee. The responses to the Referee's comments in our direct reply and within the revised manuscript are provided below. The original comments from Referee are in black, our replies are in blue and the tracked changes in the main manuscript are in red color text.

This manuscript aimed to study SOA formation from furan under photooxidation conditions with varied NOx and RH. SOA mass, O3 concentration, and SOA composition were carefully measured. The authors concluded that furan photooxidation is dominated by RO2 + NO chemistry that leads to formation of carbonyl-rich products. SOA formation was found to enhance under higher relative humidity and higher VOC/NOx concentration. The results are clearly presented, but there are a few important issues that need to be addressed before becoming publishable. My major comment is that the manuscript did not provide sufficient chemistry insights given the suite of instruments used.

Author reply:

We greatly appreciate the thoughtful and helpful comments proposed by the Referee. To have a more sufficient chemistry insights into the furan SOA formation, we have added five more experiments under a series of NOx and RH conditions for the analysis of an improved chemical identification instrument. According to the latest results that sufficiently eliminate the interference of artifacts on the Exactive-Orbitrap MS, few parts of the discussion have been modified. Spectra results and reaction mechanism have been updated as well. Further discussion is given in later sections.

Major:

1. The authors claims that the O3 maximum concentration decreases with increasing RH likely due to that high RH favors the partitioning of the NOx reservoir, RNO2 and RONO2 into the particle phase. Thus the release of NOx is limited. However, it is

unclear how much more pronounced is the RNO2 and RONO2 uptake at higher RH and whether this enhancement is sufficient to affect O3 formation. These species need to be very soluble to show distinct partitioning behavior under different RH. What are their possible structures and could the Henry's law constants be estimated? Were any RNO2 or RONO2 species enhanced in the SOA samples under higher RH? From the ESI-MS results, the authors said that the SOA composition is similar between higher RH and low RH. Does this contradict what the authors concluded earlier? You have a max SOA yield of 5% and only a small fraction of that is RNO2 or RONO2. Thus are they important enough to affect gas-phase NOx concentration. Evidence is needed. Alternatively, could wall loss of the RNO2 and RONO2 under high RH better explain the observation?

Author reply:

According to the updated HESI-Q Exactive-Orbitrap MS results in the revised manuscript, the intensities of multifunctional hydroxyl nitrates and dihydroxyl dinitrate (m/z^- 146, 225) were indeed enhanced under high RH conditions (Fig. 8). As demonstrated by a previous study, these multifunctional hydroxyl nitrates and dihydroxyl dinitrate have low volatilities and can partition into the particle phase (Schwantes et al., 2019). It should also be noted that some products generated from the furan photooxidation have C=C bonds conjugated with the carbonyl and acid groups. These products can absorb strongly in the ~200-300 nm range and contribute to the signal of O_3 concentration detected by O_3 analyzer (Strollo and Ziemann, 2013). However, under high RH conditions, these carbonyl-rich products were favourable to condense on the moist surface of particles and thus lowered the O_3 concentration detected by O_3 analyzer. This assumption is reasonable since the intensities of m/z^+ 85 and 101 carbonyl-rich products were observed to increase when RH increased from dry condition to 30%. However, the intensities of the assigned carbonyl-rich products exhibited a slight decrease under higher RH conditions. This decreasing trend resulted from the aqueous phase reactions of hydroxyfuranone (m/z^+ 101) with 4-dialdehyde (m/z$^+$ 85), leading to the appearance of the generated hemiacetal compound (m/z$^+$ 185). In addition, there is a possibility that the wall losses of the organonitrates species would inhibit the O_3 formation under high RH as suggested by the Referee. To provide more information about the decreased O_3 concentration under high RH, the following changes have been made to the revised manuscript.

Page 7, line 28:

"However, it should be noted that the apparent high O_3 concentration monitored by the O_3 analyzer was due to species other than O_3 and that have absorption around 254 nm. The generated gas-phase reaction products that have carbonyl, carboxylic acid, and ester groups conjugated with C=C bonds can absorb strongly in the ~200-300 nm range and, accordingly, contribute to the apparent intense signal of O_3 detected by the O_3 monitor (Strollo and Ziemann, 2013)."

Page 8, line 16:

"Additionally, the slight change in O_3 maximum concentration under different RH conditions may also be caused by the consumption of gas-phase reaction products that contain functional groups conjugated with C=C bonds and respond to the O_3 analyzer. This assumption is reasonable because these carbonyl-rich products were favourable to condense on the moist surface of particles and thus lowered the O_3 concentration detected by the O_3 analyzer, which has been further confirmed by the MS results with enhanced intensities of corresponding organonitrates. The wall loss of the organonitrates species would also explain the decreasing trend of O_3 concentration as RH increases."

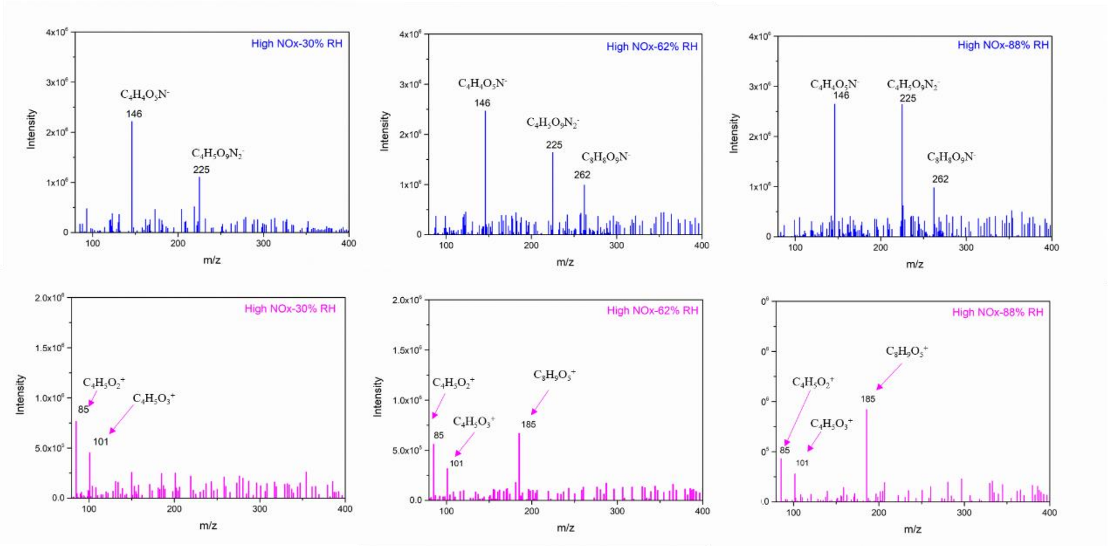

Figure 8: Selected background-subtraction HESI-Q Exactive-Orbitrap MS results of SOA in both negative (blue) and positive (pink) ion modes from the photooxidation of furan under different RH conditions.

Table 3. Ion peaks with the assigned compounds observed in the HESI-Q Exactive-Orbitrap MS. Proposed assignments are based on the formula from HESI-Q Exactive-Orbitrap MS.

Ion mode	No	Mass (m/z)	Ion Mode	Ion Formula	Delta (amu)	Proposed Structure
Positive ion mode	1	85.0018	$[M+H]^+$	$C_4H_5O_2^+$	-0.027	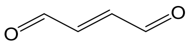
	2	101.0894	$[M+H]^+$	$C_4H_5O_3^+$	0.066	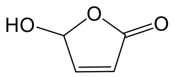 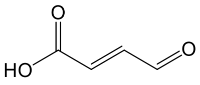 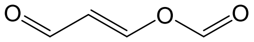
	3	185.0504	$[M+H]^+$	$C_8H_9O_5^+$	0.006	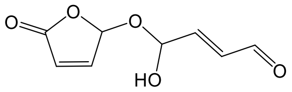
Negative ion mode	4	146.0161	$[M-H]^-$	$C_4H_4O_5N^-$	0.007	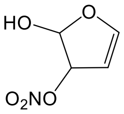 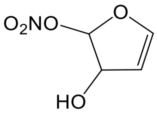 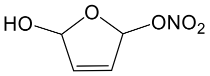
	5	225.0125	$[M-H]^-$	$C_4H_5O_9N_2^-$	0.012	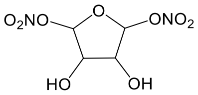
	6	262.0132	$[M-H]^-$	$C_8H_8O_9N^-$	-0.007	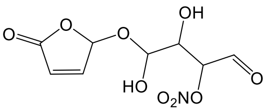

2. The ESI-MS results presented grouped ions and observed m/z 200-299 as the most abundant group. What does this mean? What are the major chemical formulas observed in this range? I think a lot more discussion of the ESI-MS results could be included here. For example:

(1) Could the authors group all nitrogen-containing species and discuss their presence?

(2) What are the ranges of O:C ratio and oxidation state?

(3) Any variation as the furan/NOx and RH changed?

(4) For soluble species uptaking onto aqueous particles, they will likely oligomerize. Do the authors see oligomers in the ESI-MS?

(5) There is a substantial decrease of large molecules under lower furan/NOx ratio and higher RH in the negative ion mode (but not in the positive ion mode). What does that suggest?

(6) what is the ion in the negative ion mode around m/z 380?

In the current form, there is very little discussion (page 11, line 16-24, page 12, line 2-7, and page 13, line 8-11)

Author reply:

A simple discussion of the m/z 200-299 parts may be confusing for a better understanding of the SOA components. In our revised manuscript, this part has been deleted and a detailed introduction of the updated Exactive-Orbitrap MS results was presented. Specifically, the nitrogen-containing species have been grouped and discussed in the revised manuscript as suggested by the Referee. Generally, three kinds of nitrogen-containing organic species were observed by the HRMS with m/z^- of 146.0161, 225.0125 and 263.0132 being detected in negative ion mode. The assignments of these ion peaks, the molecular weights, and proposed structures are summarized in Table 3. However, owing to the limits of our techniques, the ranges of O:C and oxidation state cannot be provided here. For carbonyl-rich species, these products were favourable to condense on the moist surface of particles and took part in further reactions. According to the mass results, the observed hemiacetal compound

(m/z^+ 185) was generated from the oligomerizations of hydroxyfuranone (m/z^+ 101) and 4-dialdehyde (m/z^+ 85). After removing the interference both from the sampling filter and residues from the detection instruments, new experiments have been conducted. The collected particles have been re-detected and the detected products were re-assigned in the revised manuscript. Moreover, the ESI-MS results have been significantly expanded as following:

Page 11, line 21:

"The MS spectra of generated species from different NOx level and RH conditions, which show evidence for the OH-furan reaction, are presented in Fig. 7 and Fig. 8, respectively. The major peaks are m/z^+ 85.0018, 101.0894, and 185.0504 in positive ion mode, and m/z^- 146.0161, 225.0125 and 263.0132 in the negative ion mode. The prominent peaks in the HR-MS spectra detected on negative ion mode are comprised of various functionalized hydroxyl nitrates and dihydroxyl dinitrates. However, in the positive ion mode analysis, most carbonyl components were detected. The assignments of these ion peaks, the molecular weights of the products observed, and proposed structures are summarized in Table 3. These detected compounds provide additional evidence for the proposed radical reaction mechanism."

Page 12, line 3:

"Moreover, the formed alkylperoxy radicals ($RO_2\cdot$) can either react with RO_2/HO_2 or NO to yield the corresponding alkoxy radical ($RO\cdot$), which can (i) decompose and then react with O_2 to yield 1,4-aldoester (A), (ii) react with $NO_2/NO/O_2$ to form hydroxyl nitrate compound isomers with m/z^- 146, or (iii) react with O_2 to form unsaturated products, hydroxyfuranone (B) and 1,4-aldoacid (C). The ring-opened alkylperoxy radical generated from (d) can decompose to generate an unsaturated 1,4-dialdehyde (D). The formation of 1,4-dialdehyde with a m/z^+ 85 detected in the positive ion mode suggests that these unsaturated 1,4-dicarbonyls are formed after initial OH addition at 2- or 5-positions. We note that OH radical addition at 2, 3-positions would lead to carbonyl product isomers with same m/z^+ 101. In addition, some dihydroxyl dinitrates with *m/z*$^-$ 225 were also detected in negative ion mode. However, the pathways favouring the generation of these dihydroxyl dinitrates could only take place under high NOx levels. Scheme 1 shows the formation of second-generation products hemiacetals (E) via the reactions of the hydroxyfuranone (B) with 1,4-dialdehyde (D). After uptake from the gas-phase, the combination of hydroxyfuranone with 4-dialdehyde appeared to occur by H-abstraction, followed by dehydration, thus forming *m/z*$^+$ 185 compounds. This reaction pathway has also been identified in previous studies of OH-radical initiated reactions of furans (Strollo and Ziemann, 2013; Aschmann et al., 2014). According to the results of HR-MS, this aqueous phase reaction is more favoured in aqueous particles."

Page 13, line 6:

"These carbonyl-containing products have lower volatility and contribute to the SOA formation. The peak intensities in the MS of the products (*m/z*$^+$ 85, 101) generated by the pathways involving HO_2 (as indicated by the scheme 1) decreased with the increase of NOx concentration. Additionally, more products of dihydroxyl dinitrates (*m/z*$^-$ 225) with multifunctional groups were detected under high NOx conditions. As shown in Scheme 1, the multifunctional organonitrates detected in negative ion mode are produced mostly from later-generation chemistry. Hydroxyl nitrates with *m/z*$^-$ 149 can be formed through pathways 1-a, 2-a, and 3-a by the reaction of RO_2 with NOx. We note that the *m/z*$^-$ 149 compound was detected both at low NOx levels and high NOx levels. However, the peak intensity of this product was decreased with increasing NOx concentration. This phenomenon might be caused by the later-reaction of the unsaturated hydroxyl nitrates going through a second OH-initiated reaction and leading to the formation of the dihydroxyl dinitrate with *m/z*$^-$ 225. In addition, the peak intensities changes of SOA products detected in the positive mode, such as, the peaks at *m/z*$^+$ 85 and 101 were reduced under high NOx conditions, which resulted from the fact that the RO_2 radical fate was dominated by the pathway of RO_2+NO or RO_2+NO_2. This result supports that the fate of RO_2 is not a single channel reaction. There exists a competition between RO_2 reacting with NOx and with HO_2 under high NOx conditions but the former pathway is more favourable. There are two pathways for hydroxyl nitrates formation from RO_2 radicals in the presence of NOx according to which RO_2 radicals may react with NO and NO_2 to form $RONO_2$ and $ROONO_2$, respectively (Kroll and Seinfeld, 2008). However, the formed peroxynitrates could easily thermally dissociate and convert to $RONO_2$.

Furthermore, by analyzing the OH concentration and products components, we conclude that there are two possible explanations for the increasing trend of SOA yield as the NOx level increases: (i) the SOA production is closely related to the oxidation capacity in the photooxidation experiments. Experiments conducted under different NOx levels indicate that the OH concentration is controlled by the NOx level if there is no additional OH precursor added before the start of the experiment. As shown in Fig. S3, an increase in NOx level results in more OH generation and a faster furan decay rate. This justifies the observed higher SOA mass concentration and higher SOA yield. (ii) HRMS fragments associated with multifunctional organonitrates are enhanced under high NOx conditions (Fig. 7). As presented in Scheme 1, the furan dihydroxyl dinitrates are generated from the first-generation hydroxyl nitrate reacting with OH to form a peroxy radical, which reacts thereafter reacts with NO. Together with multifunctional hydroxyl nitrates, these low-volatility species can easily partition into the particle phase and increase the SOA mass concentration. More importantly, the seed particle added initially plays an important role in the processes of gas-particle partitioning as indicated by a recent study, which showed that sufficient seed surface area at the start of the reaction largely suppressed the effects of vapour wall losses of low-volatility compounds (Schwantes et al., 2019). Therefore, the NaCl seed particle added in the present work promoted the partitioning of the formed low-volatility functional organonitrates."

Page 14, line 28:

"It is highly probable that the particle surface area increases with increasing amount of ALW as shown in Fig. S7, which likely promotes the dissolution of semi-volatile matters produced during the experiments. According to the HESI-Q Exactive-Orbitrap

MS results shown in Fig. 8, the intensities of multifunctional hydroxyl nitrates and dihydroxyl dinitrate (*m/z*$^-$ 146 and 225, respectively) exhibited positive correlations with RH. Slight peak intensities increases of m/z$^+$ 85 and 101 products were also observed under high RH conditions. This phenomenon indicates that the gas-particle phase partitioning of low-volatility compounds was enhanced under high RH conditions. Furthermore, the increased surface area under high RH conditions may also be attributed to the condensation of the produced multifunctional compounds."

Page 15, line 9:

"The appearance of *m/z*$^+$ 185 and *m/z*$^-$ 262 detected by the HESI-Q Exactive-Orbitrap MS further demonstrated that aqueous phase reactions indeed took place under high RH conditions. As shown in Scheme 1, the peak of *m/z*$^+$ 185 could form by aqueous phase reaction of the hydroxyfuranone (B) and 1,4-dialdehyde (D). The formation of hemiacetal (E) has also been detected by a previous study of the OH-initiated reaction of 3-methylfuran in the presence of NOx (Strollo and Ziemann, 2013). The proposed hemiacetal compound (E) plays a substantial role in the obvious increase of *m/z* $^+$185 product formation under high RH conditions. A pathway of organonitrate (*m/z*$^-$ 262) formation in the aqueous particles with the presence of NO_3^- was suggested in the present study based on a previous work, which indicated a radical-radical reaction pathway for organosulfate formation from aqueous OH oxidation of glycolaldehyde in the presence of sulfuric acid (Perri et al., 2010). Increasing the RH also resulted in an overall addition of peak intensities in the negative ion mode, due to the fact that the sample obtained at high RH during the SOA generation had a larger particle surface. Specifically, a relatively stronger intense band of $C_8H_8O_9N^-$ (*m/z*$^-$=262) was found under a high RH. Consequently, the heterogeneous products in wet seed particles will further contribute to the formation of SOA, because higher aerosol liquid water content enables more aqueous phase reactions.

In conclusion, the reasons for the increasing trend of SOA formation under high RH conditions may be summarized as following: firstly, higher concentration of OH radical will certainly promote the SOA formation as RH increases. A faster decay rate of furan will also contribute to the formation of products that can partition into the particle phase. In addition, it is possible that the aqueous surface of seed particles provides a new substrate for the photooxidation of furan. Previously, N_2O_5 and HNO_3 have been proven to be the key products in the VOC-NOx irradiation experiments (Wang et al., 2016). The moist surface under high RH conditions is more favorable for the condensation of products with low vapor pressure, leading to the increasing production of SOA formation. The high RH environment favors the formation of the hemiacetal compound. Moreover, the effect of RH on SOA formation in furan photooxidation can be also determined by the aqueous photochemistry under high RH conditions as discussed above. The aqueous phase reactions at the surface of particles promotes the formation of hemiacetal-like products, which likely plays an important role in the process of SOA formation. Previously, unsaturated first-generation reaction products of 3-methyl furan have also been suggested to undergo acid-catalyzed condensed-phase reactions, with SOA yields up to 15% (Strollo and Ziemann, 2013). In addition, the reinforced effect of RH on SOA yield was also ascribed from the photooxidation of other aromatic compounds, such as, benzene (Ng et al., 2007), toluene (Hildebrandt et al., 2009; Kamens et al., 2011), and xylene (Zhou et al., 2011)."

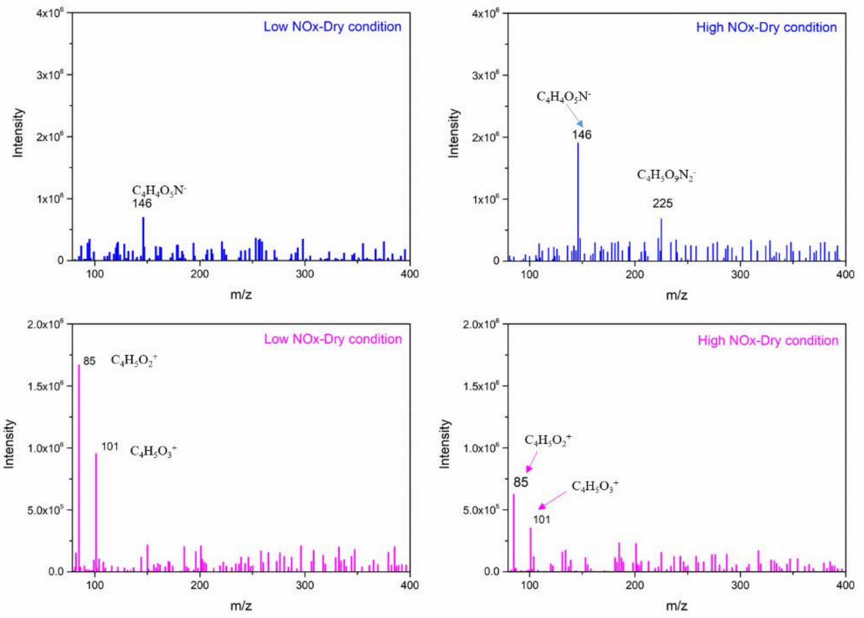

Figure 7: Selected background-subtraction HESI-Q Exactive-Orbitrap MS results of

SOA in both negative (blue) and positive (pink) ion modes from the photooxidation of furan under different RH conditions.

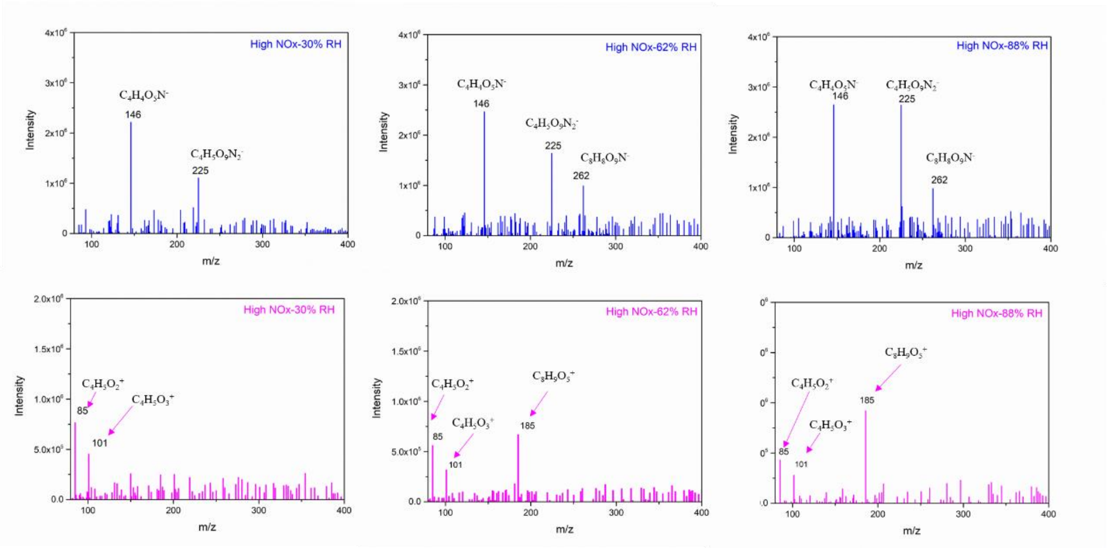

Figure 8: Selected background-subtraction HESI-Q Exactive-Orbitrap MS results of SOA in both negative (blue) and positive (pink) ion modes from the photooxidation of furan under different RH conditions.

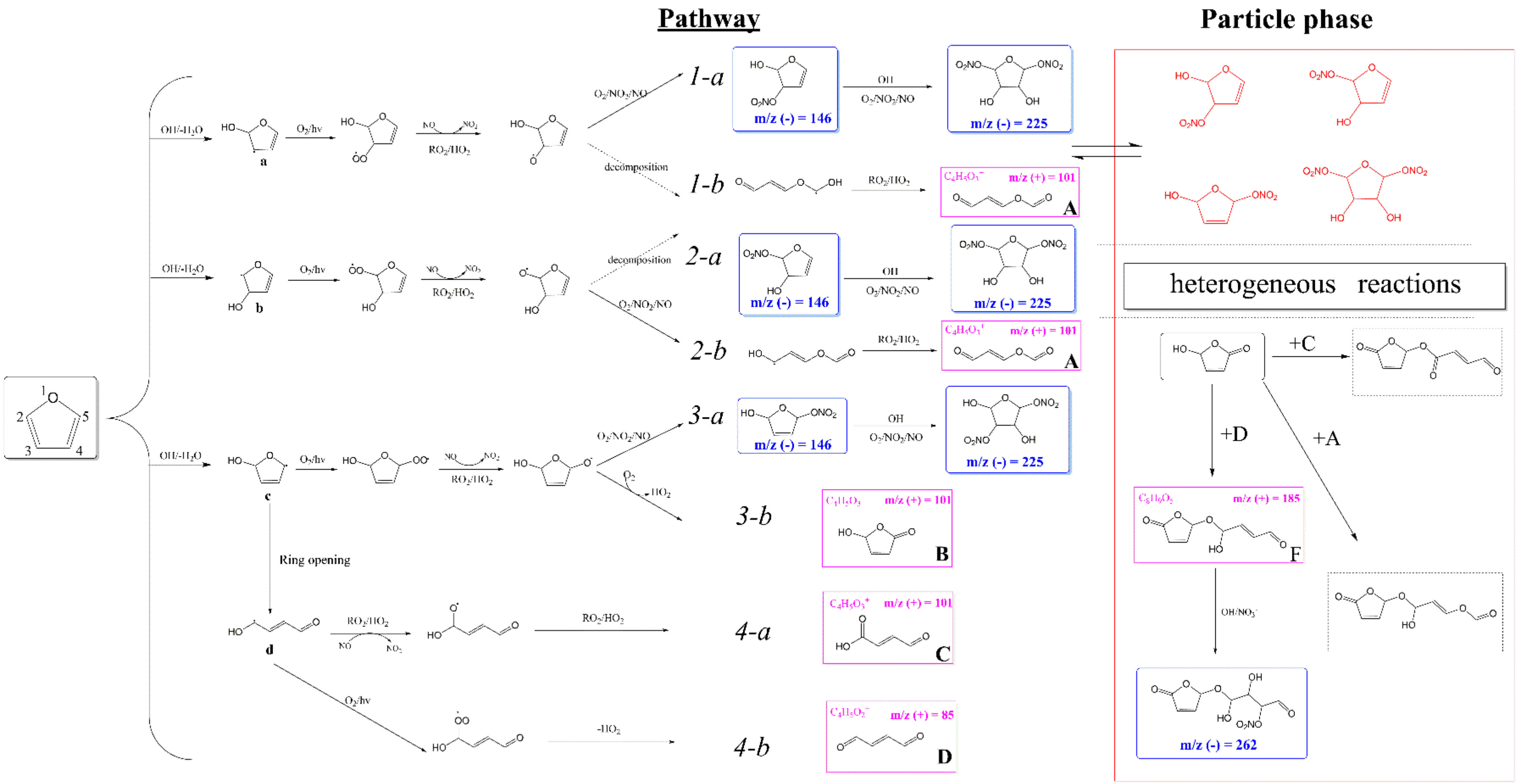

Scheme 1: Proposed chemical mechanism of furan-NOx photooxidation under different experimental conditions. SOA constituents in blue and

pink boxes are proposed SOA constituents detected by HESI-Q Exactive-Orbitrap MS under negative and positive ion mode, respectively. The detected nitrates and dinitrates in red are low-volatility organic species, which can easily partition into the particle phase and enhance the SOA formation.

3. The observation of enhanced SOA formation with increased NO is interesting, because most previous work have shown that increase of NO tend to promote RO2+NO chemistry which lead to fragmentation. Why are SOA yields higher with higher NO in the case of furan photooxidation? The authors gave these possibilities in the text, but did not further conclude it based on the mechanism. Is this because furan is a cyclic compound and the fragmentation does not break the C4 backbone? Or were OH concentrations very different between different furan/NOx experiments (as in the cases for the two referred studies)? Or both?

Author reply:

In our experiments, the OH radical was indeed produced during the photooxidation of furan instead of being added before the experiments started. But the original intension of our study was not to determine the OH effect on furan SOA formation. As indicated previously, SOA yields increase with increasing NOx concentration at low NOx levels and then decrease at higher NOx concentration (Sarrafzadeh et al., 2016a; Loza et al., 2014; Hoyle et al., 2011; Chan et al., 2010). All these studies demonstrated that the increase of SOA yield at low NOx levels was attributed to an increase of OH concentration. After eliminating the effect of OH concentration on the SOA mass growth, the SOA yield only decreased with increasing NOx concentration.

To control the effect of OH concentration on furan SOA formation in the present work, four more experiments have been added with additional injection of H_2O_2 as OH precursor before the experiments started. The results suggested that there remains a positive correlation between SOA formation and NOx concentration as shown in Table S1 and Fig. 3. To further understand the effect of NOx level on SOA formation, four more experiments were carried out for HESI-Q Exactive-Orbitrap MS detection. The MS results revealed the formation of a number of cyclical hydroxyl nitrates and dihydroxyl dinitrates with low-volatility, which can significantly contribute to the SOA formation (Schwantes et al., 2019). In addition, according to the proposed mechanism, the fragmentation can hardly break the C4 backbone for the cyclic compound furan. Many newly published studies suggested that increasing NOx concentration is beneficial to nitrates formation, which are regarded as low volatility species that can easily partition into the particle phase and enhance the SOA formation (Liu et al., 2019; Rissanen, 2018). To provide a better illustration of the NOx effect on SOA formation, the following changes have been made in the revised manuscript.

Page 7, line 2:

"To further assess the effect of OH produced during the furan-NOx photooxidation, four experiments (Table S1, Exp.13-16) were conducted by injecting H_2O_2 in the chamber before the experiments started. For Exp.6-12, different RH levels coupled with similar furan/NOx ratios were monitored to assess the RH impact on SOA formation. To analyze the SOA composition, five additional experiments (Table S2, Exp. 17-21) were carried out to analyze the HESI-Q Exactive-Orbitrap MS, which intended to compare the role of NOx and RH on the SOA formation."

Page 9, line 5:

"It is generally accepted that experiments with low NOx levels lead to higher SOA yields than those with higher NOx levels at the same VOC concentration (Song et al., 2005). However, as shown in Fig. 3, an increasing SOA mass concentration and SOA yield with increasing NOx was observed. There are two possible explanations to this phenomenon: (i) The concentration of OH radicals produced *in situ* in the present study before additional source of OH was insufficient to produce a considerable amount of SOA under low-NOx conditions. As shown in Fig. S3, the OH concentration exhibits a gradual increase with NOx concentration and there appears to be a correlation between NOx concentration, OH concentration and SOA yield. Therefore, at low-NOx conditions, the increase of SOA yield was attributed to an increase of OH concentration, which was affected by OH recycling following reaction (R6) (see Fig. 1) and contributed to the enhancement of SOA formation. This result is consistent with a previous study concerning the impact of NOx and OH on SOA formation from β-pinene photooxidation, which has proved that the positive correlation between SOA yield and NOx levels ($[VOC]_0/[NOx]_0 > 10$ ppbC/ppb) was caused by the NOx–induced increase of OH concentration (Sarrafzadeh et al., 2016b). (ii) Differently, Sarrafzadeh et al. found that after eliminating the effect of OH concentration on SOA mass growth, SOA yield only decreased with increasing NOx levels (Sarrafzadeh et al., 2016b). To further investigate the NOx effect on furan generated SOA formation under adequate OH conditions, four more experiments (see Table S1) were carried out with additional injection of H_2O_2 as the OH radical source before the start of each experiment. The SOA yield trend at different C_4H_4O/NOx ratios is also shown in Fig. 3. The continuous growth trend of SOA yield with increasing NOx concentration at a relative high NOx level may result from the partitioning of generated semi/low-volatility compounds (multifunctional nitrates and dinitrates) to the particle phase, leading to significant furan SOA formation under high NOx conditions. Similarly, SOA from OH-initiated isoprene oxidation under high-NOx conditions was comprehensively investigated by Schwantes et al., who suggested that low volatility hydroxyl nitrates and dihydroxyl dinitrates generated conspicuously more aerosol than previously thought (Schwantes et al., 2019). Our results showing the increase of SOA mass formation at high-NOx conditions also agree with a previous study, which indicated that a high level of NO_2 can participate in the OH-induced reaction of guaiacol, consequently leading to the formation of organic nitrates and the enhancement of guaiacol SOA formation (Liu et al., 2019). ”

Page 11, line 21:

“The MS spectra of generated species from different NOx level and RH conditions, which show evidence for the OH-furan reaction, are presented in Fig. 7 and Fig. 8, respectively. The major peaks are m/z^+ 85.0018, 101.0894, and 185.0504 in the positive ion mode, and m/z^- 146.0161, 225.0125 and 263.0132 in the negative ion mode. The prominent peaks in the HR-MS spectra detected on negative ion mode are comprised of various functionalized hydroxyl nitrates and dihydroxyl dinitrates. However, in the positive ion mode analysis, most carbonyl components were detected.

The assignments of these ion peaks, the molecular weights of the products observed, and proposed structures are summarized in Table 3. These detected compounds provide additional evidence for the proposed radical reaction mechanism.”

Page 12, line 4:

“(i) decompose and then react with O_2 to yield a 1,4-aldoester (A). (ii) react with $NO_2/NO/O_2$ to form hydroxyl nitrate compound isomers with m/z^- 146, or (iii) react with O_2 to form unsaturated products and hydroxyfuranone (B) and 1,4-aldoacid (C). The ring-opened alkylperoxy radical generated from (d) can decompose to generate an unsaturated 1,4-dialdehyde (D). The formation of 1,4-dialdehyde with m/z^+ 85 detected in the positive ion mode suggests that these unsaturated 1,4-dicarbonyls are formed after initial OH addition at 2- or 5-positions. We note that OH radical addition at 2, 3-positions would lead to carbonyl product isomers with same m/z^+ 101. In addition, some dihydroxyl dinitrates with m/z^- 225 were also detected in negative ion mode. However, pathways favouring the generation of these dihydroxyl dinitrates could only take place under high NOx levels. Scheme 1 shows the formation of second-generation products hemiacetals (E) via the reactions of the hydroxyfuranone (B) with 1,4-dialdehyde (D). After uptake from the gas-phase, the combination of hydroxyfuranone with 4-dialdehyde appeared to occur by H-abstraction, followed by dehydration, thus forming m/z^+ 185 compounds. This reaction pathway has also been identified in previous studies of OH-initiated reactions of furans (Strollo and Ziemann, 2013; Aschmann et al., 2014). According to the results of HR-MS, this aqueous phase reaction is more favoured in aqueous particles.”

Page 13, line 4:

“In the present study, an increasing trend of SOA formation was observed with the increase of NOx concentration. As shown in the HESI-Q Exactive Orbitrap-MS results, all the detected primary products are carbonyl-rich, and even the organonitrates have at least two carbonyl functional groups. These carbonyl-containing products have lower volatility and contribute to the SOA formation. The peak intensities in the MS of the products (*m/z*$^+$ 85, 101) generated by the pathways involving HO_2 (as indicated by the scheme 1) decreased with the increase of NOx concentration. Additionally, more products of dihydroxyl dinitrates (*m/z*$^-$ 225) with multifunctional groups were detected under high NOx conditions. As shown in Scheme 1, the multifunctional organonitrates detected in negative ion mode are produced mostly from later-generation chemistry. Hydroxyl nitrates with *m/z*$^-$ 149 can be formed through pathways 1-a, 2-a, and 3-a by the reaction of RO_2 with NOx. We note that the *m/z*$^-$ 149 compound was detected both at low NOx levels and high NOx levels. However, the peak intensity of this product was decreased with increasing NOx concentration. This phenomenon might be caused by the later-reaction of the unsaturated hydroxyl nitrates going through a second OH-initiated reaction and leading to the formation of the dihydroxyl dinitrate with *m/z*$^-$ 225. In addition, the peak intensities changes of SOA products detected in the positive mode, such as, the peaks at *m/z*$^+$ 85 and 101 were reduced under high NOx conditions, which resulted from the fact that the RO_2 radical fate was dominated by the pathway of RO_2+NO or RO_2+NO_2. This result supports that the fate of RO_2 is not a single channel reaction. There exists a competition between RO_2 reacting with NOx and with HO_2 under high NOx conditions but the former pathway is more favourable. There are two pathways for hydroxyl nitrates formation from RO_2 radicals in the presence of NOx according to which RO_2 radicals may react with NO and NO_2 to form $RONO_2$ and $ROONO_2$, respectively (Kroll and Seinfeld, 2008). However, the formed peroxynitrates could easily thermally dissociate and convert to $RONO_2$.

Furthermore, by analyzing the OH concentration and products components, we conclude that there are two possible explanations for the increasing trend of SOA yield as the NOx level increases: (i) the SOA production is closely related to the oxidation capacity in the photooxidation experiments. Experiments conducted under different NOx levels indicate that the OH concentration is controlled by the NOx level if there is no additional OH precursor added before the start of the experiment. As shown in Fig. S3, an increase in NOx level results in more OH generation and a faster furan decay rate. This justifies the observed higher SOA mass concentration and higher SOA yield. (ii) HRMS fragments associated with multifunctional organonitrates are enhanced under high NOx conditions (Fig. 7). As presented in Scheme 1, the furan dihydroxyl dinitrates are generated from the first-generation hydroxyl nitrate reacting with OH to form a peroxy radical, which reacts thereafter with NO. Together with multifunctional hydroxyl nitrates, these low-volatility species can easily partition into the particle phase and increase the SOA mass concentration. More importantly, the seed particle added initially plays an important role in the processes of gas-particle partitioning as indicated by a recent study, which showed that sufficient seed surface area at the start of the reaction largely suppressed the effects of vapour wall losses of low-volatility compounds (Schwantes et al., 2019). Therefore, the NaCl seed particle added in the present work promoted the partitioning of the formed low-volatility functional organonitrates."

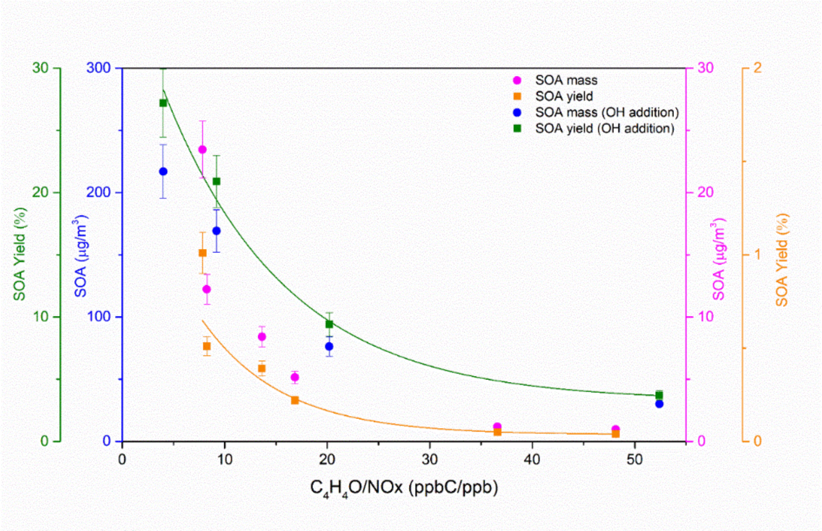

Figure 3: Dependence of the SOA mass concentration and SOA yield on the C_4H_4O/NOx ratio. Since the particle wall loss has a weak RH dependence in our chamber, a mean value of 3.6×10^{-5} s^{-1} was used for wall loss correction. A density of 1.4 g cm^{-3} was used in SMPS (Jia and Xu, 2018; Kostenidou et al., 2007).

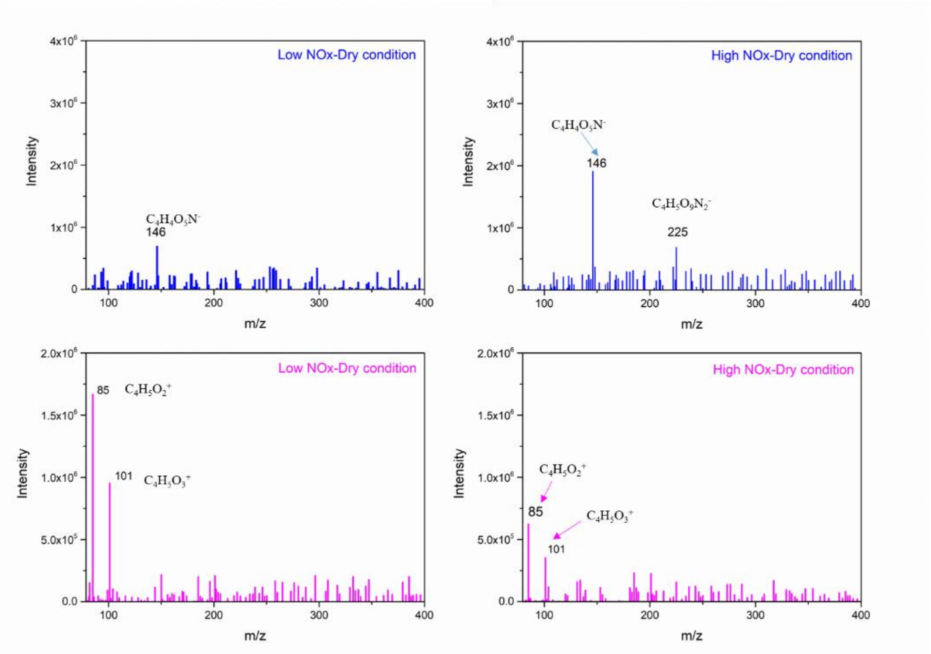

Figure 7: Selected background-subtraction HESI-Q Exactive-Orbitrap MS results of SOA in both negative (blue) and positive (pink) ion modes from the photooxidation of furan under different RH conditions.

Table S1. Summary of experimental conditions with the additional injection of H_2O_2 in the study of the NOx effect on SOA formaiton.

No.	[furan]$_0$ (ppb)	[H_2O_2]$_0$ (ppm)	[NOx]$_0$ (ppb)	RH (%)	C_4H_4O/NOx (ppbC/ppb)	SOA^e (μg m^{-3})	SOA yield (%)
13	802	1.7	15.3	< 10	52.4	30.1	3.7
14	811	1.6	40.2	< 10	20.2	76.3	9.4
15	807	1.7	87.5	< 10	9.2	169.2	20.9
16	797	1.7	200.1	< 10	4.0	216.9	27.2

Table S2. Summary of experimental conditions for HESI-Q Exactive-Orbitrap MS detection.

No.	$[furan]_0$ (ppb)	$[H_2O_2]_0$ (ppm)	$[NOx]_0$ (ppb)	RH (%)	C_4H_4O/NOx (ppbC/ppb)	Aim
17	723.5	3.5	26.4	<5	36.3	for HESI-Q Exactive-Orbitrap MS
18	748.3	6.5	152.6	<5	5.8	
19	764.8	7.2	163.5	30	5.9	
20	755.1	7.3	149.8	62	5.9	

4. The discussion of the RH effect on SOA using the mass spectral data was very vague. The authors only discussed two ions, m/z 187 and m/z 255. First, it seems the m/z 187 ion is C4H4O4Cl2 from high-resolution fitting. But how is it formed? The authors proposed Cl adduct for the major ions m/z 187, 255, and 281. It is probabaly the case for m/z 255 and 281, since they contain nitrogen and have only one Cl on the ion. But m/z 187 is probably not. The C4H4O4 compound does not exist in Scheme 1. The compound D is C4H4O3. How does it form C4H4O4 in the mechanism? Further, for the m/z 255 ion, the formulas provided in Figure 6 is incorrect. [C4H4O4]35Cl2- has an exact mass of 185.949; [C4HO9N2]35Cl- has an exact mass of 255.938; [C8H8O8N]35Cl- has an exact mass of 280.994. The authors need to make sure the chemical formula assignments are correct before discussing the mechanism.

Author reply:

We thank the Referee for the thoughtful comments. According to the revised MS results, the chemical formulae have been reassigned in the revised manuscript. The discussion part, supporting figures and chemical mechanism have been shown in our reply to Comment 2.

Minor and technical comments:

1. Abstract: The abstract should deliver the most important scientific findings. It is unnecessary to describe how the measurements were performed in the abstract (e.g., how particle mass concentration and size distribution were determined). Additionally, "the SOA mass concentration and yield increase with increasing humidity, because higher aerosol liquid water content brings more aqueous phase reactions" does not make sense. More aqueous phase reactions do not mean higher product yield.

Author reply:

We thank the referee for this suggestion. The abstract has been rewritten in the revised manuscript:

"Atmospheric furan is a primary and secondary pollutant in the atmosphere, and its emission contributes to the formation of ultrafine particles. We investigate the effects of NOx level and humidity on the formation of secondary organic aerosol (SOA) generated from the photooxidation of furan in the presence of NaCl seed particles. SOA mass concentration and yield were determined under different NOx and humidity levels. A significant difference is observed both in the variation of SOA mass concentration and SOA yield with the initial experimental conditions. Varying VOC/NOx ratios over the range 48.1 to 8.2 contributes to the effective formation of SOA in the presence of NaCl seed particles, with the SOA mass concentration and SOA yield ranging from 0.96 μg m^{-3} to 23.46 μg m^{-3} and from 0.04 % to 1.01 %, respectively. We found that there was a favourable relationship between the SOA yield and NOx concentration. Especially, the increase of SOA yield with increasing NOx concentration was continuously observed at high NOx levels owing to a corresponding increase of the amount of low-volatility hydroxyl nitrates and dihydroxyl dinitrates that can partition into particle phase. In addition, varying RH from 5% to 88% increased the SOA yield from 1.01% to 5.03%. The enhanced SOA formation from humid conditions may result from the high OH concentration, rapid furan decay rate, enhanced carbonyl-rich products condensation, and the aqueous-phase reactions. Using hybrid quadrupole-orbitrap mass spectrometer equipped with electrospray ionization (HESI-Q Exactive-Orbitrap MS), three carbonyl-rich products and three kinds of organonitrates were identified in the collected SOA. Based on the MS analysis and FTIR spectra, the reaction mechanism of furan photooxidation was proposed. This study demonstrates the effects of NOx and humidity on SOA formation during the furan-NOx-NaCl photooxidation, and provides new insights into the oxidation regime and SOA composition in furan photooxidation. The results also illustrate the importance of studying SOA formation over a comprehensive range of environmental conditions. Only such evaluations can induce meaningful SOA mechanisms to be implemented in air quality models."

2. Second sentence in the introduction puts different categories together. Remove black carbon and brown carbon.

Author reply:

We have now removed this part accordingly.

3. Page 2, line 1. Change volatile organic compound to VOC.

Author reply:

This has been changed.

4. In the introduction, some statements about cited studies are incorrect. For example, page 2, line 3-4, the Chan et al. (2010) study demonstrated that isoprene SOA formed under high NO2/NO is large, not under high-NOx conditions; the Zhang et al. (2012) as well as the Zhang et al. 2011 studies show different compositions under dry and wet conditions.

Author reply:

We have revised this part accordingly as:

Page 3, line 8

Another study of the SOA formation from the irradiation of propylene showed that the SOA yield decreased with increasing propylene/NOx ratio (Ge et al., 2017b)."

Page 3, line 12

"A study focusing on the photooxidation of toluene and m-xylene has demonstrated that aerosol yields decrease as NOx level increases (Xu et al., 2015), while another study showed that the SOA yield from photooxidation of isoprene under high NO_2/NO is 3 times more important than that measured under low NO_2/NO level (Chan et al., 2010)."

5. Page 10, line 10. What is C4H4O4Cl? Does the authors have a prediction of the possible structure? How does the NaCl interacts with the organic components in SOA to form this species? On page 11, line 24, some discussion was made, but it is still unclear how "Cl adduction of SOA product" happens.

Author reply:

According to the latest results that sufficiently eliminate the interference of artifacts, the Cl-containing products have not been detected, which indicates that there were no Cl adduction reactions happening.

6. Page 10, line 13. The carboxylic acids may not generate enough acidity to catalyze reactions as the authors mentioned, unless the authors could provide evidence.

Author reply:

We have removed this speculation from the revised manuscript.

7. Page 12, line 28. The authors said “it is highly probable that the particle surface area increases with the amount of ALW increasing”. Could the SMPS measurements provide quantitative evidence?

Author reply:

We agree with the Referee’s suggestions that the SMPS measurements could provide quantitative evidence. We have compared the surface particle sizes under different RH conditions and found that the particle surface area increases as the amount of ALW increases. To make the conclusion more persuasive, we have added the following figure in the revised version.

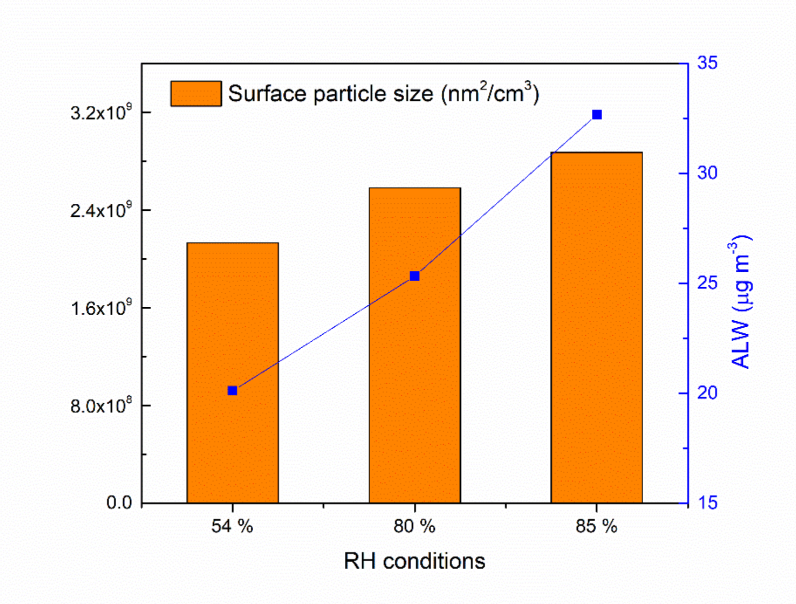

Figure S7: Variations of surface particle sizes and ALW under different experimental RH conditions.

8. Page 13, line 4. Under high RH, the acidity, if any, is likely lower due to water dilution.

Author reply:

The “acid catalyzed reactions” is now removed in the revised manuscript.

References

Aschmann, S. M., Nishino, N., Arey, J., and Atkinson, R.: Products of the OH radical initiated reactions of furan, 2-and 3-methylfuran, and 2,3-and 2,5-dimethylfuran in the presence of NO, J. Phys. Chem. A, 118, 457-466, 10.1021/jp410345k, 2014.

Chan, A. W. H., Chan, M. N., Surratt, J. D., Chhabra, P. S., Loza, C. L., Crounse, J. D., Yee, L. D., Flagan, R. C., Wennberg, P. O., and Seinfeld, J. H.: Role of aldehyde chemistry and NOx concentrations in secondary organic aerosol formation, Atmos. Chem. Phys., 10, 7169-7188, 10.5194/acp-10-7169-2010, 2010.

Hildebrandt, L., Donahue, N. M., and Pandis, S. N.: High formation of secondary organic aerosol from the photo-oxidation of toluene, Atmos. Chem. Phys., 9, 2973-2986, 10.5194/acp-9-2973-2009, 2009.

Hoyle, C. R., Boy, M., Donahue, N. M., Fry, J. L., Glasius, M., Guenther, A., Hallar, A. G., Hartz, K. H., Petters, M. D., Petaja, T., Rosenoern, T., and Sullivan, A. P.: A review of the anthropogenic influence on biogenic secondary organic aerosol, Atmos. Chem. Phys., 11, 321-343, 10.5194/acp-11-321-2011, 2011.

Jia, L., and Xu, Y.: Different roles of water in secondary organic aerosol formation from toluene and isoprene, Atmos. Chem. Phys., 18, 8137-8154, 10.5194/acp-18-8137-2018, 2018.

Kamens, R. M., Zhang, H., Chen, E. H., Zhou, Y., Parikh, H. M., Wilson, R. L., Galloway, K. E., and Rosen, E. P.: Secondary organic aerosol formation from toluene in an atmospheric hydrocarbon mixture: Water and particle seed effects, Atmos. Environ., 45, 2324-2334, 10.1016/j.atmosenv.2010.11.007, 2011.

Kostenidou, E., Pathak, R. K., and Pandis, S. N.: An algorithm for the calculation of secondary organic aerosol density combining AMS and SMPS data, Aerosol Sci. Tech., 41, 1002-1010, 10.1080/02786820701666270, 2007.

Kroll, J. H., and Seinfeld, J. H.: Chemistry of secondary organic aerosol: Formation and evolution of low-volatility organics in the atmosphere, Atmos. Environ., 42, 3593-3624, 10.1016/j.atmosenv.2008.01.003, 2008.

Liu, C., Liu, J., Liu, Y., Chen, T., and He, H.: Secondary organic aerosol formation from the OH-initiated oxidation of guaiacol under different experimental conditions, Atmos. Environ., 207, 30-37, 10.1016/j.atmosenv.2019.03.021, 2019.

Loza, C. L., Craven, J. S., Yee, L. D., Coggon, M. M., Schwantes, R. H., Shiraiwa, M., Zhang, X., Schilling, K. A., Ng, N. L., Canagaratna, M. R., Ziemann, P. J., Flagan, R. C., and Seinfeld, J. H.: Secondary organic aerosol yields of 12-carbon alkanes, Atmos. Chem. Phys., 14, 1423-1439, 10.5194/acp-14-1423-2014, 2014.

Ng, N. L., Kroll, J. H., Chan, A. W. H., Chhabra, P. S., Flagan, R. C., and Seinfeld, J. H.: Secondary organic aerosol formation from m-xylene, toluene, and benzene, Atmos. Chem. Phys., 7, 3909-3922, 10.5194/acp-7-3909-2007, 2007.

Perri, M. J., Lim, Y. B., Seitzinger, S. P., and Turpin, B. J.: Organosulfates from glycolaldehyde in aqueous aerosols and clouds: Laboratory studies, Atmos. Environ., 44, 2658-2664, 10.1016/j.atmosenv.2010.03.031, 2010.

Rissanen, M. P.: NO2 Suppression of Autoxidation-Inhibition of Gas-Phase Highly Oxidized Dimer Product Formation, Acs Earth and Space Chemistry, 2, 1211-1219, 10.1021/acsearthspacechem.8b00123, 2018.

Sarrafzadeh, M., Wildt, J., Pullinen, I., Springer, M., Kleist, E., Tillmann, R., Schmitt, S. H., Wu, C., Mentel, T. F., and Zhao, D.: Impact of NOx and OH on secondary organic aerosol formation from β-pinene photooxidation, Atmos. Chem. Phys., 16, 11237-11248, 10.5194/acp-16-11237-2016, 2016a.

Sarrafzadeh, M., Wildt, J., Pullinen, I., Springer, M., Kleist, E., Tillmann, R., Schmitt, S. H., Wu, C., Mentel, T. F., Zhao, D., Hastie, D. R., and Kiendler-Scharr, A.: Impact of NOx and OH on secondary organic aerosol formation from beta-pinene photooxidation, Atmos. Chem. Phys., 16, 11237-11248, 10.5194/acp-16-11237-2016, 2016b.

Schwantes, R. H., Charan, S. M., Bates, K. H., Huang, Y., Nguyen, T. B., Mai, H., Kong, W., Flagan, R. C., and Seinfeld, J. H.: Low-volatility compounds contribute significantly to isoprene secondary organic aerosol (SOA) under high-NOx conditions, Atmos. Chem. Phys., 19, 7255-7278, 10.5194/acp-19-7255-2019, 2019.

Song, C., Na, K. S., and Cocker, D. R.: Impact of the hydrocarbon to NOx ratio on secondary organic aerosol formation, Environ. Sci. Technol., 39, 3143-3149, 10.1021/es0493244, 2005.

Strollo, C. M., and Ziemann, P. J.: Products and mechanism of secondary organic aerosol formation from the reaction of 3-methylfuran with OH radicals in the presence of NOx, Atmos. Environ., 77, 534-543, 10.1016/j.atmosenv.2013.05.033, 2013.

Wang, Y., Luo, H., Jia, L., and Ge, S.: Effect of particle water on ozone and secondary organic aerosol formation from benzene-NO_2-NaCl irradiations, Atmos. Environ., 140, 386-394, 10.1016/j.atmosenv.2016.06.022, 2016.

Zhou, Y., Zhang, H., Parikh, H. M., Chen, E. H., Rattanavaraha, W., Rosen, E. P., Wang, W., and Kamens, R. M.: Secondary organic aerosol formation from xylenes and mixtures of toluene and xylenes in an atmospheric urban hydrocarbon mixture: Water and particle seed effects (II), Atmos. Environ., 45, 3882-3890, 10.1016/j.atmosenv.2010.12.048, 2011.

We thank the Referee for the very insightful comments. We have revised our manuscript according to the suggestions of the Referee's comments and our responses to the comments are as follows. Referee's comments are in black, authors' responses are in blue, and changes to the manuscript are in red color text.

This paper presents results from a series of simulation chamber experiments on the formation of secondary organic aerosol (SOA) from the photooxidation of furan. SOA yield was found to vary with both VOC/NOx ratio and relative humidity. Some information on the chemical composition of the SOA is presented, along with possible chemical mechanisms for the generation of several of the identified species. The experiments appear to have been conducted appropriately, however there are some aspects of the data interpretation that need to be clarified and/or improved prior to publication.

1. The effect of relative humidity in increasing SOA yield seems to be very similar to that reported for p-xylene by Healy et al. (2009), who proposed that the increase in relative humidity results in higher levels of HONO formation in the chamber which leads to increased OH concentration, a faster p-xylene decay rate, and higher aerosol mass yields. Could the same effect be happening here? Was there a change in the rate of decay of furan as the relative humidity was increased through experiments 6-12?

Author reply:

According to the Referee's suggestions, we have added a figure of relationships between relative humidity and OH concentration as well as the degradation profile of furan under different RH conditions. The effects of RH conditions on OH concentration and SOA formation found in the present study are similar to those reported by Healy et al. An increasing trend of OH concentration and a faster decay rate of furan were observed as RH increased, as shown in Fig. S3. It is possible that the faster rate of gas phase oxidation under higher OH concentrations would lead to the generation of less volatile compounds as presented previously (Chan et al., 2007). This part has been revised on page 9 and page 13.

Page 9, line 28:

“It is worth note that under high RH conditions, as shown in Fig. 1, the NO_2 hydrolysis (reaction (R11)) can generate nitrous acid (HONO), which has been considered as a major source of OH. As indicated in Fig. 4, the SOA yields obtained in the present work clearly show a gradual increase with RH. Also shown in Fig. S3 is the dependence of OH and furan concentrations on RH during the experiments determined from the decay of furan using a reaction rate coefficient of k(OH+furan) = 4.01×10^{-11} cm^3 $molecules^{-1}$ s^{-1} (Atkinson et al., 1983). It is therefore probable that the increase of RH results in high levels of HONO formation in the chamber, which leads to an increase in OH concentration, a faster furan decay rate, and higher aerosol mass yields. This result is in reasonable good agreement with previous studies, which proposed that the amount of products that can partition into the particle phase increases with the increasing rate of hydrocarbon oxidation (Healy et al., 2009; Chan et al., 2007). Moreover, the increasing RH might also enhance the SOA formation due to the fact that the functionalized gas phase components were more favoured to condense on the surface of wet particles (Liu et al., 2019). ”

Page 14, line 8:

“As shown in Fig. S3, an increase in RH leads to higher OH concentrations resulting from higher HONO levels generated by the reaction of NO_2 with H_2O. Previously, Anglada et al. confirmed, using quantum mechanical calculations, that the water component could increase the OH production (Anglada et al., 2011). The positive correlation between initial water vapour concentration and OH concentration has also been previously observed experimentally (Healy et al., 2009; Tillmann et al., 2010). Additionally, Healy et al. have also reported that increasing OH concentration promoted the decay of VOC and enhanced SOA formation (Healy et al., 2009). Similarly, in the present work, a faster decay rate of furan was also observed as RH increased, as shown in Fig. S3. It is possible that the faster rate of gas phase oxidation under higher OH concentrations will lead to the generation of less volatile compounds as presented previously (Chan et al., 2007). A higher OH concentration promotes oxidation reactions, influences the distribution of organic products, and facilitates the SOA formation (Sarrafzadeh et al., 2016)."

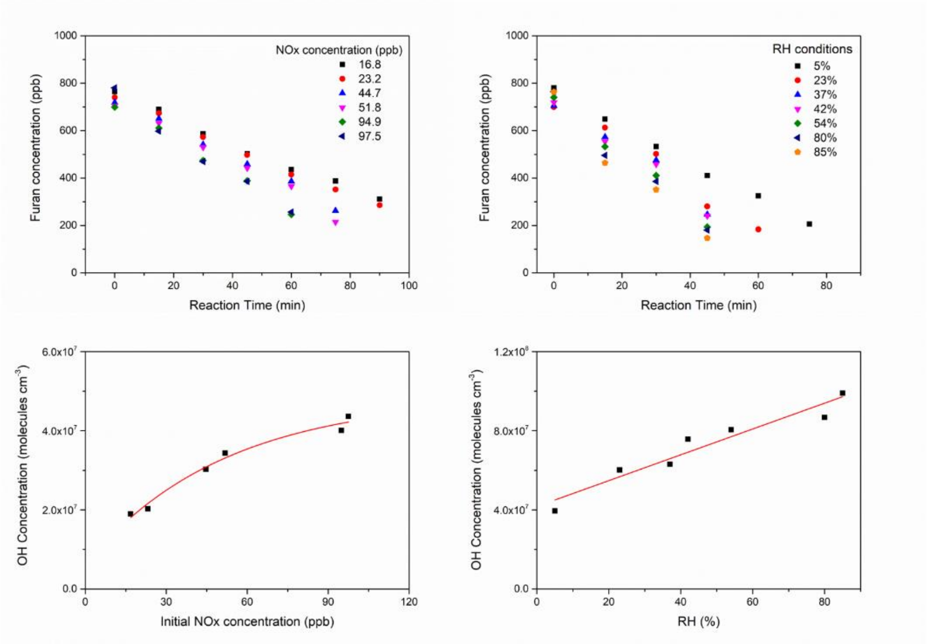

Figure S3: Relationship between relative NOx concentrations, humidity, and steady OH concentration in the furan photooxidation experiments performed under different NOx levels and RH conditions. The OH concentration was calculated based on $[OH]= \ln\frac{[furan]_0}{[furan]_t}/kt$, k=4.01× 10^{-11} cm^3 $molecules^{-1}$ s^{-1} (Atkinson et al., 1983).

2. A similar kinetic effect may also be occurring in experiments 1-5 where the VOC/NOx ratio was varied. Nitrous acid (HONO) is the main source of OH produced by heterogeneous reaction of nitrogen dioxide with water at the walls of the reactor. When NOx is increased, it is mainly in the form of NO2 and this may result in more OH formation, faster furan oxidation and more SOA formation. The authors should check the rate of furan decay in this subset of experiments and report/interpret accordingly.

Author reply:

As suggested by the Referee, the relationship between NOx level and OH concentration as well as the degradation profile of furan have been added in Fig. S3. Experiments conducted under different NOx levels indicate that the OH concentration was controlled by the NOx level if there were no additional OH precursors added before the experiment. As shown in Fig. S3, the OH concentration exhibits a gradual increase with the increase of NOx concentration and there appears to be a correlation between NOx concentration, OH concentration and SOA yield. Therefore, the increase of SOA yield was attributed to an increase of OH concentration, which was affected by OH recycling (reaction (R6), Fig. 1) and thus contributed to the enhancement of SOA formation.

Page 9, line 8:

"the concentration of OH radicals produced *in situ* in the present study before additional source of OH was insufficient to produce a considerable amount of SOA under low-NOx conditions. As shown in Fig. S3, the OH concentration exhibits a gradual increase with NOx concentration and there appears to be a correlation between NOx concentration, OH concentration and SOA yield. Therefore, at low-NOx conditions, the increase of SOA yield was attributed to an increase of OH concentration, which was affected by OH recycling following reaction (R6) (see Fig. 1) and contributed to the enhancement of SOA formation. This result is consistent with a previous study concerning the impact of NOx and OH on SOA formation from β-pinene photooxidation, which has proved that the positive correlation between SOA yield and NOx levels ($[VOC]_0/[NOx]_0 > 10$ ppbC/ppb) was caused by the NOx–induced increase of OH concentration (Sarrafzadeh et al., 2016b)."

Page 13, line 24:

"Experiments conducted under different NOx levels indicate that the OH concentration is controlled by the NOx level if there is no additional OH precursor added before the start of the experiment. As shown in Fig. S3, an increase in NOx level results in more OH generation and a faster furan decay rate. This justifies the observed higher SOA mass concentration and higher SOA yield."

Minor Comments:

1. The abstract is written in a generic manner and should be re-written to contain information specific to this work. For example, it is stated that the reaction conditions affected SOA yields. But it should state something like "varying VOC/NOx ratios over the range 48 to 8 cause SOA yields to increase from 0.04% to 0.5% under dry conditions". Some similar statements should be used to report the influence of relative humidity.

Author reply:

We thank the Referee for this suggestion. We have re-written this section as:

"Atmospheric furan is a primary and secondary pollutant in the atmosphere, and its emission contributes to the formation of ultrafine particles. We investigate the effects of NOx level and humidity on the formation of secondary organic aerosol (SOA) generated from the photooxidation of furan in the presence of NaCl seed particles. SOA mass concentration and yield were determined under different NOx and humidity levels. A significant difference is observed both in the variation of SOA mass concentration and SOA yield with the initial experimental conditions. Varying VOC/NOx ratios over the range 48.1 to 8.2 contributes to the effective formation of SOA in the presence of NaCl seed particles, with the SOA mass concentration and SOA yield ranging from 0.96 μg m^{-3} to 23.46 μg m^{-3} and from 0.04 % to 1.01 %, respectively. We found that there was a favourable relationship between the SOA yields and NOx concentration. Especially, the increase of SOA yield with increasing NOx concentration was continuously observed at high NOx levels owing to a corresponding increase of the amount of low-volatility hydroxyl nitrates and dihydroxyl dinitrates that can partition into particle phase. In addition, varying RH from 5% to 88% increased the SOA yield from 1.01% to 5.03%. The enhanced SOA formation from humid conditions may result from the high OH concentration, rapid furan decay rate, enhanced carbonyl-rich products condensation, and the aqueous-phase reactions. Using hybrid quadrupole-orbitrap mass spectrometer equipped with electrospray ionization (HESI-Q Exactive-Orbitrap MS), three carbonyl-rich products and three kinds of organonitrates were identified in the collected SOA. Based on the MS analysis and FTIR spectra, the reaction mechanism of furan photooxidation was proposed. This study demonstrates the effects of NOx and humidity on SOA formation during the furan-NOx-NaCl photooxidation, and provides new insights into the oxidation regime and SOA composition in furan photooxidation. The results also illustrate the importance of studying SOA formation over a comprehensive range of environmental conditions. Only such evaluations can induce meaningful SOA mechanisms to be implemented in air quality models."

2. On page 2 (line 27), it is mentioned that several studies have previously investigated SOA formation from furan, but they appear to focus only on kinetic and mechanistic aspects.

Author reply:

We have revised this sentence as follows:

"Although the determination of kinetics and products of furan oxidation has been performed (Cabanas et al., 2004; Liljegren and Stevens, 2013; Tapia et al., 2011), the influence of several factors including NOx level and relative humidity on SOA formation from furan has not been well examined."

3. On page 3 (line 26), it is mentioned that sea salt particles are the second most abundant particles in the atmosphere. This statement is seemingly used to justify the use of NaCl as seed particles, while it is more common to use ammonium sulfate as seeds in SOA formation experiments. Given that furan is a product of biomass burning and is also more likely to be released in urban environments than marine

environments, the use of NaCl as seeds seems rather odd. The authors should provide some more reasons why NaCl particles were used as seeds.

Author reply:

We agree that ammonium sulfate is more commonly used as seeds in smog chamber simulations compared to NaCl. But concerning the strong absorption of ammonium sulfate in mid-infrared region, the addition of ammonium sulfate would interfere the assignment of the functional groups in the FTIR spectra. Specifically, the following figure shows the characteristic peaks of ammonium sulfate: the stretching modes of the SO_4^{2-} ion are at 1089 and 975 cm^{-1}; the broad band between 3400 and 2800 cm^{-1} is assigned to NH_4^+ stretching. However, NaCl does not have the absorption band in mid-infrared region. Consequently, we decided to choose NaCl as seeds in the present experiment. To remove any confusion regarding the use of NaCl seed particles, the statement has been modified as:

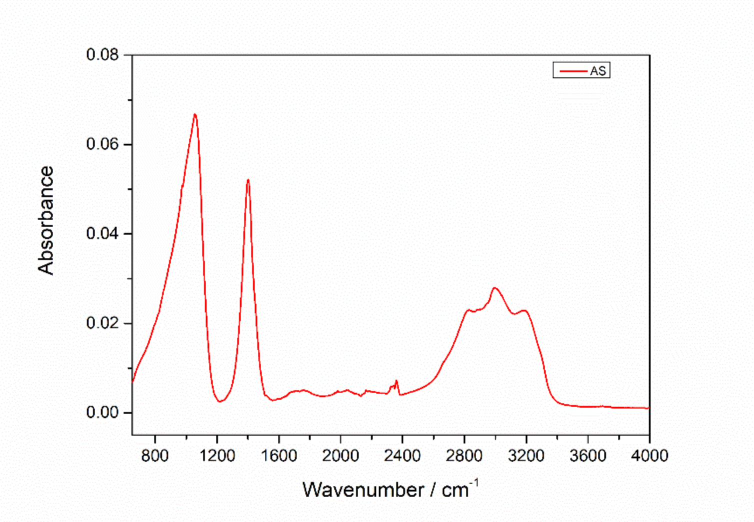

"All the experiments were conducted in the presence of NaCl seed particles, which acted as the nuclei and provided sufficient seed surface area at the beginning of the reaction to suppress the effects of vapour wall losses of semi/low-volatility species."

References

Anglada, J. M., Gonzalez, J., and Torrent-Sucarrat, M.: Effects of the substituents on the reactivity of carbonyl oxides. A theoretical study on the reaction of substituted carbonyl oxides with water, Phys. Chem. Chem. Phys., 13, 13034-13045, 10.1039/c1cp20872a, 2011.

Atkinson, R., Aschmann, S. M., and Carter, W. P.: Kinetics of the reactions of O_3 and OH radicals with furan and thiophene at 298±2 K, Int. J. Chem. Kinet., 15, 51-61, 0.1002/kin.550150106, 1983.

Chan, A. W. H., Kroll, J. H., Ng, N. L., and Seinfeld, J. H.: Kinetic modeling of secondary organic aerosol formation: Effects of particle- and gas-phase reactions of semivolatile products, Atmos. Chem. Phys., 7, 4135-4147, 10.5194/acp-7-4135-2007, 2007.

Healy, R. M., Temime, B., Kuprovskyte, K., and Wenger, J. C.: Effect of relative humidity on gas/particle partitioning and aerosol mass yield in the photooxidation of p-Xylene, Environ. Sci. Technol., 43, 1884-1889, 10.1021/es802404z, 2009.

Liu, S., Tsona, N. T., Zhang, Q., Jia, L., Xu, Y., and Du, L.: Influence of relative humidity on cyclohexene SOA formation from OH photooxidation, Chemosphere, 231, 478-486, 10.1016/j.chemosphere.2019.05.131, 2019.

Sarrafzadeh, M., Wildt, J., Pullinen, I., Springer, M., Kleist, E., Tillmann, R., Schmitt, S. H., Wu, C., Mentel, T. F., Zhao, D., Hastie, D. R., and Kiendler-Scharr, A.: Impact of NOx and OH on secondary organic aerosol formation from beta-pinene photooxidation, Atmos. Chem. Phys., 16, 11237-11248, 10.5194/acp-16-11237-2016, 2016.

Tillmann, R., Hallquist, M., Jonsson, A. M., Kiendler-Scharr, A., Saathoff, H., Iinuma, Y., and Mentel, T. F.: Influence of relative humidity and temperature on the production of pinonaldehyde and OH radicals from the ozonolysis of alpha-pinene, Atmos. Chem. Phys., 10, 7057-7072, 10.5194/acp-10-7057-2010, 2010.

Secondary organic aerosol formation from photooxidation of furan: effects of NOx and humidity

Xiaotong Jiang[1], Narcisse T. Tsona[1], Long Jia[2], Shijie Liu[1], Hailiang Zhang[2], Yongfu Xu[2], Lin Du[1,*]

[1] Environment Research Institute, Shandong University, Qingdao, 266237, China
[2] State Key Laboratory of Atmospheric Boundary Layer Physics and Atmospheric Chemistry, Institute of Atmospheric Physics, Chinese Academy of Sciences, Beijing, 100029, China

Correspondence to: Lin Du (lindu@sdu.edu.cn)

Abstract. Atmospheric furan is a primary and secondary pollutant in the atmosphere, and its emission contributes to the formation of ultrafine particles. We investigate the effects of NOx level and humidity on the formation of secondary organic aerosol (SOA) generated from the photooxidation of furan in the presence of NaCl seed particles. SOA mass concentration and yield were determined under different NOx and humidity levels. A significant difference is observed both in the variation of SOA mass concentration and SOA yield with the initial experimental conditions. Varying VOC/NOx ratios over the range 48.1 to 8.2 contributes to the effective formation of SOA in the presence of NaCl seed particles, with the SOA mass concentration and SOA yield ranging from 0.96 μg m^{-3} to 23.46 μg m^{-3} and from 0.04 % to 1.01 %, respectively. We found that there was a favourable relationship between the SOA yields and NOx concentration. Especially, the increase of SOA yield with increasing NOx concentration was continuously observed at high NOx levels owing to a corresponding increase of the amount of low-volatility hydroxyl nitrates and dihydroxyl dinitrates that can partition into particle phase. In addition, varying RH from 5% to 88% increased the SOA yield from 1.01% to 5.03%. The enhanced SOA formation from humid conditions may result from the high OH concentration, rapid furan decay rate, enhanced carbonyl-rich products condensation, and the aqueous-phase reactions. Using hybrid quadrupole-orbitrap mass spectrometer equipped with electrospray ionization (HESI-Q Exactive-Orbitrap MS), three carbonyl-rich products and three kinds of organonitrates were identified in the collected SOA. Based on the MS analysis and FTIR spectra, the reaction mechanism of furan photooxidation was proposed. This study demonstrates the effects of NOx and humidity on SOA formation during the furan-NOx-NaCl photooxidation, and provides new insights into the oxidation regime and SOA composition in furan photooxidation. The results also illustrate the importance of studying SOA formation over a comprehensive range of environmental conditions. Only such evaluations can induce meaningful SOA mechanisms to be implemented in air quality models.

1 Introduction

Atmospheric particulate matter (PM) is primarily composed of organic carbon, elemental carbon, sulfate, nitrate, and other components (Donahue et al., 2009; Zhang et al., 2011), which has adverse effects on human health and global climate forcing (Hallquist et al., 2009; Pope et al., 2013). Secondary organic aerosols (SOA) constitute a substantial portion of the total ambient aerosol particles, which mainly originate from biomass burning and atmospheric reactions of volatile organic compounds (VOCs) (Kanakidou et al., 2005). Identifying the chemical composition and major precursors of SOA is helpful to better understand their formation mechanism and strategies for the control of PM. Furan is an important five-member heteroatom-containing VOC present in the atmosphere and it can be produced by wood combustion, oil refining, coal mining and gasification, and pyrolysis of biomass, cellulose, and lignin (Shafizadeh, 1982). As shown in previous studies, furan is one of the most common products of the thermal cracking of biomass (Kahan et al., 2013; Gilman et al., 2015). Both furan and furan-related compounds have been detected in the effluent from initial smouldering of fuels, oats and soft pellets (Olsson, 2006; Perzon, 2010). In addition, furan has been identified as one of the major compounds emitted from the combustion of Ponderosa Pine, which constitute a significant fraction (5-37 % by estimated emission factor) of smoke from combustion (Hatch et al., 2015). Field measurements of hydrocarbon emissions from biomass burning in Brazil have also shown that furans consists of 52% and 72% of the oxygenated hydrocarbons emissions in the cerrado (grasslands) and selva (tropical forest) regions, respectively (Greenberg et al., 1984). Moreover, furan has been proven to be the typical trace gas of roasting/burning activities (Gloess et al., 2014; Coggon et al., 2016; Burling et al., 2010; Gilman et al., 2015; Sarkar et al., 2016; Stockwell et al., 2016; Stockwell et al., 2015; Stockwell et al., 2014), and it is also an important contribution to OH reactivity towards biomass burning emissions (Gilman et al., 2015; Sarkar et al., 2016). Furan is also a secondary pollutant produced in the photooxidation of some conjugate alkenes. Previous product studies of 1,3-butadiene oxidation have shown that furan is one of the dominant product during the OH radical-initiated reactions in the presence of NO (Sprengnether et al., 2002; Tuazon et al., 1999). Furthermore, another source of furan is the cyclization of the unsaturated 1,4-hydroxyaldehydes, which will further go through the dehydration reactions (Baker et al., 2005). There is strong evidence that furan can cause malignant tumor formation in a variety of experimental animals (IARC, 1995). Therefore, a better understanding of the atmospheric transformations of furan will be helpful to improve the air quality models for toxic species.

As an aromatic hydrocarbon, furan is very reactive according to its electrophilic substitution reactions (Villanueva et al., 2007). The measured rate constant of furan with OH radicals, O_3 and NO_3 radicals at room temperature is $(4.01\pm0.30)\times10^{-11}$, $(2.42\pm0.28)\times10^{-18}$ and $(1.4\pm0.2)\times10^{-12}$ cm^3 $molecule^{-1}$ s^{-1}, respectively (Atkinson et al., 1983; Atkinson et al., 1985). If the oxidant concentration of OH and NO_3 are assumed to be 1.6×10^{6} and 5×10^{8} molecule cm^{-3}, lifetimes of furan for reactions with OH and NO_3 are estimated to be 3 h and 18 min, respectively (Cabanas et al., 2004). In the troposphere, atmospheric furan is expected to be mainly oxidized by OH during daytime and NO_3 at night. Although the determination of kinetics and products of furan oxidation has been performed (Cabanas et al., 2004; Liljegren and Stevens, 2013; Tapia et al., 2011), the influence of several factors including NOx level and relative humidity on SOA formation from furan has not been well examined. It is important to assess the SOA formation potential of furan and its role in SOA production in biomass burning plumes. Although the SOA formation potential of furan has been studied in recent years (Cabanas et al., 2004; Liljegren and Stevens, 2013; Tapia et al., 2011), the influence of several factors including NOx levels and relative humidity (RH) on SOA formation should be further investigated. It is generally accepted that NOx level plays a critical role in SOA formation, by governing the reactions of organo-peroxy radicals (RO_2) (Song et al., 2007; Song et al., 2005). The branching ratio of RO_2

reactions with NOx and the hydroperoxyl radical (HO_2) is determined by the NOx level during experiments (Kroll and Seinfeld, 2008). A previous study showed that the mechanisms of the two reactions differ sharply under different NOx level conditions. RO_2 reacts only with NO under high NOx levels and with HO_2 under low NOx conditions (Ng et al., 2007a). The latter case produces lower volatility products than the former one. An increase in SOA yield with increasing NOx was proposed to be due to the formation of low-volatility compounds including multifunctional nitrates and dinitrates, which partitioned to the particle phase and contribute significantly to isoprene SOA under high-NOx conditions (Schwantes et al., 2019). Another study of the SOA formation from the irradiation of propylene also showed that the SOA yield decreased with increasing propylene/NOx ratio (Ge et al., 2017a). Recently, Liu et al. indicated that NO_2 could participate in the OH-initiated reaction of guaiacol, consequently resulting in the formation of organic nitrates and promoting SOA formation (Liu et al., 2019a). The effect of NOx level on SOA formation from aromatic precursors has been investigated previously but the results are inconclusive. A study focusing on the photooxidation of toluene and m-xylene has demonstrated that aerosol yields decrease as NOx level increases (Xu et al., 2015), while another study showed that the SOA yield from photooxidation of isoprene under high NO_2/NO is 3 times more important than that measured under low NO_2/NO level (Chan et al., 2010).

Besides the mixed effect of NOx level on SOA formation, the RH can significantly alter the sizes of SOA particles, depending on their hygroscopicity (Varutbangkul et al., 2006), their gas-phase reactions involving water (Jonsson et al., 2006), and the aqueous chemistry occurring at their surfaces (Lim et al., 2010; Grgic et al., 2010). The photooxidation experiments of aromatic compounds, such as toluene (Edney et al., 2000; Cao and Jang, 2010; Faust et al., 2017; Hinks et al., 2018), benzene and ethylbenzene (Jia and Xu, 2014), m-xylene (Zhou et al., 2011), and 1,3,5-trimethylbenzene (Cocker et al., 2001) have been carried out previously to study the effect of RH on SOA formation. The results exhibited large discrepancies under different experimental conditions. The yield of SOA generated under low-NOx conditions was found to be small at high RH (Cao and Jang, 2010). A little RH effect was also observed on SOA particle formation and size distributions (Bonn and Moortgat, 2002; Fry et al., 2009). Nevertheless, positive correlations between RH and SOA yield have also been observed in the presence of hygroscopic seed particles (Zhou et al., 2011), and the role of RH in SOA formation also appears to be mixed. Water vapour does not only participate in the VOC photooxidation reactions and affect the gas-phase oxidation mechanisms, but also alters the partitioning of the reaction products between the gas-phase and the particle-phase, hereby influencing the equilibrium partitioning of generated organic aerosols (Spittler et al., 2006). Moreover, the RH is connected with SOA formation due to its strong influence on seed acidity and particle liquid water concentration (Mahowald et al., 2011). A high RH environment contributes to the increase of aerosol liquid water (ALW), which promotes the hydrolysis of organic compounds and leads to other heterogeneous and aqueous phase reactions (Ervens et al., 2011). Previous studies regarding the atmospheric reactions of furan typically focused on the kinetics and mechanism (Gomez Alvarez et al., 2009; Aschmann et al., 2014).

In the present study, we used FTIR, in concert with SMPS to elucidate the roles of NOx level and RH in SOA formation from furan-NOx irradiation. All the experiments were conducted in the presence of NaCl seed particles, which acted as the nuclei and provided sufficient seed surface area at the beginning of the reaction to suppress the effects of vapour wall losses of semi/low-volatility species. Specifically, we evaluate whether the increased ALW affects the SOA mass concentration and the SOA yield. The chemical composition of furan SOA was investigated by HESI-Q Exactive-Orbitrap MS, with a focus on the formation of organic nitrates. Strong evidences that both the RH and different NOx levels have a significant effect on SOA formation from furan photooxidation are presented.

2 Experiments

2.1 SOA sample preparation

All experiments were performed in a 1.3 m^3 Teflon FEP film chamber at the Institute of Atmospheric Physics, Chinese Academy of Sciences, Beijing. To maximize and homogenize the interior light intensity, a mirror surface stainless steel was chosen as the interior wall of the enclosure. A total of 42 black-lamps (F40BLB, GE, Fairfield, CT, USA) with emission band centre at 365 nm were equipped in the facilities to simulate the spectrum of the UV band in solar irradiation. The chamber was equipped with multiple sampling ports, which allowed the introduction of clean air, seed aerosols, gas-phase reagents, and for measurements of both gas-phase and particle-phase compositions. The reaction setup used in the present study and the schematic of the smog chamber facility is shown in Fig. S1 (Liu et al., 2017; Jia and Xu, 2014, 2016; Ge et al., 2017b, a).

The zero air (generated from Zero Air Supply, Model 111 and Model 1150, Thermo Scientific) was used as the background gas for the experiments, and three big hydrocarbon traps (BHT-4, Agilent, Santa Clara, CA, USA) coupled with three activated-carbon filters were used to get further purified air. The chamber was cleaned by flowing pure air for at least 4 h prior to each experiment until residual NO, NO_2, O_3 or any other particles could not be detected in the chamber. The prepared gas-phase furan was introduced into the chamber directly by a syringe. A certain amount of NO_2 was injected into the chamber by a gas-tight syringe to achieve the initial NOx level. For the enhancement of the SOA formation, NaCl seed aerosols were injected into the chamber via atomization of NaCl aqueous solution with a constant-rate atomizer (Model 3076, TSI, USA). An aerosol neutralizer (Model 3087, TSI, USA) was used to bring particles to a steady-state charge distribution before they were introduced into the reactor. The initial seed number and mass concentrations were approximately 5×10^4 cm^{-3} and 6 μg m^{-3} on average, respectively. For different RH conditions, the dry zero air was introduced into a bottle of high-purity water to control the humidity of the background air. The humidity in the chamber was detected with a hygrometer (Model 645, Testo AG, Lenzkirch, Germany). The initial experimental conditions considered in this study are summarized in Table 1. Typically, approximate 750 ppb furan was employed. To study the effect of NOx levels on SOA formation, experiments were conducted with initial furan/NOx ratios ranging from 7.8 to 48.1, whereas to develop and test the role of RH, experiments were performed for RH values varying from 5 to 85% and with an initial average furan to NOx ratio of 7.55. The temperature of the chamber was controlled to be 308-310 K during all the experiments.

Particles and gas-phase species may get lost to the chamber walls on short timescales, hereby influencing the gas-phase chemistry and SOA formation. The wall loss rate constants for O_3, NOx and aerosol particles were 3.3×10^{-7} s^{-1}, 4.1×10^{-7} s^{-1}, and 3.6×10^{-5} s^{-1}, respectively, which were detected from our previous study conducted in the same set-up and similar experimental conditions (Ge et al., 2017a). However, no wall loss of furan was observed within the uncertainty of the detection of the instrument. Furthermore, the light intensity in the reactor was determined to be 0.34 min^{-1} by using the NO_2 photolysis rate constant as the indirect representation. Before the start of each experiment, the static electricity of the Teflon chamber was removed. After all the reactants flowed into the chamber, the reactor was maintained in the dark for at least 40 min without any activities to reach homogeneous mixing.

2.2 Gas and particle monitoring

The concentrations of O_3 and NOx were measured continuously by UV photometric O_3 analyzer (Model 49C, Thermo Environmental Instruments Inc.) and a chemiluminescence analyzer (Model 42C, Thermo Electron Corporation, USA), respectively. The sampling flow rate was 0.75 L min^{-1} for both O_3 and NOx analyzers. The uncertainty in the gas-phase measurements was below ± 1 %. The experiment samples were collected by Tenax absorption tubes (150 mm length × 6 mm O.D., 0.2 g sorbent). Furan concentrations and product samples were detected by thermal desorption-gas chromatography-mass spectrometry (TD-GC-MS): the thermal desorber (Master TD, Dani, Italy) was combined with gas chromatography (Model 7890A, Agilent Tech., USA) interfaced to a mass selective detector (5975C, Agilent Tech., USA). The initial reactants concentrations are given in Table 1. The chromatographic analytical method used for the analysis was as follows: the chromatographic column was kept at 338 K for 4 min, then heated to 598 K at a heating rate of 20 K min^{-1} and held for 5 min.

The particle size distribution and mass concentration were measured with a scanning mobility particle sizer (SMPS, Model 3936, TSI, USA) composed of a TSI 3081 differential mobility analyzer (DMA) and a TSI 3776 condensation particle counter (CPC). The sampling and sheath flow rates of the SMPS were 0.3 L min^{-1} and 3 L min^{-1}, respectively. Given this flow conditions of the SMPS, particle sizes (in counts cm^{-3}) were recorded in 64 size bins for particles in the 13.6 to 710.5 nm size range. The accuracy of the particle number concentration is ±10 % at $<3\times10^5$ cm^{-3}. The method of the reduced Dry-Ambient Size spectrometer (DASS) was used to detect the ALW (Engelhart et al., 2011). To get dry particle mass concentrations, a large diameter Nafion dryer (Permapure MD-700-48F-3) and a multi-tube Nafion dryer (Permapure PD-200T-24E-M) were added to the sampling inlet and sheath flow, respectively. This DASS method is generally accepted and widely used in the detection of ALW content, and can remove up to 90% of the water vapour without losing the organic-bound water. It should be noted that the dissloved water-soluble species would evaporate back into the gas phase during the ALW measurement when the aerosol water is removed. In fact, the repartitioning of water-soluble components between gas and particle phases was not taken into consideration. The SOA concentrations for high RH conditions were slightly underestimated, but the underestimation is extremely low and can be negligible. The results were compared with the mass concentrations detected in humid mode, in which the humid air in the chamber was introduced into the SMPS with the sheath air set at 10 L min^{-1}. The ALW was calculated as the difference between the particle mass concentrations determined at dry and humid modes (Jia and Xu, 2018). On the basis of the recorded particle volume concentration and assumed particle density, a total suspended particulate (TSP in μg m^{-3}) could be translated. As shown in Eq. (1), TSP is the sum of seed aerosol (NaCl in this work), $NaNO_3$, particle ALW, and SOA. By dissolving the SOA collected on ZnSe disks into high purity water, an ion chromatograph (IC, Dionex ICS-900, Thermo Fisher, USA) was then used to analyze the inorganic content (Cl^- and NO_3^-) in SOA. With known initial NaCl seed aerosols and their decay rates, the particle mass concentration of NaCl can be calculated, and based on the detected ALW during experiments, the SOA produced in the photooxidation of furan can be estimated from Eq. (1).

$$\mathrm{TSP} = \mathrm{NaCl} + \mathrm{NaNO_3} + \mathrm{ALW} + \mathrm{SOA} \tag{1}$$

2.3 Chemical characterization of products

The SOA particles were sampled on ungreased ZnSe disk (25 mm in diameter) using a Dekati low-pressure impactor (DLPI, Dekati Ltd., Kangasala, Finland) after the appearance of the O_3 maximum concentration. The sampling flow rate of DLPI was 10 L min^{-1} with the particles sizes from 30 nm to 10 μm, classified into 13 stages. According to the particle distribution explored from the SMPS, the SOA particles size was mainly around 150 nm after 3 h of irradiation. The ZnSe disk was placed on stage 3 to reach the maximum collection of the particles. Afterward, the ZnSe disk was put in the FTIR (Nicolet iS10, Thermos Fisher, USA) sample holder, which had been flushed with N_2 to eliminate the impact of ambient H_2O and CO_2 on the determination of the chemical composition of formed SOA particles. The spectra were recorded at 4 cm^{-1} resolution with 128 scans. The samples collected on the ZnSe disk were then dissolved with high purity water for analysing inorganic species.

To obtain chemical characterization information, the ultrahigh performance liquid chromatograph (UPLC, Ultimate 3000, Thermo Scientific, USA) -heated-electrospray ionization-high-resolution orbitrap mass spectrometer (HESI-HRMS, Q Exactive, Thermo Scientific, USA) was used for the analysis of organic compounds produced from the photooxidation of furan. Methanol (Optima™ LC/MSGrade, Fisher Chemical, USA) was used as the eluent in UPLC system. The acquired mass spectrum of SOA was in the range of 30 80-1000 Da. As a “soft ionization”, HESI can provide molecular formulae for thousands of OA substances when coupled with a high-resolution mass analyzer. The HESI source was used in both positive and negative ion modes using the optimum method for characterization of organic compounds. A total volume of 300 L was sampled at a flow rate of 0.2 L min^{-1}, and a volume of 20 μL of the extraction was used for the measurement. The addition of acetonitrile allows a lower surface tension of the solution and provides a stable electrospray ionization process (Koch et al., 2005). N_2 was used as the sheath and auxiliary gas. The desolvation gas temperature was 320 °C, and the gas flow was 200 μL min^{-1}. The capture voltage was set to 3 kV. The Thermo Scientific Xcalibur software (Thermo Fisher Scientific Inc., USA) was used to analyze the data from HRMS.

3 Results and discussion

3.1 Gas phase and SMPS results

Experiments were divided into two main groups, which were set to study the role of (i) NOx and (ii) RH on SOA formation. To keep the variables of each set of conditions consistent, almost identical initial gas phase conditions were required. The addition of furan and seed aerosol in all the experiments was nearly equal. The first set of experiments (Exp.1-6, Table 1), designed to investigate the effect of NOx level on SOA formation, used similar RH conditions with different NOx concentrations. To further assess the effect of OH produced during the furan-NOx photooxidation, four experiments (Table S1, Exp.13-16) were conducted by injecting H_2O_2 in the chamber before the experiments started. For Exp.6-12, different RH levels coupled with similar furan/NOx ratios were monitored to assess the RH impact on SOA formation. To analyse the SOA composition, five additional experiments (Table S2, Exp. 17-21) were carried out to analyse the HESI-Q Exactive-Orbitrap MS, which intended to compare the role of NOx and RH on the SOA formation. The major gas-phase inorganic chemical reactions occurred during the experiments are presented in Fig. 1. After turning on the light, the photolysis of NO_2 produced NO and O, which further reacted with O_2 to form O_3 in the chamber. As a result, a slight increase in the beginning, followed by the decrease of NOx concentrations are observed (Fig. 2). On one hand, the decrease of NOx is caused by the reaction between NO and alkyl RO_2, which are formed from the OH-initiated oxidation of furan during the experiment. On the other hand, the oxidation of NO by O_3 also contributes to the NOx decreasing trend.

The photochemical oxidation of VOCs in the presence of NOx and OH radical is an important source of tropospheric O_3 (Labouze et al., 2004). Although the atmospheric degradation mechanisms of furan is complex, the fundamental features of troposphere O_3 formation is relatively simple. The main formation pathway of O_3 in the atmosphere is the photolysis of NO_2 as presented in Fig. 1 (R1 and R2). The RO_2 and HO_2 radicals generated from the photooxidation of furan can further react with NO to form NO_2 (R5 and R6), whose photolysis will produce the ground-state oxygen atom (R1) and thus contribute to the net O_3 formation through the reaction of O_2 with O (R2). The very similar VOCs level may result in a high O_3 production with higher NOx concentrations conditions (Bowman and Seinfeld, 1994). As presented in a previous work of the ethylene-NOx-NaCl irradiations, both experimental results and model simulations showed an abundant O_3 production (approximately 500 ppb) with an initial NOx level of 142 ppb (Jia and Xu, 2016). Therefore, it is important to evaluate the O_3 production potential of VOCs in the atmosphere. As shown in Fig. 2, it shows a consistent increasing trend between O_3 concentration and SOA mass concentration, indicating that O_3 was generated during the furan photooxidation reactions with the formation of SOA. However, it should be noted that the apparent high O_3 concentration monitored by the O_3 analyzer was due to species other than O_3 and that have absorption around 254 nm. The generated gas-phase reaction products that have carbonyl, carboxylic acid, and ester groups conjugated with C=C bonds can absorb strongly in the ~200-300 nm range and, accordingly, contribute to the apparent intense signal of O_3 detected by the O_3 monitor (Strollo and Ziemann, 2013).

The O_3 maximum concentration, SOA mass concentration and SOA yield dependences on the C_4H_4O/NOx ratio are presented in Fig. 2. The results show that the O_3 maximum concentration produced during the experiments decreases with increasing C_4H_4O/NOx ratio. When the C_4H_4O/NOx ratio decreases from 16.9 to 7.8, there is a sharp increase in O_3 concentration from 197 to 382 ppb. Interestingly, experiments for which the C_4H_4O/NOx ratio changed from 48.1 to 36.60 exhibit a change of 24 ppb in O_3 maximum concentration. This result indicates that under different C_4H_4O/NOx ratio regimes, the concentration of O_3 produced varies much. There is a great change in O_3 accumulation when the C_4H_4O/NOx ratios are relatively low (<16.9), which is consistent with a previous observation from C_3H_6-NOx-NaCl irradiation experiments by Ge et al. (Ge et al., 2017a) who found that when the C_3H_6/NOx ratio was less than 11, the O_3 concentration decreased considerably with increasing ratio, whereas when the ratio was larger than 11, the O_3 concentration slightly decreased with increasing ratio. Fig. S2 shows the comparisons of the observed concentrations of the apparent O_3 and NOx from furan irradiations at different experimental conditions. With similar NOx level, the amount of O_3 formed at 5% RH was larger than that at 42% RH. The apparent O_3 maximum concentration was reduced by almost 60% as the C_4H_4O/NOx ratio increased from 7.8 to 36.6. However, the effect of RH on O_3 formation is not so obvious compared to the difference in initial C_4H_4O/NOx ratio. The influence of NOx level on O_3 is likely related to its formation mechanism. The formation of O_3 is directly connected with the NOx in two ways: the photolysis of NO_2, producing the O atom that reacts with O_2, and the NOx reacting directly with RO. However, the RH has little to no effect on O_3 formation. This formation is slightly favoured at low RH whereas, at high RH, the ONO_2- are easily transferred into the aerosol phase, thereby suppressing the O_3 formation (Jia and Xu, 2014). Additionally, the slight change in O_3 maximum concentration under different RH conditions may also be caused by the consumption of gas-phase reaction products that contain functional groups conjugated with C=C bonds and respond to the O_3 analyser. This assumption is reasonable because these carbonyl-rich products were favourable to condense on the moist surface of particles and thus lowered the O_3 concentration detected by the O_3 analyser, which has been further confirmed by the MS results with enhanced intensities of corresponding organonitrates. The wall loss of the organonitrates species would also explain in the decreasing trend of O_3 concentration as RH increases. The appearance time of O_3 maximum concentration at high C_4H_4O/NOx ratio is almost half an hour earlier than that at low initial C_4H_4O/NOx ratio. On the contrary, there is no significant difference in the balance time of NOx concentration under different experimental conditions. Similar initial C_4H_4O/NOx ratios result in a similar profile of NOx concentration during the experiment, although the final NOx concentration shows a slight difference.

The calculated SOA yield is defined as the ratio of the mass concentrations of the maximum SOA formed (M_{SOA} in μg m^{-3}, corrected by wall loss) and the reacted furan (ΔC_4H_4O in μg m^{-3}):

$$Y_{SOA} = (\mathrm{M_{SOA}}/\Delta\mathrm{C_4H_4O}) \times 100\ \% \qquad (2)$$

where M_{SOA} is obtained by subtracting the amount of NaCl and $NaNO_3$ from the total particle mass concentration measured by the SMPS, and ΔC_4H_4O is the consumption of furan during the experiments. Experiments were started with an average of 6 μg m^{-3} of NaCl seed aerosol and were conducted under different initial C_4H_4O/NOx ratios. The dependences of the SOA mass concentration and SOA yield on the C_4H_4O/NOx ratios and RH conditions are shown in Fig. 3 and Fig. 4, respectively. The numerical values of the aerosol mass concentration and SOA yield are given in Table 1. After the photooxidation reactions, the SOA mass concentrations reached maxima between 1.0 and 23.5 μg m^{-3}, with SOA yield ranging from 0.04% to 1.01%. In other experiments carried out under varying RH conditions, SOA maxima were in the range of 23.5-119.2 μg m^{-3}, with SOA yield ranging from 1.01% to 5.03%.

It is generally accepted that experiments with low NOx levels lead to higher SOA yields than those with higher NOx levels at the same VOC concentration (Song et al., 2005). However, as shown in Fig. 3, an increasing SOA mass concentration and SOA yield with increasing NOx was observed. There are two possible explanations to this phenomenon: (i) the concentration of OH radicals produced *in situ* in the present study before additional source of OH was insufficient to produce a considerable amount of SOA under low-NOx conditions. As shown in Fig. S3, the OH concentration exhibits a gradual increase with NOx concentration and there appears to be a correlation between NOx concentration, OH concentration and SOA yield. Therefore, at low-NOx conditions, the increase of SOA yield was attributed to an increase of OH concentration, which was affected by OH recycling following reaction (R6) (see Fig. 1) and contributed to the enhancement of SOA formation. This result is consistent with a previous study concerning the impact of NOx and OH on SOA formation from β-pinene photooxidation, which has proved that the positive correlation between SOA yield and NOx levels ($[VOC]_0/[NOx]_0 > 10$ ppbC/ppb) was caused by the NOx–induced increase of OH concentration (Sarrafzadeh et al., 2016b). (ii) Differently, Sarrafzadeh et al. found that after eliminating the effect of OH concentration on SOA mass growth, SOA yield only decreased with increasing NOx levels (Sarrafzadeh et al., 2016). To further investigate the NOx effect on furan generated SOA formation under adequate OH conditions, four more experiments (see Table S1) were carried out with additional injection of H_2O_2 as the OH radical source before the start of each experiment. The SOA yield trend at different C_4H_4O/NOx ratios is also shown in Fig. 3. The continuous growth trend of SOA yield with increasing NOx concentration at a relative high NOx level may result from the partitioning of generated semi/low-volatility compounds (multifunctional nitrates and dinitrates) into the particle phase, leading to significant furan SOA formation under high NOx conditions. Similarly, SOA from OH-initiated isoprene oxidation under high-NOx conditions was comprehensively investigated by Schwantes et al., who suggested that low volatility hydroxyl nitrates and dihydroxyl dinitrates generated conspicuously more aerosol than previously thought (Schwantes et al., 2019). Our results showing the increase of SOA mass formation by high-NOx conditions also agree with a previous study, which indicated that a high level of NO_2 can participate in the OH-induced reaction of guaiacol, consequently leading to the formation of organic nitrates and the enhancement of guaiacol SOA formation (Liu et al., 2019a).

It is worth note that under high RH conditions, as shown in Fig. 1, the NO_2 hydrolysis (reaction (R11)) can generate nitrous acid (HONO), which has been considered as a major source of OH. As indicated in Fig. 4, the SOA yields obtained in the present work clearly show a gradual increase with RH. Also shown in Fig. S3 is the dependence of OH and furan concentrations on RH during the experiments determined from the decay of furan using a reaction rate coefficient of k(OH+furan) = 4.01×10^{-11} cm^3 $molecules^{-1}$ s^{-1} (Atkinson et al., 1983). It is therefore probable that the increase of RH results in high levels of HONO formation in the chamber, which leads to an increase in OH concentration, a faster furan decay rate, and higher aerosol mass yields. This result is in reasonable good agreement with previous studies, which proposed that the amount of products that can partition into the particle phase increases with the increasing rate of hydrocarbon oxidation (Healy et al., 2009; Chan et al., 2007). Moreover, the increasing RH might also enhance the SOA formation due to the fact that the functionalized gas phase components were more favoured to condense on the surface of wet particles (Liu et al., 2019b).

3.2 SOA chemical composition

To get detailed information on the functional groups in SOA formed during the photooxidation of furan, the collected particles were measured by FTIR, which has been proven to be an ideal technique for the detection of functional groups and bond information in aerosol samples. The FTIR spectra of particles collected from furan-NOx-NaCl with different values of C_4H_4O/NOx ratio are shown in Fig. 5. The absorptions of organic functional groups were detected, which further confirmed the SOA formation from the photooxidation of furan. The assignment of the FTIR absorption frequencies is summarized in Table 2. The organic nitrate exhibits typical NO symmetric stretching at 868 cm^{-1}, NO_2 symmetric stretching at around 1341 cm^{-1}, and NO_2 asymmetric stretching at 1614 cm^{-1} (Jia and Xu, 2016). The absorption at 1067 cm^{-1} matches the C-O stretching vibration in C-O-C, while the sharp absorption at 1724 cm^{-1} is the C=O stretching vibration in carboxylic acid and ketones (Sakamoto et al., 2013). The carbon skeleton corresponds to the vibrations between 2850 cm^{-1} and 3100 cm^{-1}, where the ν(C-H) stretching vibration can be found. Absorptions in the ranges 2850-3000 cm^{-1} and 3000-3100 cm^{-1} represent the C-H stretching vibration in saturated carbon ring and unsaturated alkenes, respectively. Correspondingly, the C-H bending vibrations are represented by the absorption between 1350 and 1515 cm^{-1}. The strong broad vibrations at 2400-3500 cm^{-1} are interpreted as the O-H stretching vibration in carboxyl groups and hydroxyl groups (Ge et al., 2017a).

Fig. 5 illustrates the influence of NOx level on the SOA components during the photooxidation of furan. For each of the functional groups, experiments with the most pronounced SOA formation are those with the lowest initial C_4H_4O/NOx ratio. This is further confirmed by comparing the SOA yield for different NOx level conditions under approximately similar gas-phase and initial seed conditions. The calculated variations of the relative abundance of FTIR functional groups at different NOx levels are presented in Fig. S4, in which the absolute abundances are normalized with respect to the corresponding functional abundance detected at C_4H_4O/NOx=7.8. The carbonyl compound formed with 7.8 initial C_4H_4O/NOx ratio is approximately thrice more abundant than that formed with 48.1 initial C_4H_4O/NOx ratio. The absorbance of NO_2 functional groups exhibits a much stronger enhancement under initial C_4H_4O/NOx ratio of 7.8 compared to 48.1. Although at different C_4H_4O/NOx ratio conditions the intensities of C-O-C and O-H functional groups show similar trends, their variations are substantially different from the variations of other functional groups. In sum, the increased absorbance of functional groups with decreasing initial C_4H_4O/NOx ratios demonstrates that relatively high NOx level contributes to the formation of SOA.

The FTIR results in the investigation of furan photooxidation under different RH conditions are shown in Fig. 6. The absorbance of FTIR characteristic peak increases with the RH raising from 5% to 85%. Note that obvious intensities of the functional groups were observed when the RH exceeded the efflorescence RH of NaCl. In contrast, the absorptions of corresponding functional groups enhance gently when the RH is lower than 42%. This phenomenon is consistent with the results of the SOA yield discussed above and, can also be interpreted as the increasing ALW components contributing to SOA formation. The ratio of the absorbance intensities detected at low RH to that at 85% RH is used as the relative abundance to show more intuitive FTIR results. As shown in Fig. S5, for RH between 5% and 37%, the intensities of all functional groups vary weakly and are approximately one-third of the intensity at 85% RH. However, when the RH rises from 42% to 85%, the absorption intensities of O-H and NO_2 functional groups increase by factors of 2.0 and 1.9, respectively. In this RH range, the variations of relative intensities are even stronger for C=O, C-H and C-O-C, being increased by factors of 2.3, 2.3 and 2.5, respectively. A previous study has observed that in an urban environment containing aromatic hydrocarbons and NOx, the SOA yield increased by a factor of 2 to 3 under high RH compared to lower RH (Zhou et al., 2011). This trend is similar to that found in experiments with toluene in an urban aromatic hydrocarbon-NOx mixture system (Kamens et al., 2011). It should be pointed out that observed FTIR results show a high degree of consistency with the SOA mass concentration and SOA yield.

To further identify and confirm the structure of generated SOA components, more techniques, such as GC/MS and HESI-Q Exactive-Orbitrap MS were used to analyze the chemical composition. The chromatography before ESI-MS analyzes is helpful to remove the disturbances of the inorganic salts and determine the appropriate molecular compound (Surratt et al., 2007; Gao et al., 2006). However, the collected PM products were not sufficient for the chromatography owing to the limitation of the chamber volume. Furthermore, the low SOA yield of the furan photooxidation make it harder to remain enough SOA components for the better response of ESI-MS signal. Consequently, direct infusion analyzes were carried out for HESI-Q Exactive-Orbitrap MS in the present study. Five experiments of furan-NOx-NaCl photooxidation that were conducted under different initial C_4H_4O/NOx ratios and RH conditions were analyzed by HESI-Q Exactive-Orbitrap MS. The mass spectra recorded in different ion modes represent the detected compounds ionisable in either positive or negative modes (Walser et al., 2008). The MS spectra of generated species from different NOx level and RH conditions, which show evidence for the OH-furan reaction, are presented in Fig. 7 and Fig. 8, respectively. The major peaks are m/z^+ 85.0018, 101.0894, and 185.0504 in the positive ion mode, and m/z^- 146.0161, 225.0125 and 263.0132 in the negative ion mode. The prominent peaks in the HR-MS spectra detected on negative ion mode are comprised of various functionalized hydroxyl nitrates and dihydroxyl dinitrates. However, in the positive ion mode analysis, most carbonyl components were detected. The assignments of these ion peaks, the molecular weights of the products observed, and proposed structures are summarized in Table 3. These detected compounds provide additional evidence for the proposed radical reaction mechanism.

According to the identified products in this work and based on previous kinetic (Atkinson et al., 1983; Lee and Tang, 1982) and products (Villanueva et al., 2009; Aschmann et al., 2014; Tapia et al., 2011; Villanueva et al., 2007; Strollo and Ziemann, 2013) studies, a proposed chemical mechanism for SOA formation from furan in the presence of NOx is shown in Scheme 1. Additionally, on the basis of well-established mechanisms for atmospheric volatile organic compounds (Atkinson and Arey, 2003), it can be concluded that the reaction is initiated by OH addition to a C=C bond at C2 or C3 positions. Addition at the C2 position forms two cyclic alkyl radicals (a, c), one of which (a) can isomerize to form a ring-opened alkyl radical (d), whereas addition at the C3 position forms a single alkyl radical (b). The OH radical addition leading to an hydrogen abstraction generates the alkyl radicals (R·) followed by reaction with O_2 to form alkylperoxy radicals (RO_2·) (Pan and Wang, 2014). Moreover, the formed alkylperoxy radicals (RO_2·) can either react with RO_2/HO_2 or NO to yield the corresponding alkoxy radical (RO·), which can (i) decompose and then react with O_2 to yield a 1,4-aldoester (A), (ii) react with $NO_2/NO/O_2$ to form hydroxyl nitrate compound isomers with m/z^- 146, or (iii) react with O_2 to form unsaturated products and hydroxyfuranone (B) and 1,4-aldoacid (C). The ring-opened alkylperoxy radical generated from (d) can decompose to generate an unsaturated 1,4-dialdehyde (D). The formation of 1,4-dialdehyde with m/z^+ 85 detected in the positive ion mode suggests that these unsaturated 1,4-dicarbonyls are formed after initial OH addition at 2- or 5-positions. We note that OH radical addition at 2, 3-positions would lead to carbonyl product isomers with same m/z^+ 101. In addition, some dihydroxyl dinitrates with m/z^- 225 were also detected in negative ion mode. However, the pathways favouring the generation of these dihydroxyl dinitrates could only take place under high NOx levels. Scheme 1 shows the formation of second-generation products hemiacetals (E) via the reactions of the hydroxyfuranone (B) with 1,4-dialdehyde (D). After uptake from the gas-phase, the combination of hydroxyfuranone with 4-dialdehyde appeared to occur by H-abstraction, followed by dehydration, thus forming m/z^+ 185 compounds. This reaction pathway has also been identified in previous studies of OH-initiated reactions of furans (Strollo and Ziemann, 2013; Aschmann et al., 2014). According to the results of HR-MS, this aqueous phase reaction is more favoured in aqueous particles.

3.3 Effects of NOx on SOA formation

To study the NOx level effect on SOA formation from the photooxidation of furan, the experiments were conducted with varying initial C_4H_4O/NOx ratios ranging from 7.8 to 48.1. The SOA formation is found to have much lower yield under a high C_4H_4O/NOx ratio. The SOA mass concentration and SOA yield increased from 1.0 to 23.5 $\mu g\ m^{-3}$ and 0.04% to 1.01%, respectively, as the initial concentration ratio of C_4H_4O/NOx decreased from 48.1 to 7.8 (ppbC/ppb). This trend is consistent with previous studies on propylene photooxidation, which found that the SOA yield was enhanced under a low VOC/NOx ratio (Ge et al., 2017a). Another laboratory study of aerosol assessment from isoprene photooxidation concluded that under low NOx level (< 129 ppb), the SOA mass increased with increasing initial NOx level (Kroll et al., 2006). By comparing the studies of Ge et al. and Kroll et al., there is a positive correlation between NOx effect and SOA formation when the initial NOx level is relatively low (nearly below 100 ppb). These results further support our findings in the experiments of furan photooxidation. As shown in Fig. S6, SOA formed under a low C_4H_4O/NOx ratio also have a faster increase than those under large C_4H_4O/NOx ratio conditions. However, the particle number distribution under C_4H_4O/NOx=7.8 and C_4H_4O/NOx=36.6 conditions shows similar profiles.

Generally, the NOx level has two different effects in the reaction process. Firstly, increasing NOx concentration will promote the O_3 and HONO formation, leading to more OH radical formed, which in turns is favorable to SOA formation (Sarrafzadeh et al., 2016). In addition, sufficient NOx can facilitate the competition between NO and HO_2 to react with RO_2. Products with high volatility will be generated more by the NO+RO_2 reaction than by HO_2+RO_2 reaction (Kroll and Seinfeld, 2008). However, the formation of lower volatility products favors the increase of SOA yields (Chen et al., 2018). In this regard, the increasing NOx level is not conducive to SOA formation. It was shown that the yields of SOA generated from the photooxidation of *m*-xylene increased firstly and then decreased with the increase of the NOx level (Chen et al., 2018). In the present study, an increasing trend of SOA formation was observed with the increase of NOx concentration. As shown in the HESI-Q Exactive Orbitrap-MS results, all the detected primary products are carbonyl-rich, and even the organonitrates have at least two carbonyl functional groups. These carbonyl-containing products have lower volatility and contribute to the SOA formation. The peak intensities in the MS of the products (m/z^+ 85, 101) generated by the pathways involving HO_2 (as indicated by the scheme 1) decreased with the increase of NOx concentration. Additionally, more products of dihydroxyl dinitrates (m/z^- 225) with multifunctional groups were detected under high NOx conditions. As shown in Scheme 1, the multifunctional organonitrates detected in negative ion mode are produced mostly from later-generation chemistry. Hydroxyl nitrates with m/z^- 149 can be formed through pathways 1-a, 2-a, and 3-a by the reaction of RO_2 with NOx. We note that the m/z^- 149 compound was detected both at low NOx levels and high NOx levels. However, the peak intensity of this product was decreased with increasing NOx concentration. This phenomenon might be caused by the later-reaction of the unsaturated hydroxyl nitrates going through a second OH-initiated reaction and leading to the formation of the dihydroxyl dinitrate with m/z^- 225. In addition, the peak intensities changes of SOA products detected in the positive mode, such as, the peaks at m/z^+ 85 and 101 were reduced under high NOx conditions, which resulted from the fact that the RO_2 radical fate was dominated by the pathway of RO_2+NO or RO_2+NO_2. This result supports that the fate of RO_2 is not a single channel reaction. There exists a competition between RO_2 reacting with NOx and with HO_2 under high NOx conditions but the former pathway is more favourable. There are two pathways for hydroxyl nitrates formation from RO_2 radicals in the presence of NOx according to which RO_2 radicals may react with NO and NO_2 to form $RONO_2$ and $ROONO_2$, respectively (Kroll and Seinfeld, 2008). However, the formed peroxynitrates could easily thermally dissociate and convert to $RONO_2$.

Furthermore, by analysing the OH concentration and products components, we conclude that there are two possible explanations for the increasing trend of SOA yield as the NOx level increases: (i) the SOA production is closely related to the oxidation capacity in the photooxidation experiments. Experiments conducted under different NOx levels indicate that the OH concentration is controlled by the NOx level if there is no additional OH precursor added before the start of the experiment. As shown in Fig. S3, an increase in NOx level results in more OH generation and a faster furan decay rate. This justifies the observed higher SOA mass concentration and higher SOA yield. (ii) HRMS fragments associated with multifunctional organonitrates are enhanced under high NOx conditions (Fig. 7). As presented in Scheme 1, the furan dihydroxyl dinitrates are generated from the first-generation hydroxyl nitrate reacting with OH to form a peroxy radical, which reacts thereafter with NO. Together with multifunctional hydroxyl nitrates, these low-volatility species can easily partition into the particle phase and increase the SOA mass concentration. More importantly, the seed particle added initially plays an important role in the processes of gas-particle partitioning as indicated by a recent study, which showed that sufficient seed surface area at the start of the reaction largely suppressed the effects of vapour wall losses of low-volatility compounds (Schwantes et al., 2019). Therefore, the NaCl seed particle added in the present work promoted the partitioning of the formed low-volatility functional organonitrates.

3.4 Effect of RH on SOA formation

Experiments 6-12 were conducted under seven different RH conditions ranging from 5% to 85%. In this RH range, the SOA yield increases from 1.01% to 5.03%. With almost identical initial conditions except RH, the yield of furan-derived SOA formed at high RH can be a factor of two higher than that formed at low RH. A similar trend was also observed by Yu et al., who found that the SOA mass concentrations increased by a factor of six when RH increased from 18% to 82% (Yu et al., 2011). As shown in Fig. S3, an increase in RH leads to higher OH concentration resulting from higher HONO levels generated by the reaction of NO_2 with H_2O. Previously, Anglada et al. confirmed, using quantum mechanical calculations, that the water component could increase the OH production (Anglada et al., 2011). The positive correlation between initial water vapour concentration and OH concentration has also been previously observed experimentally (Healy et al., 2009; Tillmann et al., 2010). Additionally, Healy et al. have also reported that increasing OH concentration promoted the decay of VOC and enhanced SOA formation (Healy et al., 2009). Similarly, in the present work, a faster decay rate of furan was also observed as RH increased, as shown in Fig. S3. It is possible that the faster rate of gas phase oxidation under higher OH concentrations will lead to the generation of less volatile compounds as presented previously (Chan et al., 2007). A higher OH concentration promotes oxidation reactions, influences the distribution of organic products, and facilitates the SOA formation (Sarrafzadeh et al., 2016).

An obvious increase of SOA yield was observed when the RH increased from 37% to 54%. This phenomenon was mainly caused by the efflorescence transition when the seed particles were coated with SOA. It has been previously shown that SOA formation decreases both the efflorescence RH and deliquescence RH of the seed particles and results in the uptake of water by the particles (Liu et al., 2018; Takahama et al., 2007; Smith et al., 2012). It is highly possible that the NaCl seeds effloresce and deliquesce early after being coated by the new formed SOA. The effect of efflorescence contributes to the water uptake by the particles, leading to the obvious trend-changing of SOA yield. It is noted that with the NaCl seed aerosols serving as nuclei, the ALW was high at high RH. Products with water solubility produced from the photooxidation of furan can dissolve into the ALW of aerosol particles. As a result, ALW in the formed aerosols plays an important role in gas/particle partitioning. As shown in Fig. 4, the ALW was detected when the RH was higher than 54%, which was based on the deliquescence of NaCl under high RH conditions. The increase of ALW could partially explain the increase of SOA mass concentration and SOA yield. It is highly probable that the particle surface area increases with increasing amount of ALW as shown in Fig. S7, which likely promotes the dissolution of semi-volatile matters produced during the experiments. According to the HESI-Q Exactive-Orbitrap MS results shown in Fig. 8, the intensities of multifunctional hydroxyl nitrates and dihydroxyl dinitrate (m/z^- 146 and 225, respectively) exhibited positive correlations with RH. Slight peak intensities increases of m/z^+ 85 and 101 products were also observed under high RH conditions. This phenomenon indicates that the gas-particle phase partitioning of low-volatility compounds was enhanced under high RH conditions. Furthermore, the increased surface area under high RH conditions may also be attributed to the condensation of the produced multifunctional compounds.

Another possibility for the increasing trend of SOA yield with the increase of RH might result from the SOA formation through aqueous chemistry in wet aerosols (Grgic et al., 2010; Lim et al., 2010). In these atmospheric processes, alcohols, aldehydes, and ketones formed from the photooxidation of furan in the gas phase can be absorbed into the humid surface of the hygroscopic SOA at high RH. This process further contributes to the formation of low-volatility products on the SOA surface. In addition, the aqueous photochemistry of highly soluble small compounds that portioned in ALW could produce additional organic compounds and result in larger SOA yield under high RH conditions (Faust et al., 2017; Jia and Xu, 2014). The appearance of m/z^+ 185 and m/z^- 262 detected by the HESI-Q Exactive-Orbitrap MS further demonstrated that aqueous phase reactions indeed took place under high RH conditions. As shown in Scheme 1, the peak of m/z^+ 185 could form by aqueous phase reaction of the hydroxyfuranone (B) and 1,4-dialdehyde (D). The formation of hemiacetal (E) has also been detected by a previous study of the OH-initiated reaction of 3-methylfuran in the presence of NOx (Strollo and Ziemann, 2013). The proposed hemiacetal compound (E) plays a substantial role in the obvious increase of m/z^+ 185 product formation under high RH conditions. A pathway of organonitrate (m/z^- 262) formation in the aqueous particles with the presence of NO_3^- was suggested in the present study based on a previous work, which indicated a radical-radical reaction pathway for organosulfate formation from aqueous OH oxidation of glycolaldehyde in the presence of sulfuric acid (Perri et al., 2010). Increasing the RH also resulted in an overall addition of peak intensities in the negative ion mode, due to the fact that the sample obtained at high RH during the SOA generation had a larger particle surface. Specifically, a relatively stronger intense band of $C_8H_8O_9N^-$ compound (m/z^-=262) was found under a high RH. Consequently, the heterogeneous products in wet seed particles will further contribute to the formation of SOA, because higher aerosol liquid water content enables more aqueous phase reactions.

In conclusion, the reasons for the increasing trend of SOA formation under high RH conditions may be summarized as following: firstly, higher concentration of OH radical will certainly promote the SOA formation as RH increases. A faster decay rate of furan will also contribute to the formation of products that can partition into the particle phase. In addition, it is possible that the aqueous surface of seed particles provides a new substrate for the photooxidation of furan. Previously, N_2O_5 and HNO_3 have been proven to be the key products in the VOC-NOx irradiation experiments (Wang et al., 2016). The moist surface under high RH conditions is more favorable for the condensation of products with low vapor pressure, leading to the increasing production of SOA formation. The high RH environment favors the formation of the hemiacetal compound. Moreover, the effect of RH on SOA formation in furan photooxidation can also be determined by the aqueous photochemistry under high RH conditions as discussed above. The aqueous phase reactions at the surface of particles promotes the formation of hemiacetal-like products, which likely plays an important role in the process of SOA formation. Previously, unsaturated first-generation reaction product of 3-methyl furan has also been suggested to undergo acid-catalyzed condensed-phase reactions, with SOA yields up to 15% (Strollo and Ziemann, 2013). In addition, the reinforced effect of RH on SOA yield was also ascribed from the photooxidation of other aromatic compounds, such as, benzene (Ng et al., 2007b), toluene (Hildebrandt et al., 2009; Kamens et al., 2011), and xylene (Zhou et al., 2011).

4 Conclusion

The effects of NOx and RH on SOA formation from the photooxidation of furan in the presence of NaCl seed particles have been investigated in this study. The results demonstrated that the formation of SOA were promoted when the initial VOC/NOx ratio decreases. The increase of SOA yield at high VOC/NOx ratio was caused by the NOx-induced increase of OH concentration. The reason for the promotion of SOA mass at a low furan/NOx ratio is that more low-volatility products were generated from the furan photooxidation, which contributes to the formation of SOA. Additionally, the increase of RH results in the increase in the mass concentration of the produced SOA. The mechanisms controlling SOA formation may include the gas-phase photooxidation of furan, physical water uptake as RH increases, and the gas-phase reaction of water with the first-generation products and the aqueous chemistry of low-volatility products reacting at the wet surface of NaCl seed particles. Seed aerosols are important for the growth of atmospheric particles and, therefore, affect aerosol-cloud-climate interactions. Organic nitrates, detected with FTIR and ESI-Exactive-Orbitrap MS, were found as significant composition of newly formed particles. A significant amount of carbonyl-rich products were also detected in the SOA products from the photooxidation of furan. A recent study showed that the reactive nitrogen chemistry in aerosol water can be a source of atmospheric sulfate during haze events (Cheng et al., 2016). In addition, the ALW is deeply linked with air quality (Malm et al., 1994) and aqueous SOA formation (Sareen et al., 2017). The influence of the ALW component on SOA yield was examined and it was found that increased ALW amounts lead to higher SOA mass concentration and yield, therefore highlighting the importance of the ALW in photooxidation reactions. ALW plays a crucial role in atmospheric physicochemical processes. The current results could also be used to interpret ambient gas-phase measurements and reaction mechanisms inference.

Data availability. Data are available by contacting the corresponding author.

The Supplement related to this article is available online.

Competing interests

The authors declare that they have no conflict of interest.

Author contributions

LD and XJ conceived and led the studies. XJ, NT, LJ, SL and HZ carried out the experiments and analyzed the data. XJ, LD and SL interpreted the results. NT, LJ and YX discussed the results and commented on the manuscript. XJ prepared the manuscript with contributions from all co-authors.

Acknowledgments

This work was supported by National Natural Science Foundation of China (91644214, 41375129), Shandong Natural Science Foundation for Distinguished Young Scholars (JQ201705), Shandong Key R&D Program (2018GSF117040), and Fundamental Research Funds of Shandong University (2017JQ01). We thank Hartmut Herrmann for his very constructive comments at the revision stage.

References

Anglada, J. M., Gonzalez, J., and Torrent-Sucarrat, M.: Effects of the substituents on the reactivity of carbonyl oxides. A theoretical study on the reaction of substituted carbonyl oxides with water, Phys. Chem. Chem. Phys., 13, 13034-13045, 10.1039/c1cp20872a, 2011.

Aschmann, S. M., Nishino, N., Arey, J., and Atkinson, R.: Products of the OH radical initiated reactions of furan, 2-and 3-methylfuran, and 2,3-and 2,5-dimethylfuran in the presence of NO, J. Phys. Chem. A, 118, 457-466, 10.1021/jp410345k, 2014.

Atkinson, R., Aschmann, S. M., and Carter, W. P.: Kinetics of the reactions of O_3 and OH radicals with furan and thiophene at 298±2 K, Int. J. Chem. Kinet., 15, 51-61, 0.1002/kin.550150106, 1983.

Atkinson, R., Aschmann, S. M., Winer, A. M., and Carter, W. P.: Rate constants for the gas-phase reactions of nitrate radicals with furan, thiophene, and pyrrole at 295±1 K and atmospheric pressure, Environ. Sci. Technol., 19, 87-90, 0013-936X/85/0919-0087$01.50/0, 1985.

Atkinson, R., and Arey, J.: Atmospheric degradation of volatile organic compounds, Chem. Rev., 103, 4605-4638, 10.1021/cr0206420, 2003.

Baker, J., Arey, J., and Atkinson, R.: Formation and reaction of hydroxycarbonyls from the reaction of OH radicals with 1,3-butadiene and isoprene, Environ. Sci. Technol., 39, 4091-4099, 10.1021/es047930t, 2005.

Bonn, B., and Moortgat, G. K.: New particle formation during alpha- and beta-pinene oxidation by O_3, OH and NO_3, and the influence of water vapour: Particle size distribution studies, Atmos. Chem. Phys., 2, 183-196, 10.5194/acp-2-183-2002, 2002.

Bowman, F. M., and Seinfeld, J. H.: Fundamental basis of incremental reactivities of organics in ozone formation in VOC/NOx mixtures. , Atmos. Environ., 28, 3359-3368, 10.1016/1352-2310(94)00165-h, 1994.

Burling, I. R., Yokelson, R. J., Griffith, D. W. T., Johnson, T. J., Veres, P., Roberts, J. M., Warneke, C., Urbanski, S. P., Reardon, J., Weise, D. R., Hao, W. M., and de Gouw, J.: Laboratory measurements of trace gas emissions from biomass burning of fuel types from the southeastern and southwestern United States, Atmos. Chem. Phys., 10, 11115-11130, 10.5194/acp-10-11115-2010, 2010.

Cabanas, B., Baeza, M. T., Salgado, S., Martin, P., Taccone, R., and Martinez, E.: Oxidation of heterocycles in the atmosphere: Kinetic study of their reactions with NO_3 radical, J. Phys. Chem. A, 108, 10818-10823, 10.1021/jp046524t, 2004.

Cao, G., and Jang, M.: An SOA model for toluene oxidation in the presence of inorganic aerosols, Environ. Sci. Technol., 44, 727-733, 10.1021/es901682r, 2010.

Chan, A. W. H., Kroll, J. H., Ng, N. L., and Seinfeld, J. H.: Kinetic modeling of secondary organic aerosol formation: Effects of particle- and gas-phase reactions of semivolatile products, Atmos. Chem. Phys., 7, 4135-4147, 10.5194/acp-7-4135-2007, 2007.

Chan, A. W. H., Chan, M. N., Surratt, J. D., Chhabra, P. S., Loza, C. L., Crounse, J. D., Yee, L. D., Flagan, R. C., Wennberg, P. O., and Seinfeld, J. H.: Role of aldehyde chemistry and NOx concentrations in secondary organic aerosol formation, Atmos. Chem. Phys., 10, 7169-7188, 10.5194/acp-10-7169-2010, 2010.

Chen, Y., Tong, S., Wang, J., Peng, C., Ge, M., Xie, X., and Sun, J.: The effect of Titanium Dioxide on secondary organic aerosol formation, Environ. Sci. Technol., 52, 11612-11620, 10.1021/acs.est.8b02466, 2018.

Cheng, Y., Zheng, G., Wei, C., Mu, Q., Zheng, B., Wang, Z., Gao, M., Zhang, Q., He, K., Carmichael, G., Poschl, U., and Su, H.: Reactive nitrogen chemistry in aerosol water as a source of sulfate during haze events in China, Sci. Rep., 2, e1601530, 10.1126/sciadv.1601530, 2016.

Cocker, D. R., Mader, B. T., Kalberer, M., Flagan, R. C., and Seinfeld, J. H.: The effect of water on gas-particle partitioning of secondary organic aerosol: II. m-xylene and 1,3,5-trimethylbenzene photooxidation systems, Atmos. Environ., 35, 6073-6085, 10.1016/s1352-2310(01)00405-8, 2001.

Coggon, M. M., Veres, P. R., Yuan, B., Koss, A., Warneke, C., Gilman, J. B., Lerner, B. M., Peischl, J., Aikin, K. C., Stockwell, C. E., Hatch, L. E., Ryerson, T. B., Roberts, J. M., Yokelson, R. J., and de Gouw, J. A.: Emissions of nitrogen-containing organic compounds from the burning of herbaceous and arboraceous biomass: Fuel composition dependence and the variability of commonly used nitrile tracers, Geophys. Res. Lett, 43, 9903-9912, 10.1002/2016gl070562, 2016.

Coury, C., and Dillner, A. M.: A method to quantify organic functional groups and inorganic compounds in ambient aerosols using attenuated total reflectance FTIR spectroscopy and multivariate chemometric techniques, Atmos. Environ., 42, 5923-5932, 10.1016/j.atmosenv.2008.03.026, 2008.

Donahue, N. M., Robinson, A. L., and Pandis, S. N.: Atmospheric organic particulate matter: From smoke to secondary organic aerosol, Atmos. Environ., 43, 94-106, 10.1016/j.atmosenv.2008.09.055, 2009.

Duarte, R., Pio, C. A., and Duarte, A. C.: Spectroscopic study of the water-soluble organic matter isolated from atmospheric aerosols collected under different atmospheric conditions, Anal. Chim. Acta, 530, 7-14, 10.1016/j.aca.2004.08.049, 2005.

Edney, E. O., Driscoll, D. J., Speer, R. E., Weathers, W. S., Kleindienst, T. E., Li, W., and Smith, D. F.: Impact of aerosol liquid water on secondary organic aerosol yields of irradiated toluene/propylene/NOx/$(NH_4)_2SO_4$/air mixtures, Atmos. Environ., 34, 3907-3919, 10.1016/s1352-2310(00)00174-6, 2000.

Engelhart, G. J., Hildebrandt, L., Kostenidou, E., Mihalopoulos, N., Donahue, N. M., and Pandis, S. N.: Water content of aged aerosol, Atmos. Chem. Phys., 11, 911-920, 10.5194/acp-11-911-2011, 2011.

Ervens, B., Turpin, B. J., and Weber, R. J.: Secondary organic aerosol formation in cloud droplets and aqueous particles (aqSOA): A review of laboratory, field and model studies, Atmos. Chem. Phys., 11, 11069-11102, 10.5194/acp-11-11069-2011, 2011.

Faust, J. A., Wong, J. P. S., Lee, A. K. Y., and Abbatt, J. P. D.: Role of aerosol liquid water in secondary organic aerosol formation from volatile organic compounds, Environ. Sci. Technol., 51, 1405-1413, 10.1021/acs.est.6b04700, 2017.

Fry, J. L., Kiendler-Scharr, A., Rollins, A. W., Wooldridge, P. J., Brown, S. S., Fuchs, H., Dube, W., Mensah, A., dal Maso, M., Tillmann, R., Dorn, H. P., Brauers, T., and Cohen, R. C.: Organic nitrate and secondary organic aerosol yield from NO_3 oxidation of beta-pinene evaluated using a gas-phase kinetics/aerosol partitioning model, Atmos. Chem. Phys., 9, 1431-1449, 10.5194/acp-9-1431-2009, 2009.

Gao, S., Surratt, J. D., Knipping, E. M., Edgerton, E. S., Shahgholi, M., and Seinfeld, J. H.: Characterization of polar organic components in fine aerosols in the southeastern United States: Identity, origin, and evolution, J. Geophys. Res., 111, 10.1029/2005jd006601, 2006.

Ge, S., Xu, Y., and Jia, L.: Secondary organic aerosol formation from propylene irradiations in a chamber study, Atmos. Environ., 157, 146-155, 10.1016/j.atmosenv.2017.03.019, 2017a.

Ge, S., Xu, Y., and Jia, L.: Secondary organic aerosol formation from ethylene ozonolysis in the presence of sodium chloride, J. Aerosol Sci., 106, 120-131, 10.1016/j.jaerosci.2017.01.009, 2017b.

Gilman, J. B., Lerner, B. M., Kuster, W. C., Goldan, P. D., Warneke, C., Veres, P. R., Roberts, J. M., de Gouw, J. A., Burling, I. R., and Yokelson, R. J.: Biomass burning emissions and potential air quality impacts of volatile organic compounds and other trace gases from fuels common in the US, Atmos. Chem. Phys., 15, 13915-13938, 10.5194/acp-15-13915-2015, 2015.

Gloess, A. N., Vietri, A., Wieland, F., Smrke, S., Schoenbaechler, B., Lopez, J. A. S., Petrozzi, S., Bongers, S., Koziorowski, T., and Yeretzian, C.: Evidence of different flavour formation dynamics by roasting coffee from different origins: On-line analysis with PTR-ToF-MS, Int. J. Mass Spectrom., 365, 324-337, 10.1016/j.ijms.2014.02.010, 2014.

Gomez Alvarez, E., Borras, E., Viidanoja, J., and Hjorth, J.: Unsaturated dicarbonyl products from the OH-initiated photo-oxidation of furan, 2-methylfuran and 3-methylfuran, Atmos. Environ., 43, 1603-1612, 10.1016/j.atmosenv.2008.12.019, 2009.

Greenberg, J. P., Zimmerman, P. R., Heidt, L., and Pollock, W.: Hydrocarbon and carbon-monoxide emissions from biomass burning in Brazil., J. Geophys. Res., 89, 1350-1354, 10.1029/JD089iD01p01350, 1984.

Grgic, I., Nieto-Gligorovski, L. I., Net, S., Temime-Roussel, B., Gligorovski, S., and Wortham, H.: Light induced multiphase chemistry of gas-phase ozone on aqueous pyruvic and oxalic acids, Phys. Chem. Chem. Phys., 12, 698-707, 10.1039/b914377g, 2010.

Hallquist, M., Wenger, J. C., Baltensperger, U., Rudich, Y., Simpson, D., Claeys, M., Dommen, J., Donahue, N. M., George, C., Goldstein, A. H., Hamilton, J. F., Herrmann, H., Hoffmann, T., Iinuma, Y., Jang, M., Jenkin, M. E., Jimenez, J. L., Kiendler-Scharr, A., Maenhaut, W., McFiggans, G., Mentel, T. F., Monod, A., Prevot, A. S. H., Seinfeld, J. H., Surratt, J. D., Szmigielski, R., and Wildt, J.: The formation, properties and impact of secondary organic aerosol: Current and emerging issues, Atmos. Chem. Phys., 9, 5155-5236, 10.5194/acp-9-5155-2009, 2009.

Hatch, L. E., Luo, W., Pankow, J. F., Yokelson, R. J., Stockwell, C. E., and Barsanti, K. C.: Identification and quantification of gaseous organic compounds emitted from biomass burning using two-dimensional gas chromatography-time-of-flight mass spectrometry, Atmos. Chem. Phys., 15, 1865-1899, 10.5194/acp-15-1865-2015, 2015.

Healy, R. M., Temime, B., Kuprovskyte, K., and Wenger, J. C.: Effect of relative humidity on gas/particle partitioning and aerosol mass yield in the photooxidation of p-Xylene, Environ. Sci. Technol., 43, 1884-1889, 10.1021/es802404z, 2009.

Hildebrandt, L., Donahue, N. M., and Pandis, S. N.: High formation of secondary organic aerosol from the photo-oxidation of toluene, Atmos. Chem. Phys., 9, 2973-2986, 10.5194/acp-9-2973-2009, 2009.

Hinks, M. L., Montoya-Aguilera, J., Ellison, L., Lin, P., Laskin, A., Laskin, J., Shiraiwa, M., Dabdub, D., and Nizkorodov, S. A.: Effect of relative humidity on the composition of secondary organic aerosol from the oxidation of toluene, Atmos. Chem. Phys., 18, 1643-1652, 10.5194/acp-18-1643-2018, 2018.

IARC: Dry cleaning, some chlorinated solvents and other industrial chemical., IARC Monographs on the Evaluation of Carcinogenic Risk of Chemicals to Humans, 63. International Agency for Research on Cancer, Lyon, France, 558pp, 1995.

Jang, M. S., Czoschke, N. M., Lee, S., and Kamens, R. M.: Heterogeneous atmospheric aerosol production by acid-catalyzed particle-phase reactions, Science, 298, 814-817, 10.1126/science.1075798, 2002.

Jia, L., and Xu, Y.: Effects of relative humidity on ozone and secondary organic aerosol formation from the photooxidation of benzene and ethylbenzene, Aerosol Sci. Tech., 48, 1-12, 10.1080/02786826.2013.847269, 2014.

Jia, L., and Xu, Y.: Ozone and secondary organic aerosol formation from Ethylene-NO (x)-NaCl irradiations under different relative humidity conditions, J. Atmos. Chem., 73, 81-100, 10.1007/s10874-015-9317-1, 2016.

Jia, L., and Xu, Y.: Different roles of water in secondary organic aerosol formation from toluene and isoprene, Atmos. Chem. Phys., 18, 8137-8154, 10.5194/acp-18-8137-2018, 2018.

Jonsson, A. M., Hallquist, M., and Ljungstrom, E.: Impact of humidity on the ozone initiated oxidation of limonene, delta(3)-carene, and alpha-pinene, Environ. Sci. Technol., 40, 188-194, 10.1021/es051163w, 2006.

Kahan, T. F., Ormond, T. K., Ellison, G. B., and Vaida, V.: Acetic acid formation via the hydration of gas-phase ketene under ambient conditions, Chem. Phys.Lett., 565, 1-4, 10.1016/j.cplett.2013.02.030, 2013.

Kamens, R. M., Zhang, H., Chen, E. H., Zhou, Y., Parikh, H. M., Wilson, R. L., Galloway, K. E., and Rosen, E. P.: Secondary organic aerosol formation from toluene in an atmospheric hydrocarbon mixture: Water and particle seed effects, Atmos. Environ., 45, 2324-2334, 10.1016/j.atmosenv.2010.11.007, 2011.

Kanakidou, M., Seinfeld, J. H., Pandis, S. N., Barnes, I., Dentener, F. J., Facchini, M. C., Van Dingenen, R., Ervens, B., Nenes, A., Nielsen, C. J., Swietlicki, E., Putaud, J. P., Balkanski, Y., Fuzzi, S., Horth, J., Moortgat, G. K., Winterhalter, R., Myhre, C. E. L., Tsigaridis, K., Vignati, E., Stephanou, E. G., and Wilson, J.: Organic aerosol and global climate modelling: A review, Atmos. Chem. Phys., 5, 1053-1123, 10.5194/acp-5-1053-2005, 2005.

Koch, B. P., Witt, M. R., Engbrodt, R., Dittmar, T., and Kattner, G.: Molecular formulae of marine and terrigenous dissolved organic matter detected by electrospray ionization Fourier transform ion cyclotron resonance mass spectrometry, Geochim. Cosmochim. Ac., 69, 3299-3308, 10.1016/j.gca.2005.02.027, 2005.

Kostenidou, E., Pathak, R. K., and Pandis, S. N.: An algorithm for the calculation of secondary organic aerosol density combining AMS and SMPS data, Aerosol Sci. Tech., 41, 1002-1010, 10.1080/02786820701666270, 2007.

Kroll, J. H., Ng, N. L., Murphy, S. M., Flagan, R. C., and Seinfeld, J. H.: Secondary organic aerosol formation from isoprene photooxidation, Environ. Sci. Technol., 40, 1869-1877, 10.1021/es0524301, 2006.

Kroll, J. H., and Seinfeld, J. H.: Chemistry of secondary organic aerosol: Formation and evolution of low-volatility organics in the atmosphere, Atmos. Environ., 42, 3593-3624, 10.1016/j.atmosenv.2008.01.003, 2008.

Labouze, E., Honoré, C., Moulay, L., Couffignal, B., and Beekmann, M.: Photochemical ozone creation potentials, Int. J. Life Cycle Ass., 9, 187-195, 10.1016/j.jclepro.2006.03.002, 2004.

Lee, J. H., and Tang, I. N.: Absolute rate constants for the hydroxyl radical reactions with ehtane, furan, and thiophene at roon temperature, J. Chem. Phys., 77, 4459-4463, 10.1063/1.444367, 1982.

Liljegren, J. A., and Stevens, P. S.: Kinetics of the reaction of OH radicals with 3-methylfuran at low pressure, Int. J. Chem. Kinet., 45, 787-794, 10.1002/kin.20814, 2013.

Lim, Y. B., Tan, Y., Perri, M. J., Seitzinger, S. P., and Turpin, B. J.: Aqueous chemistry and its role in secondary organic aerosol (SOA) formation, Atmos. Chem. Phys., 10, 10521-10539, 10.5194/acp-10-10521-2010, 2010.

Liu, C., Liu, J., Liu, Y., Chen, T., and He, H.: Secondary organic aerosol formation from the OH-initiated oxidation of guaiacol under different experimental conditions, Atmos. Environ., 207, 30-37, 10.1016/j.atmosenv.2019.03.021, 2019a.

Liu, S., Jia, L., Xu, Y., Tsona, N. T., Ge, S., and Du, L.: Photooxidation of cyclohexene in the presence of SO_2: SOA yield and chemical composition, Atmos. Chem. Phys., 17, 13329-13343, 10.5194/acp-17-13329-2017, 2017.

Liu, S., Tsona, N. T., Zhang, Q., Jia, L., Xu, Y., and Du, L.: Influence of relative humidity on cyclohexene SOA formation from OH photooxidation, Chemosphere, 231, 478-486, 10.1016/j.chemosphere.2019.05.131, 2019b.

Liu, T., Huang, D. D., Li, Z., Liu, Q., Chan, M., and Chan, C. K.: Comparison of secondary organic aerosol formation from toluene on initially wet and dry ammonium sulfate particles at moderate relative humidity, Atmos. Chem. Phys., 18, 5677-5689, 10.5194/acp-18-5677-2018, 2018.

Mahowald, N., Ward, D. S., Kloster, S., Flanner, M. G., Heald, C. L., Heavens, N. G., Hess, P. G., Lamarque, J.-F., and Chuang, P. Y.: Aerosol impacts on climate and biogeochemistry, in, Annu. Rev. Env. Resour., 45-74, 2011.

Malm, W. C., Sisler, J. F., Huffman, D., Eldred, R. A., and Cahill, T. A.: Spatial and seasonal trends in particle concentration and optical extinction in the United States J. Geophys. Res., 99, 1347-1370, 10.1029/93jd02916, 1994.

Ng, N. L., Chhabra, P. S., Chan, A. W. H., Surratt, J. D., Kroll, J. H., Kwan, A. J., McCabe, D. C., Wennberg, P. O., Sorooshian, A., Murphy, S. M., Dalleska, N. F., Flagan, R. C., and Seinfeld, J. H.: Effect of NOx level on secondary organic aerosol (SOA) formation from the photooxidation of terpenes, Atmos. Chem. Phys., 7, 5159-5174, 10.5194/acp-7-5159-2007, 2007a.

Ng, N. L., Kroll, J. H., Chan, A. W. H., Chhabra, P. S., Flagan, R. C., and Seinfeld, J. H.: Secondary organic aerosol formation from m-xylene, toluene, and benzene, Atmos. Chem. Phys., 7, 3909-3922, 10.5194/acp-7-3909-2007, 2007b.

Olsson, M.: Wheat straw and peat for fuel pellets - organic compounds from combustion, Biomass Bioenerg., 30, 555-564, 10.1016/j.biombioe.2006.01.005, 2006.

Pan, S., and Wang, L.: Atmospheric Oxidation Mechanism of m-Xylene Initiated by OH Radical, J. Phys. Chem. A, 118, 10778-10787, 10.1021/jp506815v, 2014.

Perri, M. J., Lim, Y. B., Seitzinger, S. P., and Turpin, B. J.: Organosulfates from glycolaldehyde in aqueous aerosols and clouds: Laboratory studies, Atmos. Environ., 44, 2658-2664, 10.1016/j.atmosenv.2010.03.031, 2010.

Perzon, M.: Emissions of organic compounds from the combustion of oats - a comparison with softwood pellets, Biomass Bioenerg., 34, 828-837, 10.1016/j.biombioe.2010.01.027, 2010.

Pope, C. A., III, Ezzati, M., and Dockery, D. W.: Fine particulate air pollution and life expectancies in the United States: The role of influential observations, J. Air Waste Manage., 63, 129-132, 10.1080/10962247.2013.760353, 2013.

Sakamoto, Y., Inomata, S., and Hirokawa, J.: Oligomerization reaction of the criegee intermediate leads to secondary organic aerosol formation in ethylene ozonolysis, J. Phys. Chem. A, 117, 12912-12921, 10.1021/jp408672m, 2013.

Sareen, N., Waxman, E. M., Turpin, B. J., Volkamer, R., and Carlton, A. G.: Potential of aerosol liquid water to facilitate organic aerosol formation: Assessing knowledge gaps about precursors and partitioning, Environ. Sci. Technol., 51, 3327-3335, 10.1021/acs.est.6b04540, 2017.

Sarkar, C., Sinha, V., Kumar, V., Rupakheti, M., Panday, A., Mahata, K. S., Rupakheti, D., Kathayat, B., and Lawrence, M. G.: Overview of VOC emissions and chemistry from PTR-TOF-MS measurements during the SusKat-ABC campaign: high acetaldehyde, isoprene and isocyanic acid in wintertime air of the Kathmandu Valley, Atmos. Chem. Phys., 16, 3979-4003, 10.5194/acp-16-3979-2016, 2016.

Sarrafzadeh, M., Wildt, J., Pullinen, I., Springer, M., Kleist, E., Tillmann, R., Schmitt, S. H., Wu, C., Mentel, T. F., Zhao, D., Hastie, D. R., and Kiendler-Scharr, A.: Impact of NOx and OH on secondary organic aerosol formation from beta-pinene photooxidation, Atmos. Chem. Phys., 16, 11237-11248, 10.5194/acp-16-11237-2016, 2016.

Schwantes, R. H., Charan, S. M., Bates, K. H., Huang, Y., Nguyen, T. B., Mai, H., Kong, W., Flagan, R. C., and Seinfeld, J. H.: Low-volatility compounds contribute significantly to isoprene secondary organic aerosol (SOA) under high-NOx conditions, Atmos. Chem. Phys., 19, 7255-7278, 10.5194/acp-19-7255-2019, 2019.

Shafizadeh, F.: Introduction to pyrolysis of biomass, J. Anal. Appl. Pyrol., 3, 283-305, 10.1016/0165-2370(82)80017-x, 1982.

Smith, M. L., Bertram, A. K., and Martin, S. T.: Deliquescence, efflorescence, and phase miscibility of mixed particles of ammonium sulfate and isoprene-derived secondary organic material, Atmos. Chem. Phys., 12, 9613-9628, 10.5194/acp-12-9613-2012, 2012.

Song, C., Na, K. S., and Cocker, D. R.: Impact of the hydrocarbon to NOx ratio on secondary organic aerosol formation, Environ. Sci. Technol., 39, 3143-3149, 10.1021/es0493244, 2005.

Song, C., Zaveri, R. A., Alexander, M. L., Thornton, J. A., Madronich, S., Ortega, J. V., Zelenyuk, A., Yu, X.-Y., Laskin, A., and Maughan, D. A.: Effect of hydrophobic primary organic aerosols on secondary organic aerosol formation from ozonolysis of alpha-pinene, Geophys. Res. Lett, 34, 10.1029/2007gl030720, 2007.

Spittler, M., Barnes, I., Bejan, I., Brockmann, K. J., Benter, T., and Wirtz, K.: Reactions of NO_3 radicals with limonene and alpha-pinene: Product and SOA formation, Atmos. Environ., 40, S116-S127, 10.1016/j.atmosenv.2005.09.093, 2006.

Sprengnether, M., Demerjian, K. L., Donahue, N. M., and Anderson, J. G.: Product analysis of the OH oxidation of isoprene and 1,3-butadiene in the presence of NO, J. Geophys. Res., 107, 4268, 10.1029/2001jd000716, 2002.

Stockwell, C. E., Yokelson, R. J., Kreidenweis, S. M., Robinson, A. L., DeMott, P. J., Sullivan, R. C., Reardon, J., Ryan, K. C., Griffith, D. W. T., and Stevens, L.: Trace gas emissions from combustion of peat, crop residue, domestic biofuels, grasses, and other fuels: configuration and Fourier transform infrared (FTIR) component of the fourth Fire Lab at Missoula Experiment (FLAME-4), Atmos. Chem. Phys., 14, 9727-9754, 10.5194/acp-14-9727-2014, 2014.

Stockwell, C. E., Veres, P. R., Williams, J., and Yokelson, R. J.: Characterization of biomass burning emissions from cooking fires, peat, crop residue, and other fuels with high-resolution proton-transfer-reaction time-of-flight mass spectrometry, Atmos. Chem. Phys., 15, 845-865, 10.5194/acp-15-845-2015, 2015.

Stockwell, C. E., Jayarathne, T., Cochrane, M. A., Ryan, K. C., Putra, E. I., Saharjo, B. H., Nurhayati, A. D., Albar, I., Blake, D. R., Simpson, I. J., Stone, E. A., and Yokelson, R. J.: Field measurements of trace gases and aerosols emitted by peat fires in Central Kalimantan, Indonesia, during the 2015 El Nino, Atmos. Chem. Phys., 16, 11711-11732, 10.5194/acp-16-11711-2016, 2016.

Strollo, C. M., and Ziemann, P. J.: Products and mechanism of secondary organic aerosol formation from the reaction of 3-methylfuran with OH radicals in the presence of NOx, Atmos. Environ., 77, 534-543, 10.1016/j.atmosenv.2013.05.033, 2013.

Surratt, J. D., Kroll, J. H., Kleindienst, T. E., Edney, E. O., Claeys, M., Sorooshian, A., Ng, N. L., Offenberg, J. H., Lewandowski, M., Jaoui, M., Flagan, R. C., and Seinfeld, J. H.: Evidence for organosulfates in secondary organic aerosol, Environ. Sci. Technol., 41, 517-527, 10.1021/es062081q, 2007.

Takahama, S., Pathak, R. K., and Pandis, S. N.: Efflorescence transitions of ammonium sulfate particles coated with secondary organic aerosol, Environ. Sci. Technol., 41, 2289-2295, 10.1021/es0619915, 2007.

Tapia, A., Villanueva, F., Salgado, M. S., Cabanas, B., Martinez, E., and Martin, P.: Atmospheric degradation of 3-methylfuran: Kinetic and products study, Atmos. Chem. Phys., 11, 3227-3241, 10.5194/acp-11-3227-2011, 2011.

Tillmann, R., Hallquist, M., Jonsson, A. M., Kiendler-Scharr, A., Saathoff, H., Iinuma, Y., and Mentel, T. F.: Influence of relative humidity and temperature on the production of pinonaldehyde and OH radicals from the ozonolysis of alpha-pinene, Atmos. Chem. Phys., 10, 7057-7072, 10.5194/acp-10-7057-2010, 2010.

Tuazon, E. C., Alvarado, A., Aschmann, S. M., Atkinson, R., and Arey, J.: Products of the gas-phase reactions of 1,3-butadiene with OH and NO_3 radicals, Environ. Sci. Technol., 33, 3586-3595, 10.1021/es990193u, 1999.

Varutbangkul, V., Brechtel, F. J., Bahreini, R., Ng, N. L., Keywood, M. D., Kroll, J. H., Flagan, R. C., Seinfeld, J. H., Lee, A., and Goldstein, A. H.: Hygroscopicity of secondary organic aerosols formed by oxidation of cycloalkenes, monoterpenes, sesquiterpenes, and related compounds, Atmos. Chem. Phys., 6, 2367-2388, 10.5194/acp-6-2367-2006, 2006.

Villanueva, F., Barnes, I., Monedero, E., Salgado, S., Gómez, M. V., and Martin, P.: Primary product distribution from the Cl-atom initiated atmospheric degradation of furan: Environmental implications, Atmos. Environ., 41, 8796-8810, 10.1016/j.atmosenv.2007.07.053, 2007.

Villanueva, F., Cabañas, B., Monedero, E., Salgado, S., Bejan, I., and Martin, P.: Atmospheric degradation of alkylfurans with chlorine atoms: Product and mechanistic study, Atmos. Environ., 43, 2804-2813, 10.1016/j.atmosenv.2009.02.030, 2009.

Walser, M. L., Desyaterik, Y., Laskin, J., Laskin, A., and Nizkorodov, S. A.: High-resolution mass spectrometric analysis of secondary organic aerosol produced by ozonation of limonene, Phys. Chem. Chem. Phys., 10, 1009-1022, 10.1039/b712620d, 2008.

Wang, Y., Luo, H., Jia, L., and Ge, S.: Effect of particle water on ozone and secondary organic aerosol formation from benzene-NO_2-NaCl irradiations, Atmos. Environ., 140, 386-394, 10.1016/j.atmosenv.2016.06.022, 2016.

Xu, J., Griffin, R. J., Liu, Y., Nakao, S., and Cocker, D. R., III: Simulated impact of NOx on SOA formation from oxidation of toluene and m-xylene, Atmos. Environ., 101, 217-225, 10.1016/j.atmosenv.2014.11.008, 2015.

Yu, K.-P., Lin, C.-C., Yang, S.-C., and Zhao, P.: Enhancement effect of relative humidity on the formation and regional respiratory deposition of secondary organic aerosol, J. Hazard. Mater., 191, 94-102, 10.1016/j.jhazmat.2011.04.042, 2011.

Zhang, Q., Jimenez, J. L., Canagaratna, M. R., Ulbrich, I. M., Ng, N. L., Worsnop, D. R., and Sun, Y.: Understanding atmospheric organic aerosols via factor analysis of aerosol mass spectrometry: A review, Anal. Bioanal. Chem., 401, 3045-3067, 10.1007/s00216-011-5355-y, 2011.

Zhou, Y., Zhang, H., Parikh, H. M., Chen, E. H., Rattanavaraha, W., Rosen, E. P., Wang, W., and Kamens, R. M.: Secondary organic aerosol formation from xylenes and mixtures of toluene and xylenes in an atmospheric urban hydrocarbon mixture: Water and particle seed effects (II), Atmos. Environ., 45, 3882-3890, 10.1016/j.atmosenv.2010.12.048, 2011.

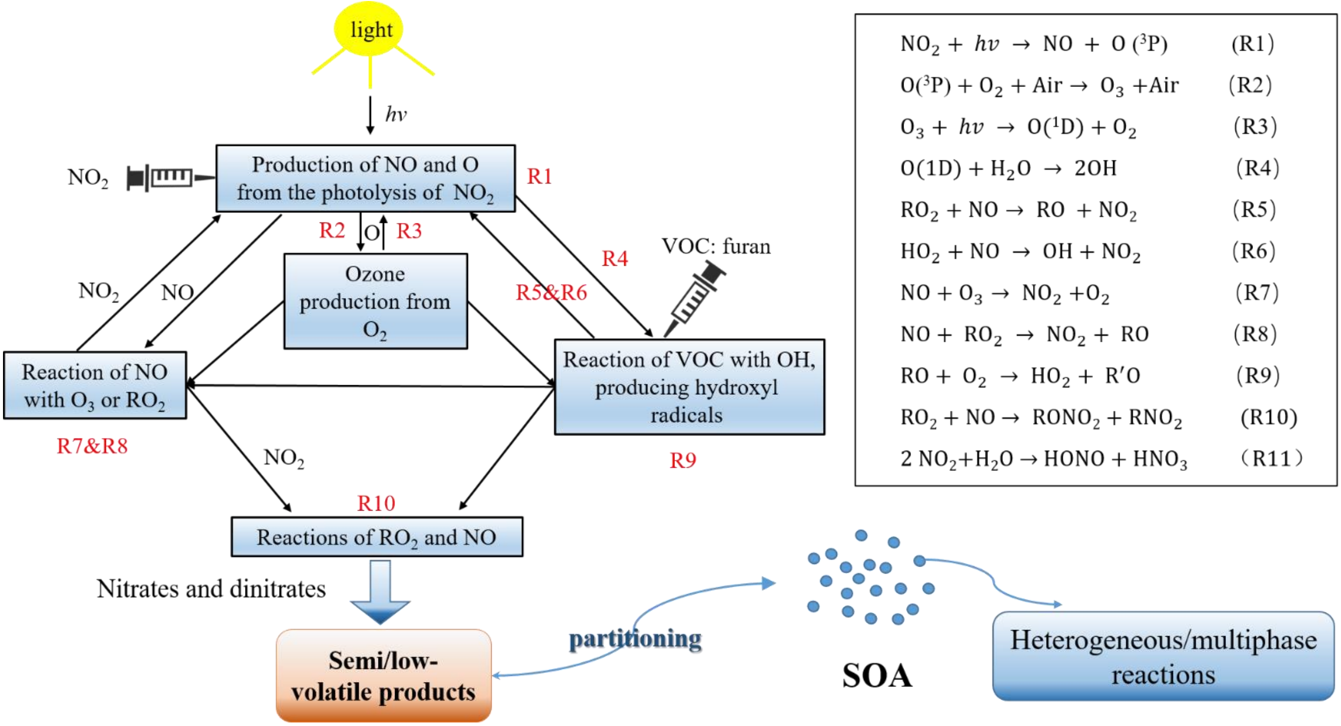

Figure 1: Major chemical reactions during the experiments.

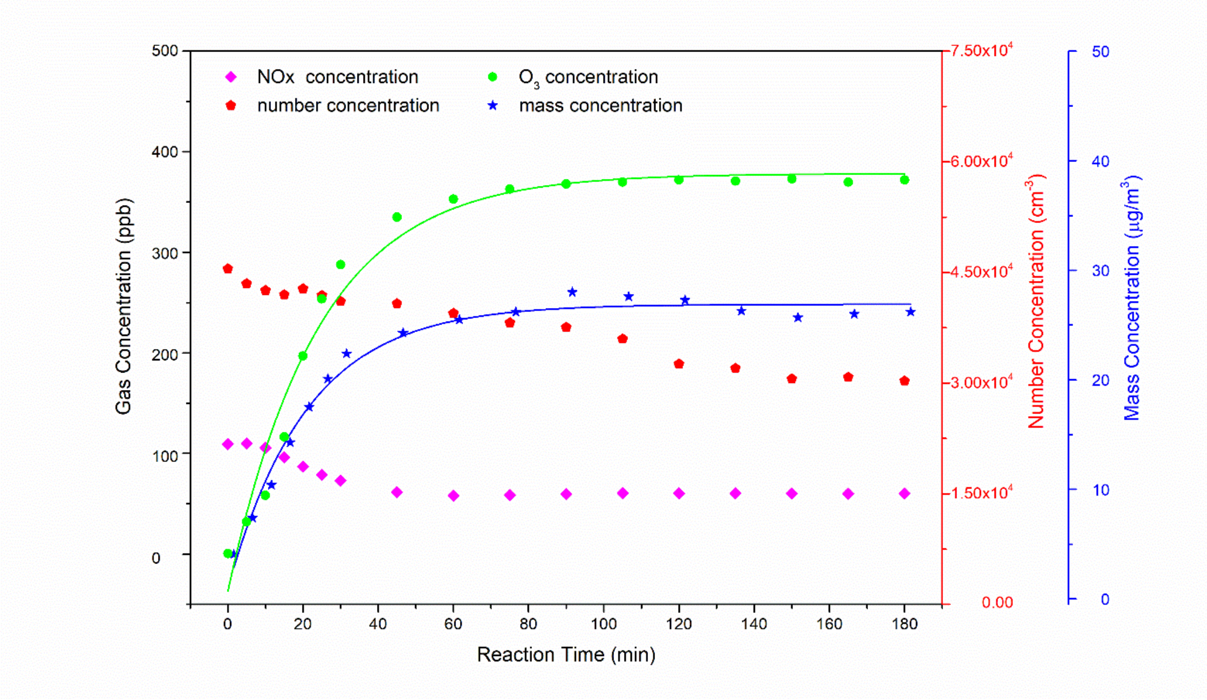

Figure 2: Profile of the gas-phase concentrations of reactants (NO, NO_2, NOx and O_3) and particle number/mass concentrations (corrected with wall loss) over time. The C_4H_4O/NOx ratio is 7.9 and RH = 23%. Since the particle wall loss has a weak RH dependence in our chamber, a mean value of 4.7×10^{-5} s^{-1} was used for wall loss correction. A density of 1.4 g cm^{-3} was used in the SMPS (Jia and Xu, 2018; Kostenidou et al., 2007).

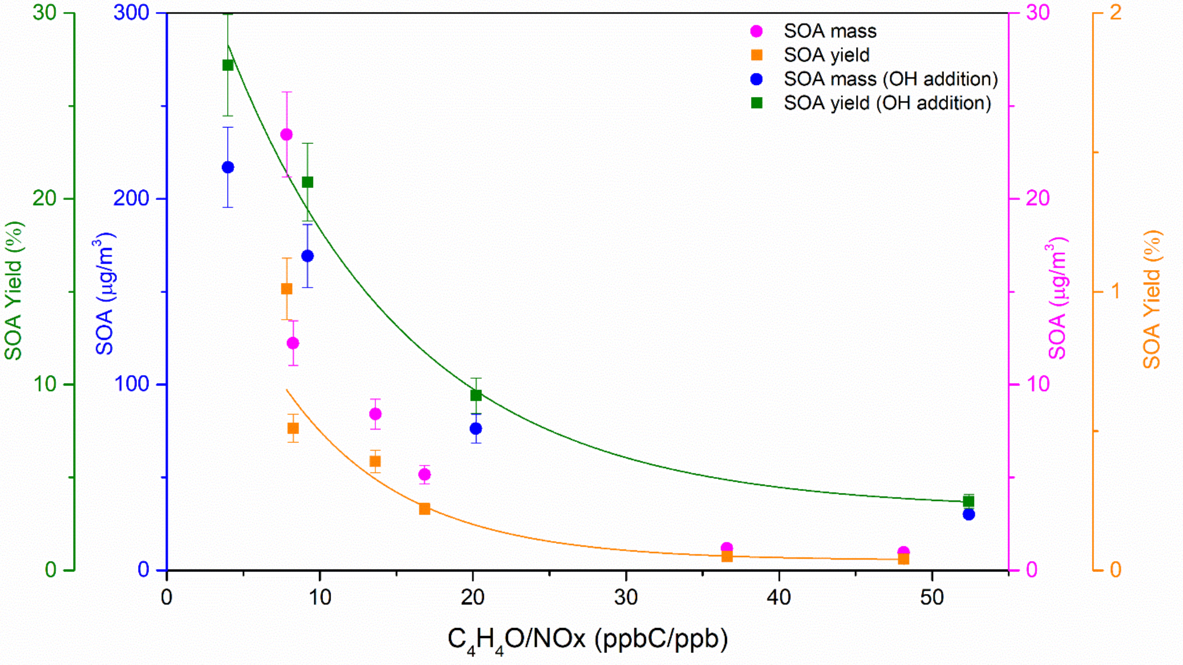

Figure 3: Dependence of the SOA mass concentration and SOA yield on the C_4H_4O/NOx ratio. Since the particle wall loss has a weak RH dependence in our chamber, a mean value of 3.6 × 10^{-5} s^{-1} was used for wall loss correction. A density of 1.4 g cm^{-3} was used in SMPS (Jia and Xu, 2018; Kostenidou et al., 2007).

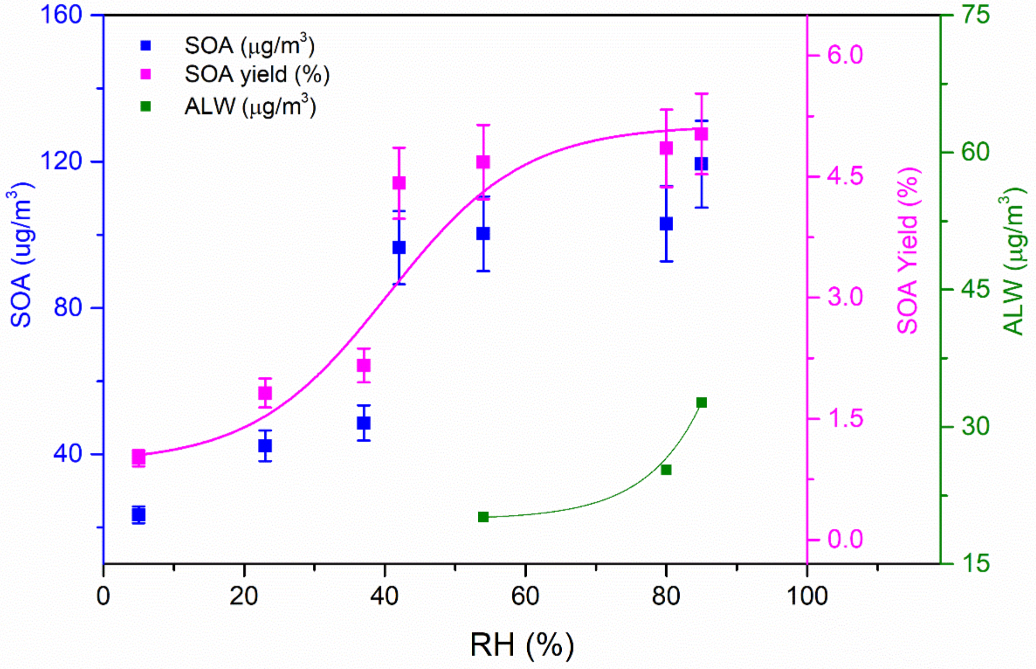

Figure 4: Dependences of the SOA mass concentration, SOA yield and ALW on relative humidity (RH).

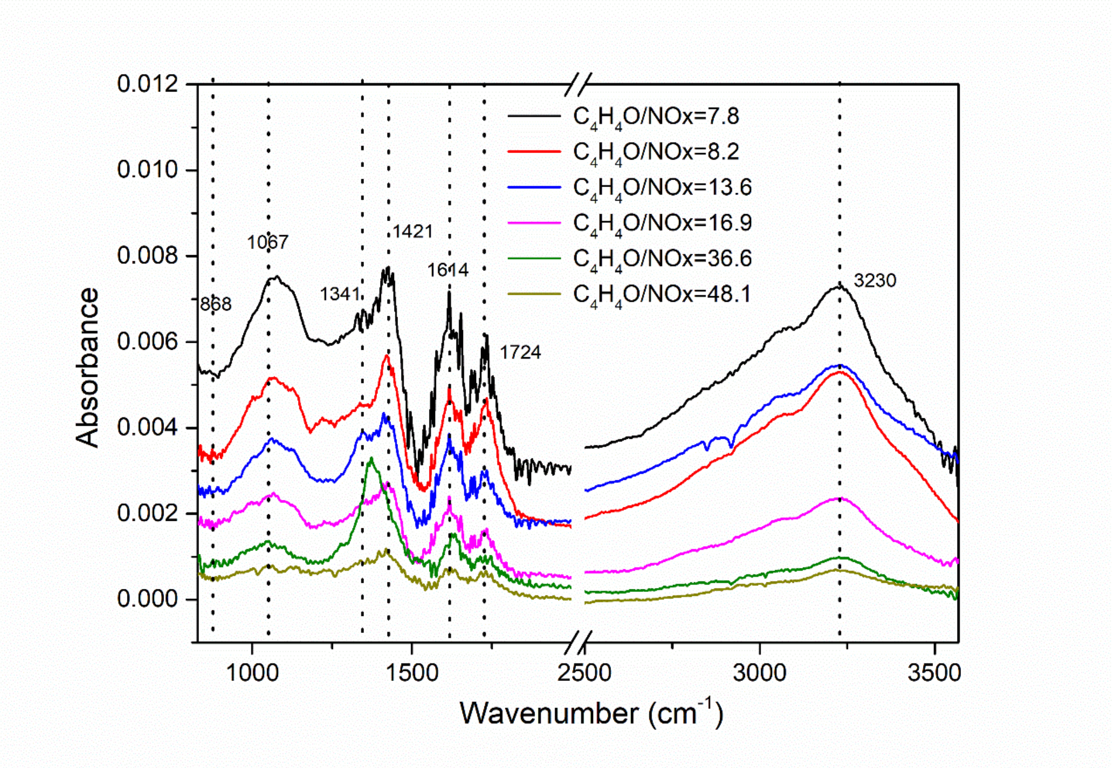

Figure 5: FTIR spectra of particles collected from furan-NOx-NaCl photooxidation experiments with different values of C_4H_4O/NOx ratio ranging from 7.3 to 48.1.

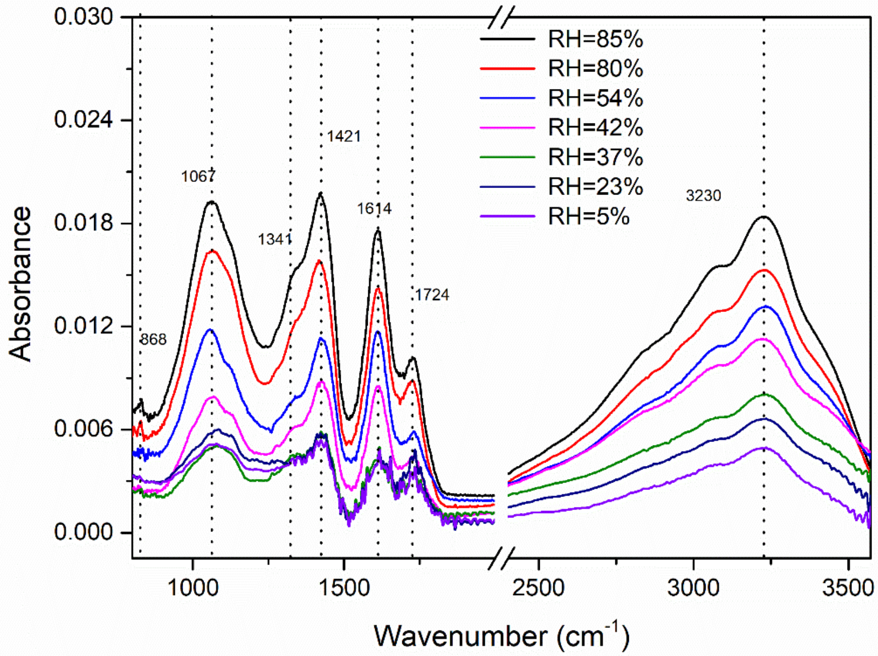

Figure 6: FTIR spectra of particles collected from furan-NOx-NaCl photooxidation experiments with different values of RH ranging from 5 % to 85 %.

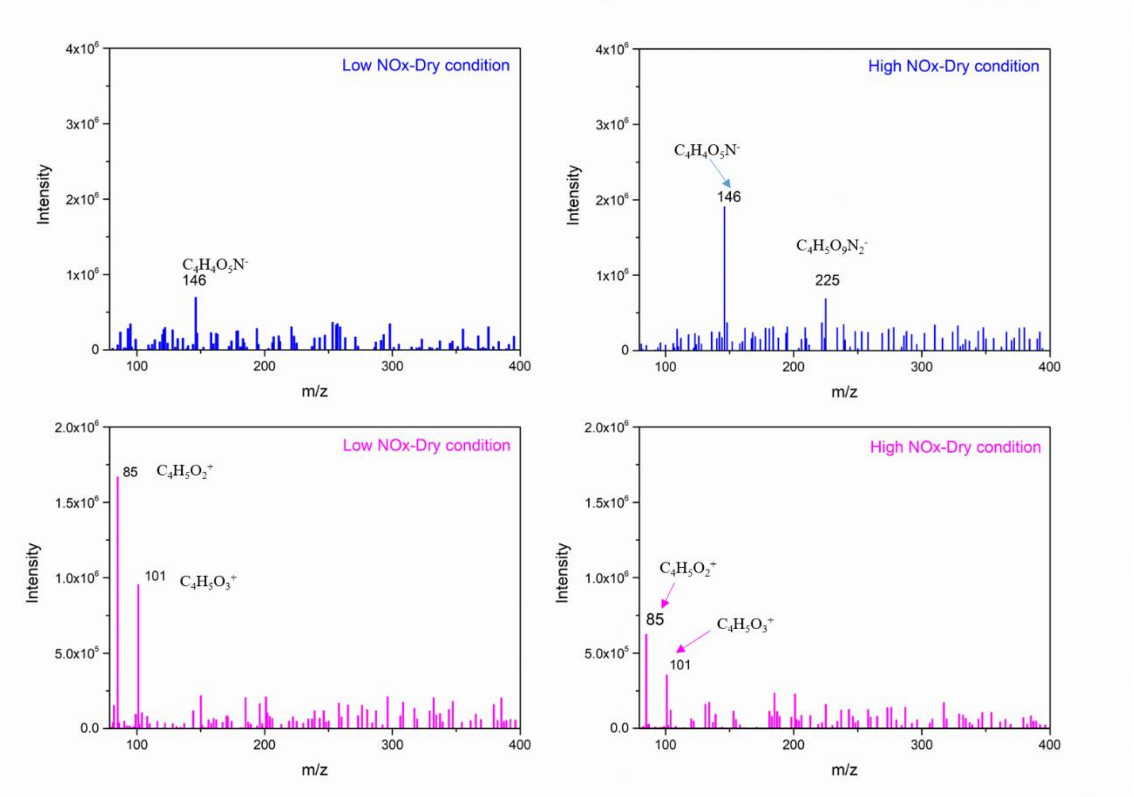

Figure 7: Selected background-subtraction HESI-Q Exactive-Orbitrap MS results of SOA in both negative (blue) and positive (pink) ion modes from the photooxidation of furan under different RH conditions.

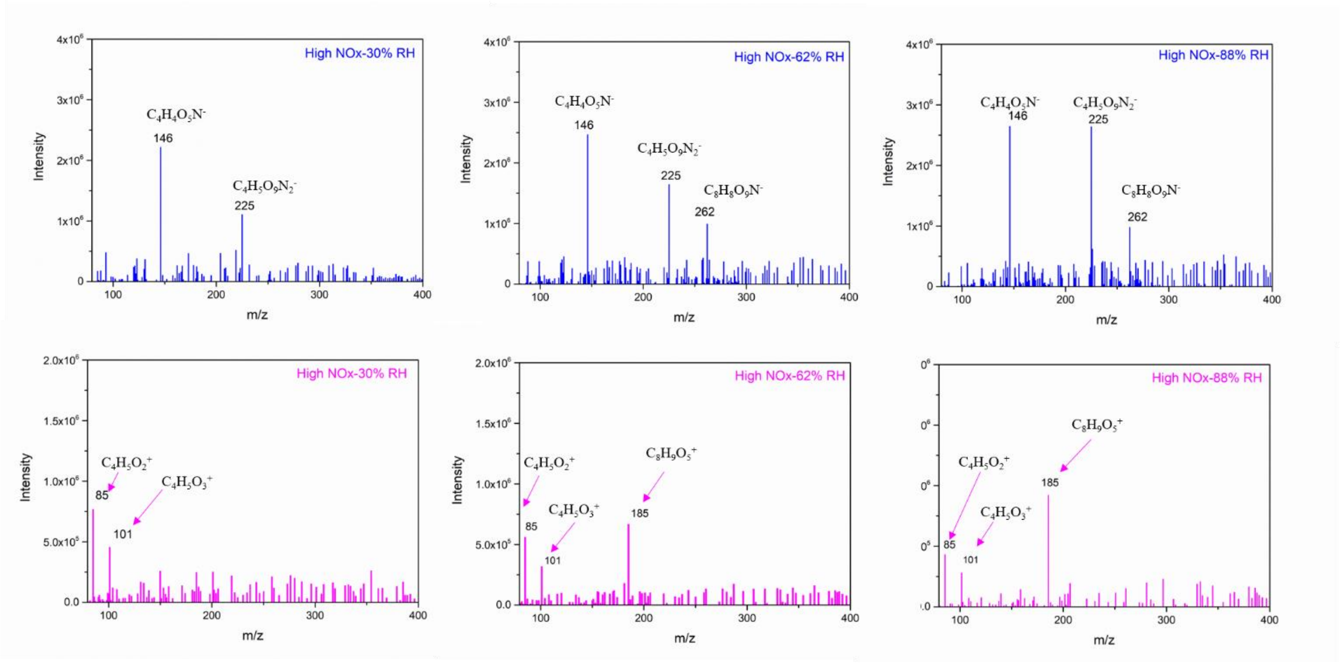

Figure 8: Selected background-subtraction HESI-Q Exactive-Orbitrap MS results of SOA in both negative (blue) and positive (pink) ion modes from the photooxidation of furan under different RH conditions.

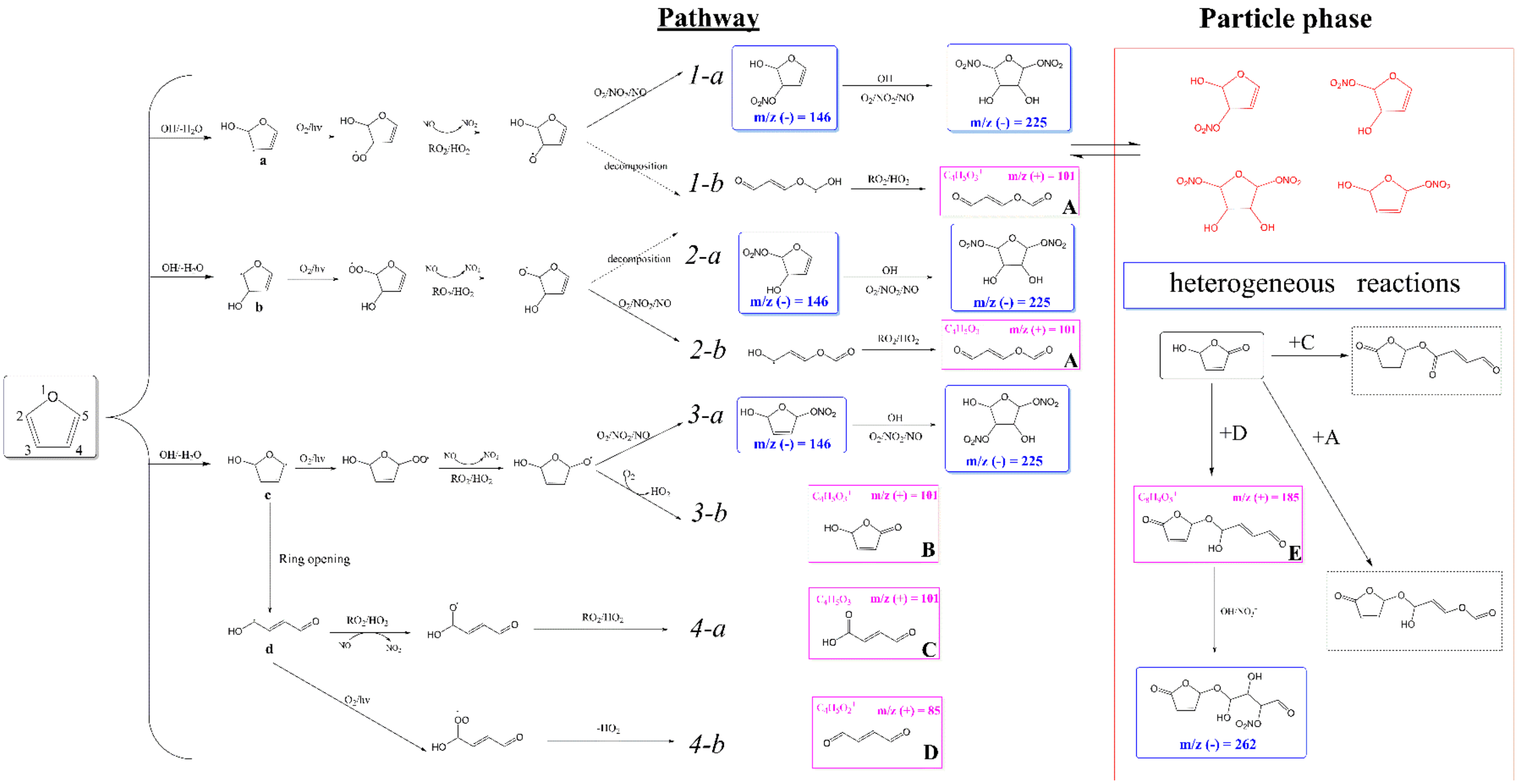

Scheme 1: Proposed chemical mechanism of furan-NOx photooxidation under different experimental conditions. SOA constituents in blue and pink boxes are proposed SOA constituents detected by HESI-Q Exactive-Orbitrap MS under negative and positive ion mode, respectively. The detected nitrates and dinitrates in red are low-volatility organic species, which can easily partition into the particle phase and enhance the SOA formation.

Table 1. Summary of initial conditions, O_3 concentrations and particle mass concentrations in furan-NOx-NaCl photooxidation experiments.

Exp No	Initial conditions				SOA formation results						
	$[\text{furan}]_0$ (ppb)	$[\text{NO}]_x$ (ppb)	RH (%)	C_4H_4O/NOx (ppbC/ppb)	O_3 (ppb)	PM[a] (μg m^{-3})	NaCl[b] (μg m^{-3})	$NaNO_3$[c] (μg m^{-3})	ALW[d] (μg m^{-3})	SOA[e] (μg m^{-3})	SOA yield (%)
1	708.4	16.8	<5 %	48.1	91	12.2	11.3	3.5	--	1.0±0.1	0.04±0.01
2	749.0	23.2	<5 %	36.6	115	15.4	10.7	1.6	--	1.2±0.2	0.05±0.01
3	752.5	44.7	<5 %	16.9	197	21.3	14.1	2.1	--	5.1±0.5	0.3±0.02
4	705.8	51.8	<5 %	13.6	250	23.5	12.6	2.5	--	8.4±0.9	0.3±0.03
5	783.4	94.9	<5 %	8.2	372	29.1	13.5	3.9	--	12.2±1.3	0.5±0.05
6	763.4	97.5	<5 %	7.8	382	38.6	11.5	3.5	--	23.5±2.3	1.0±0.1
7	764.8	96.7	23 %	7.9	359	55.5	10.4	3.8	--	42.3±4.2	1.9±0.2
8	740.1	97.3	37 %	7.6	353	64.2	11.2	4.5	--	48.6±4.9	2.2±0.3
9	719.0	100.2	42 %	7.2	329	111.1	9.4	5.2	--	96.4±9.7	4.5±0.5
10	704.8	92.9	54 %	7.6	280	138.7	12.0	6.2	20.1	100.2±10.1	4.7±0.4
11	699.3	102.9	80 %	6.8	253	144.1	8.2	7.6	25.3	103.0±10.3	4.8±0.5
12	780.7	98.1	85 %	8.0	241	173.0	10.0	11.1	32.6	119.2±10.4	5.0±0.5

[a] PM: particle mass concentration in the chamber was determined from the SMPS and was the sum of NaCl, $NaNO_3$, ALW, and SOA at the end of the experiments.22

[b] NaCl: the amount of NaCl at the end of the experiments;

[c] $NaNO_3$: the amount of $NaNO_3$ at the end of the experiments;

[d] ALW: the amount of aerosol liquid water content at the end of the experiments;

[e] SOA: the amount of secondary organic aerosol at the end of the experiments.

Table 2. Assignment of the observed FTIR absorption frequencies (cm^{-1}).

Absorption frequencies	Functional group	Assignment
1222-868	C-C and C−O	Stretching in alcohols (Coury and Dillner, 2008) C−O of COOH group (Duarte et al., 2005)
1067	C−O−C	C−O stretching (Jang et al., 2002)
1515-1350	−CH	Bending vibration of −C−H group
868	-NO	NO symmetric stretching (Jia and Xu, 2016)
1614, 1341	$-ONO_2$	NO_2 symmetric stretching and asymmetric stretching
1724	C=O	Stretching vibration in carboxylic acid and ketones
3000-2850	C−H	C−H stretching vibration in the saturated carbon ring
3100-3000	C−H	C−H stretching vibration in unsaturated alkene
3200-2400	O−H	Stretching vibration in carboxyl groups
3100-3500	O−H	Stretching vibration in hydroxyl groups

Table 3. Ion peaks with the assigned compounds observed in the HESI-Q Exactive-Orbitrap MS. Proposed assignments are based on the formula from HESI-Q Exactive-Orbitrap MS.

Ion mode	No	Mass (m/z)	Ion Mode	Ion Formula	Delta (amu)	Proposed Structure
Positive ion mode	1	85.0018	$[M+H]^+$	$C_4H_5O_2^+$	-0.027	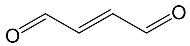
	2	101.0894	$[M+H]^+$	$C_4H_5O_3^+$	0.066	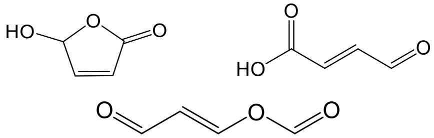
	3	185.0504	$[M+H]^+$	$C_8H_9O_5^+$	0.006	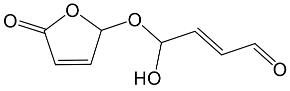
Negative ion mode	4	146.0161	$[M-H]^-$	$C_4H_4O_5N^-$	0.007	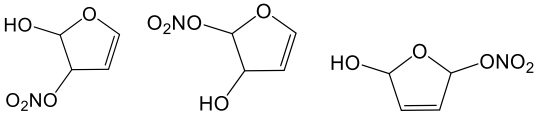
	5	225.0125	$[M-H]^-$	$C_4H_5O_9N_2^-$	0.012	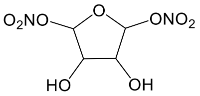
	6	262.0132	$[M-H]^-$	$C_8H_8O_9N^-$	-0.007